Global observations of aerosol-cloud-precipitation-climate interactions

Daniel Rosenfeld[1], Meinrat O. Andreae[2], Ari Asmi[3], Mian Chin[4], Gerrit de Leeuw[3,5], David P. Donovan[6], Ralph Kahn[4], Stefan Kinne[7], Niku Kivekäs[5,8], Markku Kulmala[3], William Lau[4], K. Sebastian Schmidt[9], Tanja Suni[3], Thomas Wagner[10], Martin Wild[11], and Johannes Quaas[12]

[1]Institute of Earth Sciences, The Hebrew University of Jerusalem, Israel, [2]Biogeochemistry Department, Max Planck Institute for Chemistry, Mainz, Germany, [3]Department of Physics, University of Helsinki, Helsinki, Finland, [4]Earth Science Division, NASA Goddard Space Flight Center, Greenbelt, Maryland, USA, [5]Atmospheric Composition Research Unit, Finnish Meteorological Institute, Helsinki, Finland, [6]Royal Netherlands Meteorological Institute (KNMI), AE De Bilt, The Netherlands, [7]Max Planck Institute for Meteorology, Hamburg, Germany, [8]Division of Nuclear Physics, Department of Physics, Lund University, Lund, Sweden, [9]Laboratory for Atmospheric and Space Physicsand Department for Atmospheric and Oceanic Sciences, University of Colorado Boulder, Boulder, Colorado, USA, [10]Satellite remote sensing group, Max Planck Institute for Chemistry, Mainz, Germany, [11]Institute for Atmospheric and Climate Science, ETH Zurich, Zurich, Switzerland, [12]Institute for Meteorology, Universität Leipzig, Leipzig, Germany

Abstract Cloud drop condensation nuclei (CCN) and ice nuclei (IN) particles determine to a large extent cloud microstructure and, consequently, cloud albedo and the dynamic response of clouds to aerosol-induced changes to precipitation. This can modify the reflected solar radiation and the thermal radiation emitted to space. Measurements of tropospheric CCN and IN over large areas have not been possible and can be only roughly approximated from satellite-sensor-based estimates of optical properties of aerosols. Our lack of ability to measure both CCN and cloud updrafts precludes disentangling the effects of meteorology from those of aerosols and represents the largest component in our uncertainty in anthropogenic climate forcing. Ways to improve the retrieval accuracy include multiangle and multipolarimetric passive measurements of the optical signal and multispectral lidar polarimetric measurements. Indirect methods include proxies of trace gases, as retrieved by hyperspectral sensors. Perhaps the most promising emerging direction is retrieving the CCN properties by simultaneously retrieving convective cloud drop number concentrations and updraft speeds, which amounts to using clouds as natural CCN chambers. These satellite observations have to be constrained by in situ observations of aerosol-cloud-precipitation-climate (ACPC) interactions, which in turn constrain a hierarchy of model simulations of ACPC. Since the essence of a general circulation model is an accurate quantification of the energy and mass fluxes in all forms between the surface, atmosphere and outer space, a route to progress is proposed here in the form of a series of box flux closure experiments in the various climate regimes. A roadmap is provided for quantifying the ACPC interactions and thereby reducing the uncertainty in anthropogenic climate forcing.

1. Introduction

1.1. The Background and Objectives of This Review

Cloud active aerosols, i.e., cloud condensation nuclei (CCN) and ice nuclei (IN), can modify cloud microstructure, precipitation forming processes, and the meteorological and radiative responses of clouds and the atmosphere. These effects impact both the atmospheric circulation systems and the thermodynamic and radiative energy budgets over a cascade of scales from local to global.

Observations of these cloud aerosol interactions are reviewed to provide context for novel concepts for ground and satellite-based studies on aerosol-cloud-precipitation-climate interactions. CCN and IN are important because they affect clouds and precipitation, which regulate a large fraction of Earth's energy budget. Low bright clouds have a strong cooling effect by reflecting back to space much of the incoming solar energy, whereas high, semitransparent clouds have a net warming effect by shielding the upwelling thermal emission from escaping to space, which outweighs the cooling by their weak reflectance of the solar radiation. The latent heat, which is released when condensation creates precipitating clouds, supplies much of the energy that the atmosphere loses by radiating to space.
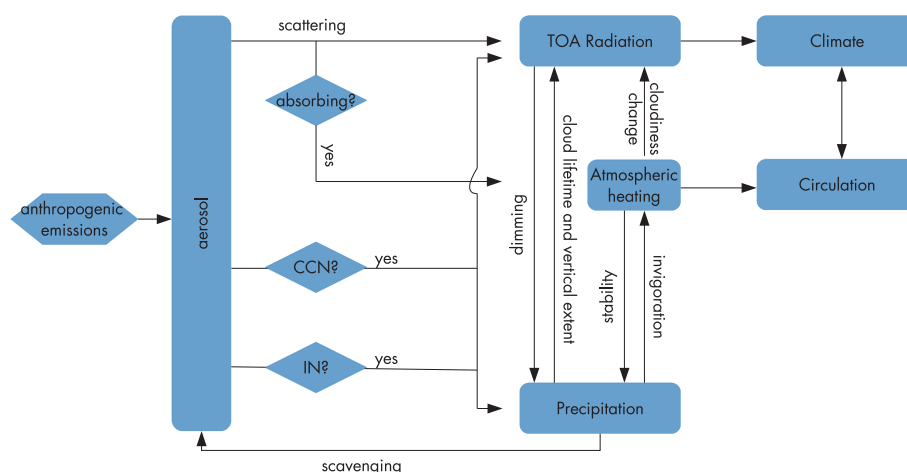
Figure 1. Illustration of ways by which aerosol particles suppress or increase local precipitation and alter thermal radiation and latent heating profiles, thus altering the hydrological cycle and climate. After *Lau et al.* [2008].

Cloud-mediated aerosol effects are recognized by the Intergovernmental Panel on Climate Change (IPCC) as one of the key sources of uncertainty in our knowledge of Earth's energy budget and anthropogenic climate forcing in particular. In view of this unanswered scientific and practical question, we provide here a condensed review of the relevant knowledge, followed by plans for addressing this question effectively by consolidating scattered ongoing efforts into the well-coordinated critical mass that is required for this research.

The overall goal of this review is to outline what is known about the mechanisms of aerosol cloud-mediated climatic impacts and the ways to observe and quantify these effects, to assess what we know and identify the gaps, and then suggest possible ways to move forward. Here we address tropospheric aerosols, because clouds form in the troposphere. Although stratospheric aerosols may interact with upper tropospheric clouds, they are not addressed in this review.

The same aerosols can have very different impacts at different scales, because primary effects that are clearly observed at the individual cloud scale can be either buffered or amplified by system response and adjustment at larger scales. Therefore, the assessment has to be done at several scales ranging from the individual cloud element (few kilometers and tens of minutes), through the scale of the cloud system lifecycle (tens to few hundred kilometers and few to 24 h), regional (few hundred to thousands of kilometers and few days), and to the global extent at climate time scales.

After a general background introduction (section 1), section 2 provides an expanded review of the role of aerosols in aerosol-cloud-precipitation-climate (ACPC) interactions. Section 3 reviews the challenge of measuring CCN and IN, especially from satellites at a global scale, and presents possible solutions. Section 4 reviews the present capabilities and limitations of observing cloud aerosol interactions, mainly due to the challenges of making adequate measurements of the cloud-active aerosol particles. Section 5 provides a proposed framework for quantifying the various aerosol effects on the atmospheric energy budget and air motions, which at present are so poorly known. Finally, section 6 provides a summary and makes recommendations.

1.2. Aerosols Modulate Cloud Properties and Precipitation in Many Ways

The composition and radiative properties of both shallow and deep clouds are affected by the aerosol particles that serve as cloud condensation nuclei (CCN) and ice nuclei (IN). In addition, the direct radiative effects of the aerosol particles can modify clouds by locally changing atmospheric heating rates. These changes in cloud properties also affect precipitation formation processes, which in turn feed back on to the cloud dynamic properties in highly nonlinear ways. This, in turn, feeds back onto the clouds' radiative properties that alter the thermal structure that further changes the cloud dynamics, and so on, as illustrated in Figure 1. Because the vertical profiles of heating rates are often dominated by latent heating processes (e.g., release during condensation, freezing, or precipitation; uptake during evaporation or melting), aerosol impacts on these processes (e.g., cloud development or precipitation formation processes) can cascade to influence atmospheric circulation. Therefore, the impacts of aerosols on cloud properties are not independent of the meteorological

environment and might even feed back into it. Therefore, it is even possible that disentangling the two may not be a fully correct approach for quantifying the aerosol effects, as they may include the meteorological response. Addressing the possible impacts of aerosols on clouds, precipitation, and the resultant changes in the atmospheric structure (i.e., meteorology), and energy budget requires measuring the CCN at a useful accuracy (better than within a factor of 1.5) on a global scale. The effects of CCN on clouds and subsequently on radiation may be approximated as a logarithmic dependency. Thus, the upper limit to the required measurement accuracy for CCN is bound to the desired limit of the uncertainty in the radiative forcing. In practice, global-scale measurements are possible only when using satellite measurements. However, doing this is a major challenge, which will be addressed with new concepts in section 3.

There is some evidence that aerosol effects often occur such that a perturbation of the system in one direction creates a compensating effect in another [*Stevens and Feingold*, 2009]. Under some circumstances, the system can bifurcate into different stable regimes that have rather different precipitation properties and cloud radiative effects. Such bifurcations occur in marine layer clouds upon their transitions between the fully cloudy closed and the partially cloudy, open cells [*Ackerman et al.*, 1993; *Rosenfeld et al.*, 2006a]. They also occur as the transitions between the full cover of supercooled layer clouds and broken semitransparent ice clouds [*Morrison et al.*, 2012].

This highly complex situation of poorly quantified aerosol-cloud-precipitation-climate (ACPC) feedbacks, some of which have opposite signs, causes high uncertainty in the resulting climate forcing. These complex relationships and their potential climate impacts were reviewed by *Rosenfeld et al.* [2013].

1.3. The ACPC Initiative

To meet the challenge of quantifying the aerosol cloud-mediated effects on the climate system, the ACPC initiative was established as a joint project of the International Geosphere–Biosphere Programme (IGBP) and the World Climate Research Program (WCRP). The initiative has been developed through the cooperation of the Integrated Land Ecosystem–Atmosphere Processes Study (iLEAPS) and International Global Atmospheric Chemistry (IGAC) core projects of IGBP, and the Global Energy and Water Cycle Experiment (GEWEX), a core project of the WCRP. The goal of the ACPC initiative is to obtain a quantitative understanding of the interactions between aerosols, clouds and precipitation, and their role in the climate system, mainly by facilitating international cooperation and providing the conceptual framework of related research projects. The latter is done in the ACPC science plan and implementation strategy [*Andreae et al.*, 2009], mostly in the form of major field campaigns in which a closure of components of energy fluxes in their various forms within a limited domain will be sought.

Due to the global scale of the ACPC related questions, satellite-based observations are essential to capture the spatial distributions of cloud, aerosol, and precipitation properties, as well as the thermodynamic properties of the atmosphere and the surface, which is done mainly by sensing radiative fluxes at selected wavelength regions. This requires the formulation of a strategic approach, which is a major task within the ACPC initiative and has been termed Remote Sensing of Aerosol-Cloud-Precipitation-Climate interactions (SAT-ACPC). In this review, we identify the main challenges and follow with suggesting possible ways to address them using satellite remote sensing. We focus on the ways by which these satellite measurements can be used in conjunction with aircraft in situ and ground-based remotely sensed measurements, and on ways by which the satellite data can be integrated in the framework of numerical simulations.

In addition, we introduce principles for planning closure box experiments with the goal of measuring the fluxes of energy and matter in all their relevant forms in various cloud regimes, and the ways these fluxes are affected by the variability in aerosol amount as well as in their chemical, physical, and optical properties. Satellite methodologies are important components in the design of these experiments.

2. The Role of Aerosols in ACPC

2.1. CCN Microphysical Impacts on Clouds and Precipitation Forming Processes
2.1.1. The CCN and Cloud Base Updraft Controls on N_a
The number of activated cloud drops at cloud base (N_a) is a potentially observable cloud property of fundamental importance. N_a is determined by the supersaturation (S) activation spectra of the cloud condensation nuclei (CCN) and by cloud base updraft velocity (W_b). The fraction of CCN that is actually activated into cloud drops increases for larger W_b and smaller number concentrations of CCN (N_{ccn}). At the extreme, in a CCN-limited

environment with very small N_{ccn} values of a few hundreds cm^{-3}, N_a is determined by N_{ccn}. At the other extreme, where N_{ccn} exceeds several thousands cm^{-3}, N_a is determined by W_b. Therefore, the latter situation is called updraft limited [*Reutter et al.,* 2009]. The conditions over pristine ocean are mostly CCN limited, and even over land, the updraft limited condition is reached only in highly polluted atmospheres. Therefore, for a given W_b, changes in N_{ccn} concentrations are manifested as respective changes in N_a, a relationship which tends to approach saturation at very high N_{ccn}. Giant CCN reduce S at cloud base and hence decrease N_a, because the condensation rate is disproportionally larger for big droplets. This becomes important where there is a high concentration of sea spray droplets under stormy conditions, or in dust storms. In polluted conditions, the effect of condensable trace gases will also reduce the critical supersaturation and so enhance the CCN activity of the small aerosols [e.g., *Laaksonen et al.,* 1998; *Charlson et al.,* 2001].

2.1.2. Primary Cloud Drop Nucleation and Conditions for Secondary Nucleation Aloft

Most cloud drops of convective clouds nucleate at cloud base; therefore, observing cloud properties above cloud base can also be useful for retrieving N_a in such clouds, as will be shown in section 3.5. Consequently, it is important to characterize the conditions in which most cloud drops nucleate near cloud base. This does no longer apply when significant secondary nucleation of cloud drops occurs at some distance above cloud base or when the drop size decreases due to partial evaporation caused by homogeneous mixing of the cloud with the ambient air, or when drops grow significantly by coalescence. When secondary cloud drop nucleation occurs above cloud base, cloud drop size distribution can no longer be tracked back to its origin at cloud base; and thus, N_a cannot be retrieved. However, as described in section 3.5, these processes have little impact on cloud drop size below the height where cloud drop effective radius reaches about 14 μm and the coalescence accelerates and initiates warm rain. Secondary nucleation can occur in convective clouds when coalescence and precipitation scavenging of the cloud drops decrease the combined surface area over which condensation can occur, and hence, S can exceed the maximum S that was reached near cloud base [*Pinsky and Khain*, 2002]. Secondary nucleation occurs in nonprecipitating convective clouds mostly in updraft-limited conditions, when the updraft speed accelerates significantly with height. This can occur mainly over near-coastal ocean in polluted air, where N_{ccn} is high and W_b is reduced by giant CCN originating from sea spray aerosol [*Rosenfeld et al.,* 2002] and can be identified in clouds by the appearance of a new mode of small cloud drops.

2.1.3. Vertical Profiles of Cloud Microstructure and Precipitation Forming Processes

Satellite retrievals of cloud drop number concentrations at cloud base are based on the retrieved vertical development of cloud drop effective radius in convective clouds [*Freud et al.,* 2011]. Therefore, in order to provide the necessary background, the cloud drop growth with height and the initiation of rain is described here. It is particularly necessary to be able to determine the height at which coalescence starts to add a significant growth rate to cloud drop effective radius beyond growth by condensation of vapor. This is done by satellite retrieval of both cloud top temperature (T) and cloud drop effective radius (r_e) for the same pixels in convective cloud elements reaching different heights above their base and relating r_e to T.

The subsequent growth with height of the drops nucleated at cloud base is initially dominated by condensation. Because the coalescence rate is proportional to the fifth power of the cloud drop effective radius [*Freud et al.,* 2011], the growth of drops by coalescence becomes very efficient when r_e exceeds a critical radius, $r_{e,crit}$, of ~14 μm, where warm rain starts developing quickly [e.g., *Rosenfeld and Gutman*, 1994; *Gerber*, 1996; *Rangno and Hobbs*, 2005; *Suzuki et al.,* 2010; *Freud and Rosenfeld*, 2012; *Rosenfeld et al.,* 2012a]. The height above cloud base that is required for r_e to exceed $r_{e,crit}$ and hence for the onset of warm rain linearly depends on N_a for a cloud water mixing ratio profile that scales with an adiabatic one. This has been documented extensively for a wide range of conditions around the world [*Freud and Rosenfeld*, 2012]. The shapes of the satellite-retrieved cloud-top temperature (T)–cloud top r_e relationships in convective clouds were used to infer five vertical microphysical zones in growing convective elements [*Rosenfeld and Lensky*, 1998]. The T-r_e relationships are composed from the measured T and r_e of a cloud ensemble of various top heights. A remotely observed area that includes the clouds has many cloudy satellite pixels, each with a pair for T and r_e values. The T-r_e relationships are obtained by calculating the mean r_e for each 1°C interval of T. For this purpose, it is assumed that the vertical evolution of r_e at cloud top along its growth is the same as the vertical profile of T-r_e of the cloud ensemble when examined at a snap shot. This assumption was corroborated in a study by *Lensky and Rosenfeld* [2006]. They tracked clouds with a 3 min sequence of satellite data and showed that the time evolution of T-r_e of a growing cloud was the same as the T-r_e that was obtained as a snap shot at the same
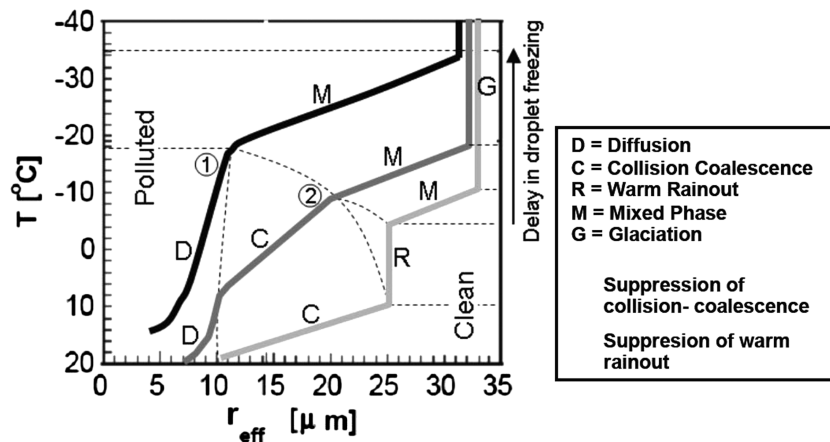
Figure 2. Conceptual diagram describing five microphysical stages (droplet growth by diffusion, collision-coalescence, warm rainout, ice-water mixed phase, and glaciated phase) common to deep convective clouds and their response to the concentration of pollution aerosols. The dashed line divide the parameter space to the microphysical zones, as denoted in the legend. For example, areas 1 and 2 show the domains of cloud drop growth by diffusion and coalescence, respectively. The bottom curve shows the case of a maritime environment with low CCN concentration and ample warm rain processes; the middle curve corresponds to moderately polluted continental clouds, where the larger number of CCN aerosols helps to suppress warm rain process and glaciation starts at slightly lower temperatures; the top curve represents extremely polluted cases where the very large number of CCNs produce smaller and more numerous droplets at cloud base suppressing the beginning of collision-coalescence processes and postponing the start of droplet freezing to lower temperatures. Intermediate situations to the above curves are also possible. Figure from *Martins et al.* [2011] who adapted it from *Rosenfeld and Woodley* [2003].

time for a cloud ensemble that had different cloud top heights. The satellite-retrieved vertical microphysical zones are [*Rosenfeld and Lensky*, 1998; *Rosenfeld and Woodley*, 2003]

1. Condensation-dominated growth of cloud drops: This is where $r_e < r_{e,crit}$, and warm rain processes have not significantly progressed [*Suzuki et al.*, 2010]. The depth of this region is determined mainly by N_a and cloud base temperature. Because N_a is dominated by N_{ccn}, except for updraft-limited conditions, the depth of the diffusional growth zone is dominated by N_{ccn}.
2. Coalescence-dominated growth of cloud drops: Cloud drops grow by coalescence into raindrops much faster than they would just by condensation, even in an adiabatic cloud parcel. Therefore, this zone is reached when the retrieved r_e exceeds its adiabatic value.
3. Rainout zone: When the warm rain is fully developed at the top of growing convective clouds the largest drops that fall from the cloud tops balance the additional growth by coalescence. This is manifested as a stabilization of r_e with further vertical growth at the size of about 25 μm.
4. Mixed phase zone: The development of the ice phase is indicated by an apparent additional increase of the indicated r_e, when the retrieval algorithm assumes a water cloud.
5. Glaciated zone: When all cloud drops are glaciated, or at least when the radiative signature is dominated by the ice phase, the r_e reaches its peak size, because there is no effective mechanism for additional growth of the ice particles. Above that height, the retrieved r_e remains stable or decreases, due to secondary ice nucleation aloft [*Yuan et al.*, 2010].

The shapes of the T-r_e relations that define these microphysical zones are illustrated in Figure 2. These inferred microphysical zones can be validated by surface and space borne radar measurements [*L'Ecuyer et al.*, 2009; *Suzuki et al.*, 2010, 2011]. Not all microphysical zones are necessarily realized in any given convective vertical profile. They are determined by a combination of N_{ccn}, ice nuclei number concentration (N_{IN}), updraft speed, and cloud base and top temperatures.

In tropical convective clouds with warm bases, the depth of the condensation-dominated growth zone is determined by N_a. The coalescence zone and formation of warm rain can be delayed to above the freezing level in highly polluted atmospheres. For example, aircraft measurements have documented clouds with base temperatures of 25°C over the Indogangetic plain, which did not produce warm rain and whose r_e

remained below 14 μm up to the −5°C isotherm level [*Konwar et al.,* 2012; *Khain et al.,* 2013]. Precipitation was initiated in these clouds as supercooled raindrops that froze at −12 to −17°C.

The updraft speed does not change the depth of the condensation-dominated growth zone for a given N_a, although it can increase N_a for a given N_{ccn}. However, satellite observations showed that stronger updrafts aloft can delay the development of mixed phase and glaciation to greater heights and colder temperatures [*Rosenfeld et al.,* 2008b]. Ultimately, in severe convective storms with very strong updrafts aloft (larger than 40 m s^{-1}), glaciation is delayed to the homogeneous ice nucleation temperature of nearly −38°C, as documented by in situ aircraft measurements [*Rosenfeld et al.,* 2006b]. In clouds with high and cool bases and with large N_{ccn} and therefore high N_a, in situ aircraft measurements have documented that cloud drops that were mostly formed at cloud base reached the homogeneous ice nucleation temperature with updrafts that did not exceed 15 m s^{-1} [*Rosenfeld and Woodley*, 2000]. These cloud drops did not freeze earlier because they remained too small to produce supercooled drizzle and rain drops, which freeze much faster than small cloud drops. Apparently, ice nuclei concentrations could not have been very high in this situation, which would have otherwise allowed the cloud drops to freeze heterogeneously before reaching the homogeneous ice nucleation temperature. The cloud drops therefore froze into similarly small ice particles, which at these heights had no mechanism to coalesce and precipitate, but rather detrained from the anvil and evaporated.

In agreement with the observed impacts of high CCN concentrations on delaying the precipitation and glaciation to greater heights in convective clouds, *Sherwood* [2002a] and *Jiang et al.* [2009] found, based on satellite data, that biomass burning aerosols were associated with smaller ice particle r_e in the anvils of tropical deep convective clouds. The smaller ice particles precipitate more slowly and evaporate at higher levels, potentially delivering more water vapor to levels where they can reach the upper troposphere and lower stratosphere [*Sherwood*, 2002b; *Chen and Yin*, 2011; *Wang et al.*, 2011; *Nielsen et al.*, 2011; *Fan et al.*, 2012b], thus producing positive radiative forcing due to the increased extent of colder anvils and greater detrainment of water vapor.

2.1.4. Simulations of Cloud-Aerosol Interactions

Cloud models are the computational tools that we use for integrating our quantitative knowledge about the various processes and calculating the resultant clouds and precipitation under various scenarios of meteorological, thermodynamic, and aerosol conditions. Cloud models simulate clouds by solving the dynamic equations of motion of the air that forms the clouds, the thermodynamic processes that energize the cloud, and the microphysical processes of aerosol nucleation into cloud drops, their coalescence into raindrops, the nucleation of ice in the cloud, and the development of cloud ice and precipitation.

The most detailed and accurate type of model is the spectral bin microphysics model [e.g., *Khain et al.,* 2000, 2004]. This class of models calculates explicitly the particle size distributions of the CCN, cloud and rain drops, various hydrometeor types, and ice crystals. The size spectra are represented by the number of particles in 30 to 40 size bins, hence the name spectral bin model. This model calculates explicitly the interactions between all the particle types of all sizes, such as collisions and their outcomes. The interactions with the environment describe nucleation of CCN and IN into cloud drops and ice crystals, drop condensational growth and evaporation, etc. Due to the required amount of calculations, such models can only be used for simulating individual clouds or cloud clusters. When it comes to simulations at a regional scale, simplifications must be made to allow the model to run in practical execution times. This is done mostly by approximating the spectra of the various species by using some assumed shapes and constitutes the bulk microphysics models.

There is a very large number of bulk microphysics schemes of various degrees of accuracy, which is usually inversely proportional to their run time. For global simulations of general circulation models, even the bulk models are too slow, and the global models do not resolve the clouds at all but rather use cloud parameterizations. Incorporating the cloud aerosol processes accurately in such cloud parameterization schemes is rather challenging.

2.2. Adjustment Processes to the CCN-Induced Changes in Cloud Microstructures,
2.2.1. Marine *Stratocumulus*

The impact of aerosols on cloud albedo via increasing the cloud drop number density consists of a decrease in the mean particle size (for a fixed cloud water path), resulting in an increase in the overall cloud drop surface area and hence an increase in the cloud optical thickness [*Twomey*, 1977]. This effect (called the Twomey effect) has been considered until recently as being the main aerosol-cloud-mediated radiative effect [*IPCC*, 2007]. However, cases have been observed and simulated, for which the cloud liquid and/or ice water

path do not remain constant. The Twomey effect can be counteracted to a large extent by loss of cloud water due to enhanced mixing and evaporation that is caused by the smaller size of the cloud drops, especially in nonprecipitating clouds. This was both simulated in idealized case studies [*Ackerman et al.,* 2004; *Bretherton et al.,* 2007] and observed to the extent that 30% of the ship tracks in closed marine stratocumulus clouds had a smaller albedo than the background, instead of the expected larger albedo due to the Twomey effect [*Chen et al.,* 2012]. Also, from satellite data, it has been shown that often smaller droplet radii due to larger amounts of aerosols are associated with smaller liquid water path, which reduces the cloud albedo [e.g., *Lebsock et al.,* 2008], so that the impact of cloud-mediated aerosol radiative forcing at the cloud system scale may be smaller than what individual cloud scale process studies may suggest. The reduced liquid water path in such cases is due to faster evaporation of cloud drops, which induces faster mixing with the ambient dry air and hence loss of cloud water. The difference in the response at the scales of individual clouds and the cloud system is a result of a dynamic response to the aerosol impacts on precipitation-forming processes or on the rate of cloud drop evaporation. For example, the observed change in cloud drop effective radius due to changes in CCN can alter the precipitation and resultant downdrafts, which is in fact a dynamic response that often changes the cloud organization.

In the previous sections, we showed that significant rain forms when cloud drop r_e exceeds about 14 μm. The cloud depth that is required for reaching this threshold (D^*) is linearly related to N_a, such that D^* increases by nearly 300 m for each additional 100 cm^{-3} of nucleated CCN at cloud base, in both marine stratocumulus [*Gerber*, 1996] and deep convective clouds [*Freud and Rosenfeld*, 2012]. This means that D^* is reached at the top of a 600 m deep marine stratocumulus if N_a is about 100 cm^{-3} (based on Figure 2 in *Rosenfeld et al.* [2013]). Because N_a <100 cm^{-3} is typical for the aerosol limited regime, N_a under such conditions represents N_{ccn} fairly well. Simulations show that almost all CCN are nucleated in an aerosol-limited regime and even more so for smaller CCN concentrations [*Reutter et al.,* 2009]. The strong dependence of the precipitation on cloud top r_e and cloud optical depth was shown by comparing CLOUDSAT radar-measured rain reflectivities in clouds with MODIS (Moderate Resolution Imaging Spectrometer onboard the Terra and Aqua satellites) measured cloud top r_e, as illustrated in Figure 3 (from *Suzuki et al.* [2010]). Figures 3a and 3f show that clouds do not precipitate regardless of their optical depth, when r_e at their top is less than 10 μm. Figures 3c–3f and 3h–3j show that clouds precipitate almost regardless of their optical depth when r_e > 15 μm. The transition thus occurs between r_e of 10 and 15 μm. Within this transition, it is evident that rain tends to start for optically deep clouds at smaller r_e, probably due to the sea-spray-generated giant CCN that initiate some raindrops even in clouds with suppressed coalescence.

When marine stratocumulus clouds start to drizzle heavily, they often cannot maintain full cloud cover any longer and break into a regime of open cells. This was shown by both observations [e.g., *Stevens et al.,* 2005] and simulations [e.g., *Ackerman et al.,* 1993; *Wang and Feingold*, 2009a]. Heavy drizzling and breakup of the clouds occur when cloud top r_e exceeds $r_{e,crit}$, as evident from satellite observations [*Rosenfeld et al.,* 2006a] and simulations [*Rosenfeld et al.,* 2012a]. Satellite observations have shown that at least in some circumstances, the addition of aerosols to open cells can close them again into large decks of full cloud cover [*Goren and Rosenfeld*, 2012]. Such aerosol-induced transitions between open and closed cells can cause a negative cloud radiative effect in excess of −100 W m^{-2}, on a 24 h average. A cloud radiative effect is the difference in the net radiation at the top of the atmosphere between the situation with the cloud and a hypothetical cloud-free state under otherwise the same conditions. This means that when the added aerosols are anthropogenic, as was the case observed by *Goren and Rosenfeld* [2012], this can be regarded as a local radiative forcing. *Goren and Rosenfeld* [2012] showed that the Meteosat Second Generation (MSG) satellite allows tracking the microphysical evolution of clouds over several days and can help to attribute the observed changes to their possible causes by back tracking the aerosol and synoptic history of the air mass. The present U.S. geostationary satellites lack the spectral resolution that would allow a similar day and night tracking of the marine stratocumulus, but the upcoming GOES-R will provide these capabilities. The METEOSAT third generation will have even better spectral and spatial resolutions that will make it possible to quantify the time-dependent processes more accurately and on a near-global basis.

2.2.2. Deep Convective Clouds

2.2.2.1. Aerosols Impact Deep Convection by Affecting Their Precipitation Processes

As in the case of shallow layer clouds, the main impacts of aerosols on deep clouds are mediated by the cloud dynamic response to the changes in cloud microstructure and resulting changes in precipitation-forming processes within the cloud. These changes occur due to changes in the vertical condensate loading and
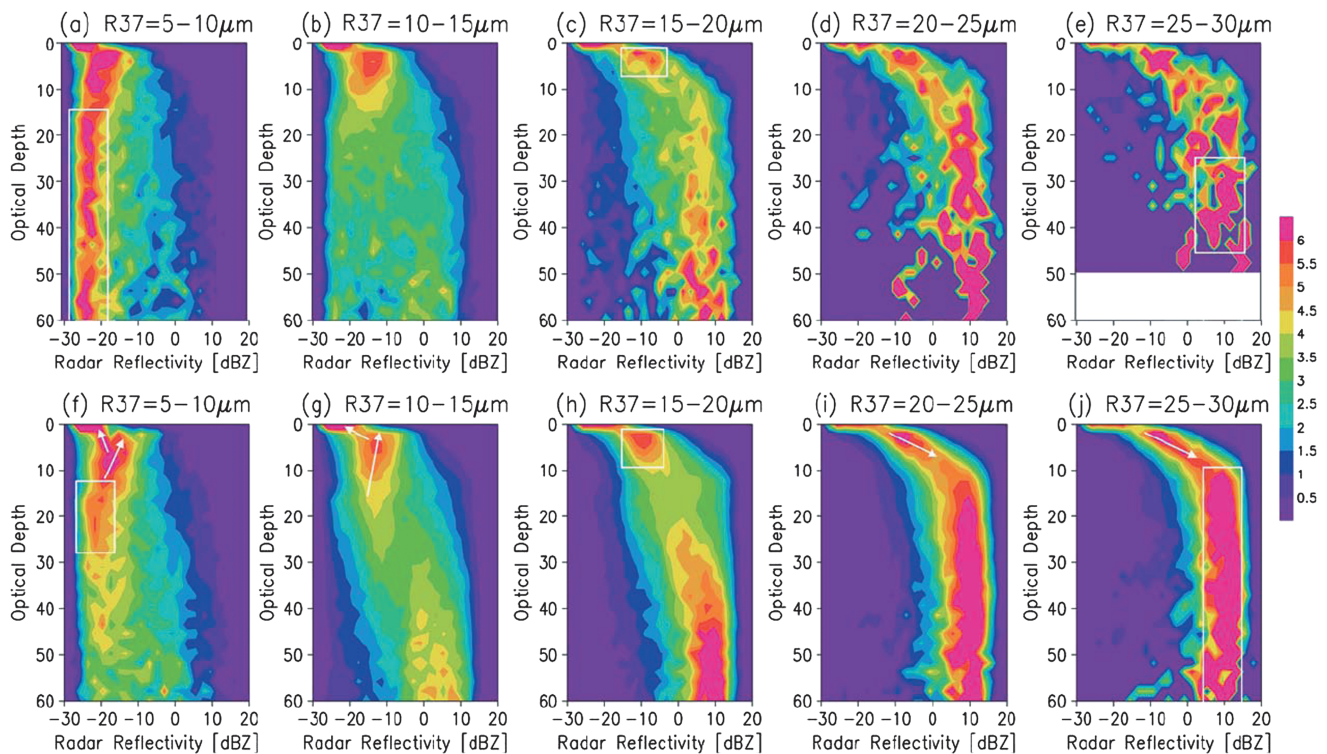
Figure 3. Relative frequencies of occurrences of CLOUDSAT radar-measured rain reflectivities in clouds with MODIS measured cloud top drop effective radius as denoted above the panels. The top and bottom rows are for clouds over land and ocean, respectively, during June-July-August. The unit of color shading is relative frequency in % dBZ. The white box on the left panels shows that cloud drops with $r_e < 10$ μm have very small reflectivities, which means no rain. The white box on the right panels shows that large cloud drops with $r_e > 25$ μm have high reflectivities, which means rain. The changeover from no rain to rain occurs through drizzle, shown in the white box in the middle panels, where r_e crosses 15 μm. Adapted from *Suzuki et al.* [2010].

latent heating profiles, which both affect the buoyancy, the cloud environment, and hence the cloud dynamics and their subsequent development. In the following we present several examples of possible effects at the scale of individual clouds. A comprehensive review of the physical basis and simulations of aerosol cloud interactions of mostly deep convective clouds was published by *Tao et al.* [2012]. Here we highlight the processes that can in principle be observed and quantified from satellites and add some perspectives that are important for understanding the ways in which they can be measured from space.

2.2.2.2. The Aerosol Convective Invigoration Hypothesis

When aerosols are very scarce, cloud drop surface area becomes too small for effective adjustment of the vapor saturation in clouds. Large supersaturations of several percent can develop above the base of extremely pristine convective clouds, with few tens of CCN cm^{-3} or less. When CCN concentrations increase beyond these low concentrations, the supersaturation diminishes to below 1% and the previously supersaturated vapor condenses and releases added latent heat of condensation, which invigorates the shallow convective clouds compared to the ultrapristine background [*Koren et al.*, 2014]. The drops in such pristine clouds coalesce very quickly and precipitate as rain through the updraft. When pristine clouds become very deep, the updrafts have to exceed the raindrop terminal fall velocity for a substantial amount of water to rise above the 0°C isotherm, freeze and electrify the clouds, and create thunderstorms [*Atlas and Williams*, 2003].

A different kind of deep convective invigoration occurs when aerosol-induced decrease in cloud drop effective radius slows the coalescence process, delays the formation of warm rain to greater heights, and consequently postpones the development of the downdraft. This allows the continued growth and intensification of the updraft and invigorates the convection. This scenario is supported by satellite observations of taller trade wind cumuli with smaller r_e in a Hawaiian volcanic plume [*Yuan et al.*, 2011a]. The suppression of rainout from the rising cloud parcel means that more cloud water reaches the freezing level and freezes onto ice hydrometeors. The additional latent heat of freezing released by this process increases the buoyancy of the cloud. Updraft invigoration can occur when the additional thermal buoyancy overcomes the added condensate loading

[*Rosenfeld et al.,* 2008a]. When the cloud drop coalescence zone and significant warm rain processes are not reached by the freezing level, a large amount of supercooled water is available to grow on relatively few precipitation particles, and then they can grow into large hail, especially when strong updrafts exist. The formation of large ice hydrometeors allows a faster unloading of the precipitation from the updraft, slower evaporation and less evaporative cooling, which further invigorate the storm. Observational support for this was obtained from reports of severe convective storms [*Rosenfeld and Bell*, 2011] and from satellite observations that statistically relate satellite-observed cloud tops becoming higher and more expansive with increasing aerosol loading, which usually is quantified by the aerosol optical depth [*Koren et al.,* 2005, 2008a, 2010a, 2012]. The enhancement of updrafts, with more supercooled water and ice hydrometeors, is expected to produce greater cloud electrification [*Williams et al.,* 2002]. Indeed, clouds ingesting MODIS-observed volcanic smoke over large areas of the western Pacific were observed to produce much more lightning than unperturbed clouds [*Yuan et al.,* 2011b]. Similar relations between smoke aerosols and TRMM-LIS (Lightning Imaging Sensor onboard the Tropical Rainfall Measuring Mission satellite) observed lightning were observed also over the Eastern Pacific near Mexico [*Kucienska et al.,* 2012].

This process of invigoration and enhanced hail has been simulated by spectral bin models, whereas bulk models produce the opposite effects [*Khain et al.,* 2011; *Morrison*, 2012; *Fan et al.,* 2012a]. The bulk microphysical parameterization is considered less reliable.

Aerosol-induced changes in primary convective clouds are communicated to the environment and affect the overall cloud organization in various ways. The changes in precipitation intensity and particle size affect the rate of its evaporative cooling and in turn the temperature of the downdrafts and the resultant cold pools of air near the surface. The increased hydrometeor size and decreased concentration reduce evaporative cooling and therefore decrease the cold pools and in turn the intensity of the gust fronts [*van den Heever et al.,* 2011]. The increase in hydrometeor size with decrease in cloud drop size has been already observed by a combination of satellites and disdrometers (rain gauges that measure rain drop size distributions) [*Rosenfeld and Ulbrich*, 2003] and can now readily be observed by combining the satellite retrieved r_e with polarimetric radar measurements of rain drop sizes. Satellite observations have shown that this effect occurs at a global scale [*Koren et al.,* 2012].

2.2.2.3. Adjustment Mechanisms and Their Potential Buffering Effect, as Obtained From Simulations

To account properly for the aerosol effects on deep convective clouds, it is necessary to include the various adjustment mechanisms of the environment and the circulation systems. While simulations of aerosol impacts on the scale of individual clouds showed clearly the invigoration effects, as discussed in section 2.2.2.2, simulations at larger scales with bulk cloud-resolving models indicated buffering of the invigoration when feedback with the large-scale environment was considered [*Morrison and Grabowski*, 2013]. When the aerosol perturbation is introduced into the whole model domain, simulations of aerosol convective adjustments are eventually constrained by the external energy budget, such as the amounts of solar radiative heating and the emitted thermal radiation to space. This results in convergence of the results of any aerosol perturbation, with little overall effect on the radiative forcing and precipitation amount [*Grabowski and Morrison*, 2011]. However, aerosol perturbations occur mostly on subregional scales, i.e., at the scale of several hundreds of kilometers, which is the scale of large cloud systems. Simulating localized effects at the scale of the cloud system (with a cloud resolving model at a spatial resolution of 2 km), while allowing the interactions with the larger regional scale, did show invigoration of the aerosol perturbed cloud systems, while inducing regional circulation systems [*Fan et al.,* 2012b; *Morrison and Grabowski*, 2013]. Accounting for these effects requires that simulations be done on domains extensive enough to include the full life cycle of large convective cloud systems, such as ~500 × 500 km, but leaving the surrounding areas unperturbed.

2.2.2.4. Aerosol Effects on Invigorating Severe Convective Storms

In situations with high wind shear and instability, weakening of the cold pools by less evaporative cooling of precipitation can prevent the undercutting of the updraft by the weakened gust front and allow the transition from multicell to supercell convection. This, in turn, can trigger more tornadoes, as shown by simulation studies [*Snook and Xue*, 2008; *Lerach et al.,* 2008]. The updraft intensity above the height for onset of precipitation can be inferred indirectly from satellite observations due to the fact that cloud drops in stronger updrafts have shorter time to grow and glaciate, thereby having a smaller r_e for a given cloud top temperature T, and also a colder glaciation temperature (T_g). Any large hydrometeors that might be sustained by the strong updrafts fall from the cloud top deeper into the cloud, and respectively do not appear in the

satellite view. The r_e at T_g is also smaller for stronger updrafts. *Rosenfeld et al.* [2008b] have shown that this can be used as a predictor of severe convective storms and called it "severe storm microphysical signature." This signature is comprised of reduced r_e above the height of precipitation initiation, colder glaciation temperature, and smaller r_e of the anvil ice particles, as compared to the nearby nonsevere convective storms.

Climatological evidence for the aerosol impact on severe convective storms is seen in the weekly cycle of lightning [*Bell et al.,* 2009], hail, and tornadic storms in the southeastern USA [*Rosenfeld and Bell,* 2011]. In warm-base clouds and low wind-shear environments, adding aerosols can lead to invigoration of the updrafts, increased cloud top heights, and enhanced peak precipitation intensities and downdrafts [*Rosenfeld et al.,* 2008a; *Fan et al.,* 2009] by the mechanism discussed above. For clouds with warm bases and moderate wind shear, this can lead to a transition from unorganized convection to squall lines [*Khain et al.,* 2005].

2.2.2.5. Aerosol Effects on Deep Convection at a Regional Scale

Simulations of aerosol effects on deep convective storms at a regional scale were performed for different cloud base temperature and vertical wind shear situations, using a spectral-bin-microphysics cloud-resolving model [*Fan et al.,* 2012b]. The results showed that the invigoration of deep tropical clouds was not limited to the clouds themselves. The environmental adjustment to invigoration included enhanced regional low-level convergence and upper level divergence. The compensating effects occurred outside of the domain with the aerosol perturbation. This served as a positive feedback that probably enhanced the primary effects on the original clouds. This result disagrees with the simulations of *Grabowski and Morrison* [2011] and demonstrates that modeling the regional nature of the perturbation is essential. Subsequent simulations of perturbation at a limited regional scale within the domain showed long-lasting invigoration for the duration of the simulation (several days) that can induce a regional circulation [*Morrison and Grabowski,* 2013]. The simulation results of a regional aerosol perturbation are supported by the observation of a weekly invigoration cycle in precipitation over the southeast USA during the summer months. The weekly cycle of work days causes more aerosols during week days compared to weekends, and was associated with a similar weekly cycle of midweek enhanced convection and rain intensities. This cycle is coupled to a weekly cycle modulating the low-level midweek convergence and upper level divergence components over land, a phenomenon mirrored by subsidence over the adjacent oceans [*Bell et al.,* 2008]. The weekly cycle was absent in the western USA and during winter, because the invigoration by the mechanism of suppression of rain that leads to a greater release of latent heat of freezing aloft works best with warm cloud bases. Such warm bases occur during summer in the southeastern USA, but not in Europe or the western USA.

The simulations of *Fan et al.* [2012b] with spectral bin microphysics reproduced the invigoration and the microphysical anvil expansion effects, as well as moistening of the upper troposphere. The simulations showed that the negative solar radiative forcing of $-3.0\,\mathrm{W\,m}^{-2}$ at the top of the atmosphere was overwhelmed by a positive long-wave radiative forcing of $+6.6\,\mathrm{W\,m}^{-2}$. The net forcing was $+3.6\,\mathrm{W\,m}^{-2}$ at the top of the atmosphere and $-2.0\,\mathrm{W\,m}^{-2}$ at the surface, thus warming the atmosphere by $5.6\,\mathrm{W\,m}^{-2}$. However, this overall warming effect might be the result of the anvils in this particular single event growing and lingering during nighttime, where only long-wave forcing exists. Similar month-long simulations with a cloud-resolving model of aerosol-perturbed deep convective cloud systems showed that the solar negative forcing was slightly larger than the thermal positive radiative forcing, leading to a net slightly negative aerosol forcing of nearly $-3\,\mathrm{W\,m}^{-2}$ [*Fan et al.,* 2013].

Satellite observations of these effects will need to measure, in addition to the radiation budget, the water and ice cloud particle r_e, the cloud top temperatures, and the UTLS water vapor amount and divergence.

2.2.2.6. Aerosol Effects on Intensifying Extratropical Cyclones Over Ocean

Aerosols transported from East Asia into the North Pacific were observed to invigorate the storm track intensity there. This was quantified by computing the temporal trend of transient eddy meridional heat flux (EMHF) at 850 hPa along with the trend of aerosol emissions. EMHF is defined as the average of $V'_{850}\,T'_{850}$, where V' and T' denote the eddy meridional velocity and eddy temperature departure from the mean seasonal cycles, respectively. This observation was replicated by a regional cloud resolving model, which was validated by satellite data. The simulations also showed increasing cloud top heights, indicating that the aerosols had strengthened the energy of the storm track through invigoration of convective clouds and release of extra latent heat that was associated with 7% added precipitation. This was also associated with a radiative forcing of $-1\,\mathrm{W\,m}^{-2}$ at the top of the atmosphere [*Wang et al.,* 2014a, 2014b]. Enhancing the storm

track intensity may modulate the planetary waves and the patterns of the global circulation. This subject is still to be addressed in the future.

2.2.2.7. Effects of Aerosols on Modulating the Intensity of Tropical Cyclones

Aerosols affect convective storms at all scales. The ultimate manifestation of deep convection is the tropical cyclone. It has been both observed and simulated that aerosols ingested into tropical cyclones invigorate their peripheral clouds at the expense of convergence toward the eyewall, thereby decreasing the maximum wind speed of the storm [*Rosenfeld et al.,* 2007, 2012b; *Zhang et al.,* 2007, 2009a; *Khain et al.,* 2008; *Carrió and Cotton*, 2011]. In contrast to the microphysical effect, simulations show that the radiative effects of absorbing aerosols around the tropical cyclones add energy and invigorate the storm by absorbing solar radiation [*Wang et al.,* 2014c].

Many of these aerosol effects can be inferred from satellite measurements of the microphysical profiles of the growing convective elements and the retrieved vertical microphysical zones and severe storm signatures [*Rosenfeld and Lensky*, 1998; *Rosenfeld et al.,* 2008c]. For example, a microphysical satellite analysis showed clearly how air pollution ingested to the peripheral cloud bands of a tropical cyclone suppresses the warm rain there, as indicated by elevating the height at which cloud drop effective radius exceeds 14 μm rain threshold to the −14°C isotherm, as compared to 12°C in the nonpolluted spiral bands [*Rosenfeld et al.*, 2012b, Figure 6]. Further into the storm along the spiral cloud bands, TRMM Precipitation Radar showed that precipitation reflectivities above the freezing level intensify substantially and are associated with a large number of TRMM-LIS measured lightning flashes, which are absent from the other nonpolluted spiral cloud bands [*Rosenfeld et al.*, 2012b, Figure 7]. This supports the hypothesis that aerosols invigorate the outer convective cloud bands at the expense of the intensity of the eye wall [*Rosenfeld et al.,* 2012b]. The precipitation can be more directly measured from spaceborne radars such as TRMM, CLOUDSAT, and GPM (Global Precipitation Mission).

The large contrast between the number of lightning flashes for a given amount of precipitation has been recognized as characterizing the different regimes of marine and continental deep convection [*Zipser*, 1994]. The new generation of geostationary satellites will have lightning sensors. This will be helpful for differentiating the different regimes of deep convective clouds, in the context of the other measurements, which will help quantify the aerosol effects on these cloud systems.

2.2.3. Mixed-Phase Layer Clouds

Satellite observations have shown that supercooled and mixed-phase cloud tops are the most common types over the Southern Ocean and North Pacific [*Morrison et al.,* 2011]. Supercooled layer clouds are also very common in the Arctic area. The lifetime and maintenance of these clouds depends on the balance between CCN and IN concentrations. This is an important factor because when supercooled layer clouds glaciate, their condensate content precipitates as snow and the clouds reflect much less solar radiation. Therefore, the glaciation produces a positive cloud radiative effect. This is partially compensated by the reduced thermal emissivity of the glaciated cloud. Obviously, during the polar night the sole effect is the thermal cloud radiative forcing. It was shown observationally that adding IN to supercooled layer clouds can glaciate them and convert them to semitransparent ice clouds or can clear the clouds altogether. This was shown to occur with advertent cloud seeding [*Langmuir*, 1961] and by aerosols from aircraft exhausts [*Heymsfield et al.,* 2010]. *Morrison et al.* [2012] have shown that the longevity of the supercooled layer clouds is caused by their constant rejuvenation by reverse convection that is propelled by radiative cooling at their tops, similarly to marine stratocumulus. The cloud layer dissipates when the cloud water removal rate by freezing and precipitation exceeds the cloud water condensation rate. This is again similar to the process in marine stratocumulus, where the cloud layer breaks up when the drizzle becomes sufficiently heavy to deplete the cloud water. Satellite measurements of cloud top temperature, r_e, and hydrometeor phase can provide insights to the glaciation temperature and the parameters that control the changes in cloud regime from a supercooled to a glaciated state. For example, satellite observations show that clouds glaciate at higher temperatures for the same aerosols when cloud drops at the −5°C isotherm are larger [*Rosenfeld et al.,* 2011]. Aircraft seeded tracks of AgI ice nuclei were shown by satellite to glaciate supercooled layer clouds [*Rosenfeld et al.,* 2005].

2.3. Separating the Components of Aerosol-Induced Cloud Forcing
2.3.1. The Radiative Forcing Components and Separating Them in Shallow Clouds
2.3.1.1. Separating the RF Into Twomey, LWP, and Cloud Cover Effects

Radiative forcing is defined as the change in cloud radiative effect due to added anthropogenic aerosols. A major unresolved question is the magnitude of the natural aerosol background that present-day aerosol

concentrations have to be compared with *Carslaw et al.* [2013]. The few available estimates of preindustrial aerosol background levels over land are highly uncertain [*Andreae*, 2007; *Andreae and Rosenfeld*, 2008]. This is a leading source of uncertainty in the aerosol-mediated cloud radiative forcing.

Aerosol-induced cloud radiative forcing can be broken down into three components resulting from changes in cloud drop number concentrations (N_d) (Twomey effect), liquid water path (LWP), and fractional cloud cover (f). The metrics defined so far do not distinguish these three forcing components; rather, they characterize the respective changes in physical cloud properties. The Aerosol Cloud Interactions (ACI) effect on r_e has been defined as

$$ACI_r = \partial \ln r_e / \partial \ln \alpha \qquad (1)$$

where α represents the CCN concentration, often estimated using satellite-measured aerosol optical depth (AOD) [*Feingold et al.*, 2003; *Nakajima and Schulz*, 2009; *Sorooshian et al.*, 2010]. If expressed in terms of the effective radius r_e, rather than in terms of N_d, the partial derivative, i.e., the derivative at constant LWP, has to be evaluated for given LWP. Using a measurement or retrieval of N_d overcomes this problem [*Brenguier et al.*, 2000; *Quaas et al.*, 2006]. Similarly, the impact on cloud optical thickness (τ) is defined as

$$ACI_\tau = \partial \ln \tau / \partial \ln \alpha \qquad (2)$$

and the impact on cloud fractional cover (f) is given by

$$ACI_f = \partial \ln f / \partial \ln \alpha \qquad (3)$$

The Twomey effect is in fact ACI_τ for a fixed LWP and f, i.e., the effect only due to aerosol-induced change in r_e with everything else held constant. At nonabsorbing wavelengths (visible and UV), cloud reflectance is directly related to τ. In the near infrared (NIR), water drops do absorb (with a direct dependence on drop size and optical thickness). Therefore, broadband solar reflectance is somewhat smaller for clouds having the same τ but larger r_e. The separation of the cloud radiative forcing into the N_d, LWP, and f components is important, as it can provide insights into the relative importance of the primary microphysical effects on cloud properties, as manifested by the r_e effect, versus the importance of the dynamical changes in the clouds, given by the cloud fraction and LWP effects. The partitioning between the effects of f and LWP can provide additional insights with respect to the dynamical and regime changes in cloud systems, such as transitions between open and closed cell regimes in marine stratocumulus. *Goren and Rosenfeld* [2013] developed a methodology for separating N_d, LWP, and f, and applied it to 50 MODIS observed adjacent pairs of closed and open marine stratocumulus in adjacent cloudy areas with different aerosol amounts, assuming the same meteorology. They found that the Twomey effect accounted for only about one fourth of the overall difference of $-110\,W\,m^{-2}$ of the cloud radiative effect, LWP accounted for one third, and the cloud cover effect accounted for the remaining 42%. These large values occur on the transitions between open and closed marine stratocumulus (Sc). A more climatically representative study, which analyzed the whole central Atlantic Ocean (20°S–5°N), showed average aerosol cloud mediated radiative forcing of $-9.5\,W\,m^{-2}$, out of which only $-1.5\,W\,m^{-2}$ was due to the albedo effect [*Kaufman et al.*, 2005a].

2.3.1.2. Attribution of Observed Aerosol Effects to Anthropogenic Causes

Attributing changes in cloud radiative effects to aerosols is difficult, because one has to exclude, or at least account for, other meteorological and surface factors contributing to the observed differences in cloud properties. Furthermore, the cloud radiative effects can be regarded as "anthropogenic radiative forcing" only when the changes in aerosols can be attributed to anthropogenic causes.

These challenges were addressed by a satellite study of *Goren and Rosenfeld* [2012], who tracked the emission of aerosols from ships and the subsequent growth and expansion of clouds from the original ship tracks and showed cases where the overcast cloud regime could be unambiguously attributed to anthropogenic sources. This is in general agreement with satellite observations over the global oceans [*Sekiguchi et al.*, 2003], where the Twomey effect was less than half of the overall aerosol induced cloud radiative forcing. This might explain why, at a large scale (i.e., where one can no longer assume the same meteorology for the different clouds), it is still challenging to obtain clear evidence for an anthropogenic effect on the overall cloud radiative forcing. For example, average cloud top r_e was observed to be 0.9 µm smaller in the Northern Hemisphere than in the Southern Hemisphere oceans due to the much larger abundance of anthropogenic aerosols in the Northern Hemisphere [*Rotstayn et al.*, 2007; *Cai et al.*, 2010]. But the retrieved LWP of the two

hemispheres gave grossly inconsistent results when calculated in different ways from the observations [Table 3 of *Feng and Ramanathan*, 2010]. Because the Twomey effect is defined for a given LWP, it cannot be assessed confidently without a reliable measurement of the LWP, noting that the cloud optical depth is proportional to LWP but (inversely) dependent only on the cube root of the cloud droplet number concentration.

Another challenge to our understanding is the observation that at a large scale, there is no significant difference in cloud properties between the windward and leeward sides of shipping lanes [*Peters et al.,* 2011]. This stands in contrast to the observations of *Yuan et al.* [2011a] showing large impacts of volcanic aerosols from Hawaii on the trade wind clouds downwind, as well as to the observations that aerosols originating from land appear to dominate the cloud properties over the downwind ocean, as illustrated in Figure 4 [*George et al.,* 2013]. Perhaps the amounts of aerosol emission from ships are insufficient to completely suppress the rain from most of the marine clouds, except under special conditions when ship tracks are observed to close very shallow open marine stratocumulus [*Goren and Rosenfeld*, 2012]. As long as the rain has not been fully suppressed, it may be scavenging the aerosols very efficiently, as evident by the sharp transition between closed and open cells, which is associated with a drastic decrease by a factor of about 3 in the cloud drop number concentrations [*Goren and Rosenfeld*, 2013]. However, the much larger amounts of aerosols that are drifting from the continents appear to delay the opening of the closed cells, as shown in Figure 4.

2.3.1.3. The Dominance of Aerosol Impacts on Precipitating With Respect to Nonprecipitating Clouds

There are both observational and simulation-based indications that adding CCN to nonprecipitating clouds may enhance their mixing and evaporation due to faster evaporation of the smaller drops, thus the loss of cloud water counteracting the negative radiative forcing due to the Twomey effect [e.g., *Small et al.,* 2009]. For very large aerosol amounts that include black carbon (BC), the direct radiative heating of the aerosols can actually produce a "cloud burning" effect, by either warming the air that includes the clouds and/or blocking the solar heating of the ground that propels the convection [*Koren et al.,* 2004; *Feingold et al.,* 2005]. This means that not much negative forcing is incurred when aerosols are added to nonprecipitating clouds. This leaves most of the observed effects of negative radiative forcing to those situations where aerosols are added to precipitating clouds or at least where the added aerosols keep the clouds from starting to precipitate. This means, in turn, that the dynamical response of the cloud systems to the aerosols very likely dominates the cloud radiative forcing, in agreement with the few observational indications that are available so far [*Goren and Rosenfeld*, 2012, 2013; *Koren et al.,* 2014].

The background air masses over land rarely have a dearth of aerosols to the extent that low clouds would start raining analogously to marine Sc. As described above, the main cloud radiative effect in marine Sc comes from the adjustment processes to the development or suppression of rain by the dearth or abundance of aerosols. These precipitation-driven adjustment processes would not occur in the nonprecipitating or weakly precipitating continental Sc. This might be a reason why the aerosol effect on cloud albedo has been observed over ocean [e.g., *Schwartz et al.,* 2002; *Yuan et al.,* 2011a; *Werner et al.,* 2013] but not yet over land. Over Europe, a strong weekly cycle is identified in aerosols and also in cloud droplet number concentration but is not evident in cloud albedo [*Quaas et al.,* 2009]. In contrast, a positive response of the clouds to the aerosol weekly cycle was found during summer in the southeastern USA. The reasons for this difference are discussed in section 2.2.2.4. Distinct "dimming" and "brightening" trends are found in surface solar radiation for clear skies but less clearly for cloudy skies [*Wild*, 2005; *Wild et al.,* 2009; *Wild*, 2012; *Norris and Wild*, 2007; *Ruckstuhl et al.,* 2008].

2.3.1.4. Large Sensitivity of Climate Effects and Geoengineering Potential Effectiveness

Pristine efficiently precipitating marine low clouds cannot persist in full cloud cover due to the dynamic response to the precipitation [*Rosenfeld et al.,* 2006a, 2006b; *Feingold et al.,* 2010; *Feingold and Koren*, 2013]. Therefore, adding a minimum critical amount of aerosols that suppress rain in pristine marine stratocumulus can dramatically increase the cloud cover and induce a negative cloud radiative forcing greater than $-100\,\mathrm{W\,m^{-2}}$ [*Goren and Rosenfeld*, 2012]. The cloud albedo effect [*Twomey*, 1977] is only about a quarter of the overall aerosol cloud radiative effect [*Goren and Rosenfeld*, 2013]. This process is not yet captured well in general circulation models, which might therefore be underestimating the aerosol cloud radiative forcing due to this process. Furthermore, this has implications with respect to geoengineering aimed at cooling the climate system by seeding marine stratocumulus clouds with ultrafine sea spray aerosols in order to brighten them [e.g., *Latham et al.,* 2012]. These schemes have taken into account until now only the cloud brightening effect, i.e, the Twomey albedo effect. However, they did not consider the much greater effect on cloud radiative forcing due to the
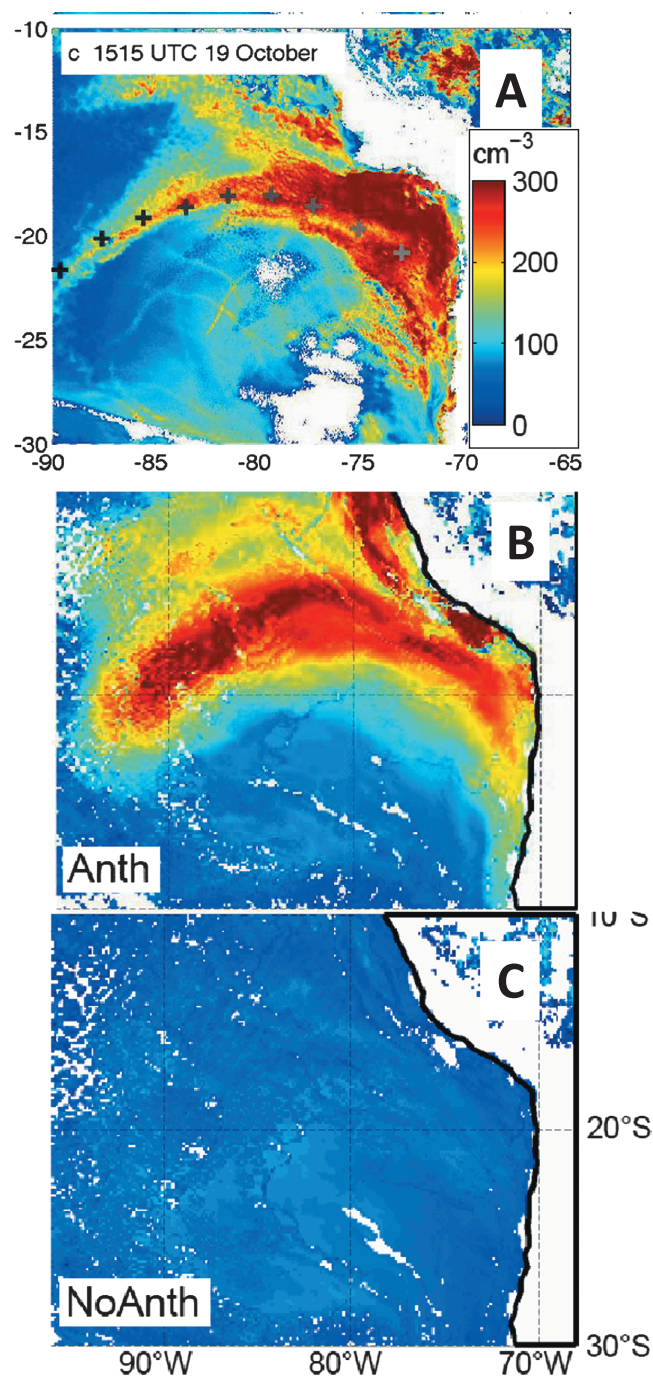
Figure 4. The impact of anthropogenic aerosols on marine stratocumulus to the west of South America. (a) Satellite observed and (b) model simulated drop number concentrations of the marine stratocumulus on 19 October 2008, 15:15 UTC. (c) Simulated clouds without anthropogenic aerosols remain pristine with very small drop number concentrations. The plus marks in Figure 4a represent the locations of trajectories from coastal pollution sources. Adapted from *George et al.* [2013].

adjustment process of the clouds to the suppressed precipitation, which can greatly increase the cloud cover. Simulations of seeding open cells of marine stratocumulus were not able to convert the cloud field into overcast [*Wang and Feingold*, 2009b; *Latham et al.,* 2012], despite observations of ship tracks being able to do so [*Goren and Rosenfeld*, 2012]. This means that the proposed techniques for seeding marine stratocumulus might have much greater effect by increasing cloud cover than has been recognized until now, where emphasis was on the Twomey effect. If so, it means that mankind might be able to tamper with Earth' energy budget to a much greater extent than has been appreciated until now. This calls for great care in the consideration of any potential application of such techniques. Continuing the research on the adjustment of cloud dynamical properties to cloud-aerosol interactions in marine low clouds on a more global basis is likely to provide much needed quantification of these potentially very large effects.

2.3.2. The Forcing Components From Deep Convective Clouds

The components of aerosol-cloud-mediated forcing from deep convective clouds can be divided into radiative and thermodynamic, i.e., changes in the vertical distribution of the latent heating. The radiative effects can be further divided into effects in the solar and thermal radiation bands. Measuring these effects directly by satellites represents even greater challenges than those for shallow clouds. The Twomey-, LWP-, and cloud cover effects operate as for the shallow clouds, but with the added complications that come from the inability to quantify the respective contributions of water and ice particles to the cloud optical depth and to the liquid water and ice path. Furthermore, additional important mechanisms for the deep clouds are

1. Cloud top cooling effect: When cloud top temperature decreases in aerosol-invigorated clouds, the outgoing thermal radiation emitted from the cloud tops is decreased, thereby incurring positive radiative forcing [*Koren et al.*, 2010a, 2010b], as illustrated with the upward arrow at the right in Figure 5.
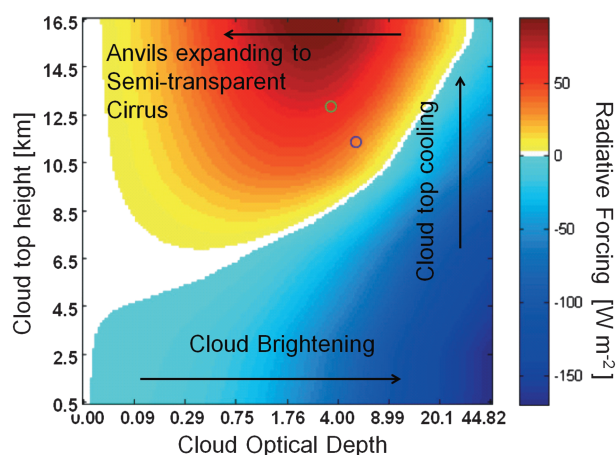
Figure 5. Cloud radiative effect over ocean in a tropical atmosphere as a function of cloud optical thickness and top temperature. The arrows show the direction of the process denoted in their labels. Adapted from *Koren et al.* [2010b].

2. Anvil expansion effect: When a large number of small ice crystals are formed in the upper troposphere, they can detrain from the cloud tops, producing larger and longer-lived anvils and subsequent cirrus clouds, as seen in both observations [*Sherwood*, 2002a; *Jiang et al.,* 2009] and simulations [*Fan et al.,* 2012b, 2013]. These semitransparent ice clouds have a positive radiative effect [*Koren et al.,* 2010a, 2010b], as illustrated at the top of Figure 5. When caused by an increase in aerosols, this effect can be regarded as a positive radiative forcing.

3. Upper troposphere and lower stratosphere (UTLS) moistening effect: The additional amount of detrained ice crystals eventually evaporates and moistens the upper troposphere. To

the extent that overshooting tops detrain, extra ice is also introduced into the lower stratosphere, which could produce moistening there as well. Added vapor in UTLS is a potent greenhouse gas and causes additional positive radiative forcing [*Sherwood*, 2002b; *Chen and Yin*, 2011; *Wang et al.,* 2011; *Nielsen et al.,* 2011]. It has also been stated that anthropogenic aerosols may have increased upper tropospheric humidity in the twentieth century [*Bister and Kulmala*, 2011].

Except for cloud top temperature, the cloud radiative effects on the thermal radiation are much less sensitive to cloud microphysical properties than the effects on solar radiation, because cloud thermal emissivity approaches saturation at visible optical depths of slightly more than one. The cloud microstructure still dominates the emissivity of very thin clouds, which are semitransparent in the infrared.

2.4. Impacts of Clouds on Aerosols

Associations of aerosol variability with changes in cloud radiative effects do not necessarily reflect the impacts of aerosols on clouds. The reverse, i.e., clouds affecting aerosols, can occur just as frequently. Here we review the pathways by which this can occur.

2.4.1. Chemical Production of Aerosols in Water Clouds

Cloud water provides an effective medium for heterogeneous chemical reactions, which can convert aerosol precursor gases into aerosol particles. When clouds evaporate, the aerosols formed in clouds will remain in the air, seen as "new particles" that can serve as CCN. The well-known heterogeneous chemical processes include oxidation of SO_2 to form sulfate [e.g., *Hoffmann and Edwards*, 1975; *Penkett et al.,* 1979] and oxidation of reactive nitrogen oxides (NO, NO_2, NO_3, N_2O_5) to form nitrate [e.g., *Chameides*, 1986; *Jacob*, 1986]. There are several reaction pathways of SO_2 oxidation that lead to sulfate formation, including SO_2 oxidation by dissolved hydrogen peroxide (H_2O_2), ozone (O_3), oxygen (O_2), and NO_2 [*Lee and Schwartz*, 1983; *Martin*, 1984; *Hoffmann and Calvert*, 1985]. Among those, SO_2 oxidation by H_2O_2 is by orders of magnitudes faster than other reactions in acidified clouds (pH < 5), and the rate is mostly independent of pH within the range of the cloud water concentrations in the atmosphere [*Seinfeld and Pandis*, 1998]. In less acidic cloud water (pH > 5.5), the rate of SO_2 oxidation by O_3 becomes faster. Overall, it is believed that the aqueous-phase oxidation of SO_2 is the major chemical process for sulfate formation, accounting for 60–80% of sulfate formation globally, with the rest produced via gas-phase reactions of SO_2 with hydroxyl radicals (OH) [e.g., *Chin et al.,* 1996, 2000; *Koch et al.,* 1999; *Barth et al.,* 2000; *Textor et al.,* 2006]. For nitrate formation, the most active reactions are thought to be the hydrolysis of N_2O_5, which is formed from $NO_2 + NO_3$ during nighttime and reacts rapidly with water to produce nitrate [e.g., *Seinfeld and Pandis*, 1998].

Organic aerosols can also be formed in cloud water. Organic aerosol formed via chemical reactions is usually referred to as "secondary organic aerosol" (SOA), to differentiate it from primary organic aerosol that is directly emitted to the atmosphere. There are many gas phase organic species, called volatile organic compounds

(VOC), in the atmosphere, which serve as SOA precursors and which have different functional groups, solubility, and chemical reactivity to form SOA. Significant progress has been made in the past decade on understanding SOA abundance and formation mechanisms, with most attention given to gas phase reactions. However, some recent studies suggest a significant role for cloud chemistry that can produce SOA as effectively as gas phase reactions, with the highest contributions from biogenic emissions of the SOA precursor gases, such as isoprene. Formation of new aerosol particles from very low volatile organic gases is also possible within a cloud [*Kulmala et al.,* 2006]. Interestingly, SOA can also be formed on hydrated aerosol particles that are coated with water [*Ervens et al.,* 2011]. Liquid-phase chemical reactions can also modify the composition of ambient SOA particles and alter their hygroscopicity [*Lee et al.,* 2011, 2012]. Detailed mechanisms and recent progress on aqueous phase SOA formation can be found in a recent review paper [*Ervens et al.,* 2011, and references therein].

2.4.2. Scavenging of Aerosols by Clouds

Although aerosols can be produced in clouds via aqueous phase chemical reactions as described in the previous subsection, they can also be efficiently removed from the atmosphere via in-cloud scavenging and precipitation, processes collectively called "wet removal" or "wet deposition." Wet removal is considered to be the major loss mechanism for removing aerosols (especially submicron size particles) from the atmosphere, thus determining their lifetime [e.g., *Liu et al.,* 2001; *Chin et al.,* 2002]. A multimodel intercomparison study including a dozen of global models indicated that globally 50% to more than 90% of submicron aerosol particles of sulfate, BC, and organic matter were removed from the atmosphere by wet deposition [*Textor et al.,* 2006].

Wet removal processes involve multiple phases that are affected not only by the properties of aerosols and precursor gases but also by the prevailing cloud type (convective, large scale, warm, ice). The term "rainout" usually refers to in-cloud scavenging of aerosols by precipitation, whereas "washout" refers to below-cloud scavenging by precipitation [e.g., *Liu et al.,* 2001; *Seinfeld and Pandis*, 1998]. Global model simulations also demonstrated that the process of aerosol scavenging in the deep convective cloud updrafts must be included in the models to realistically simulate aerosol vertical profiles [*Balkanski et al.,* 1993; *Liu et al.,* 2001]. The scavenging rates of each process are usually parameterized as a function of cloud and precipitation type, precipitation duration and rate, and aerosol removal efficiency that depends among other things on species chemical and physical properties [*Giorgi and Chameides*, 1986]. However, quantifying the wet removal rate still remains one of the largest uncertainties in estimating the amount of aerosol in the atmosphere, because of the complexity of the removal processes that are often not directly observable.

It has been shown that the differences in the treatment of wet scavenging in global models are one of the determining factors causing the large diversity in model-simulated aerosol vertical distributions. For example, a recent multiple-model comparison, made using the BC aerosol vertical profiles measured in the High-performance Instrumented Airborne Platform for Environmental Research (HIAPER) Pole-to-Pole (HIPPO) project over the Pacific Ocean, showed that the BC concentrations in the middle and upper troposphere were overestimated by all models up to an order of magnitude, with an average overestimation by a factor of 5 [*Schwarz et al.*, 2010]. Such an overestimation may be attributed mostly to the insufficient wet removal of BC in the models. By incorporating an increased wet scavenging efficiency scheme and considering nucleation scavenging in the model, the high bias was significantly reduced to agree within a factor 2 with the observations [*Wang et al.,* 2014d]. These model experiments have pointed out the importance of wet removal parameters in the models. The difficulty is that there is limited systematic observability of the parameters involved in estimating aerosol removal rates. Such parameters include cloud water/ice profiles, temperature-dependent scavenging efficiency, and reevaporation rates. Therefore, the model parameters have to be "tuned" in order to get the best agreement with the observations [*Laakso et al.,* 2003].

2.4.3. Alteration of Aerosol Chemical and Physical Properties Through Cloud Processing

In addition to the chemical reactions forming aerosols in clouds described in section 2.4.1, aerosol composition and size distribution can be transformed by a variety of mechanisms during cloud processing, as observed in laboratory studies and field measurements. First, a fraction of aerosol particles can act as CCN to form cloud droplets, while the rest remain interstitial particles in cloud. This is often described as "nucleation scavenging" of aerosols [e.g., *Hobbs*, 2003]. Cloud droplets collect more interstitial aerosol particles by collision or by dissolution of soluble particles (such as sulfate, nitrate, and sea salt) or coalesce among themselves. If the cloud is precipitating, aerosol particles collected in the precipitating droplets will be removed from the atmosphere via wet deposition, as described in section 2.4.2. However, a large fraction of clouds are nonprecipitating and instead eventually evaporate [*Lin and Rossow*, 1996];
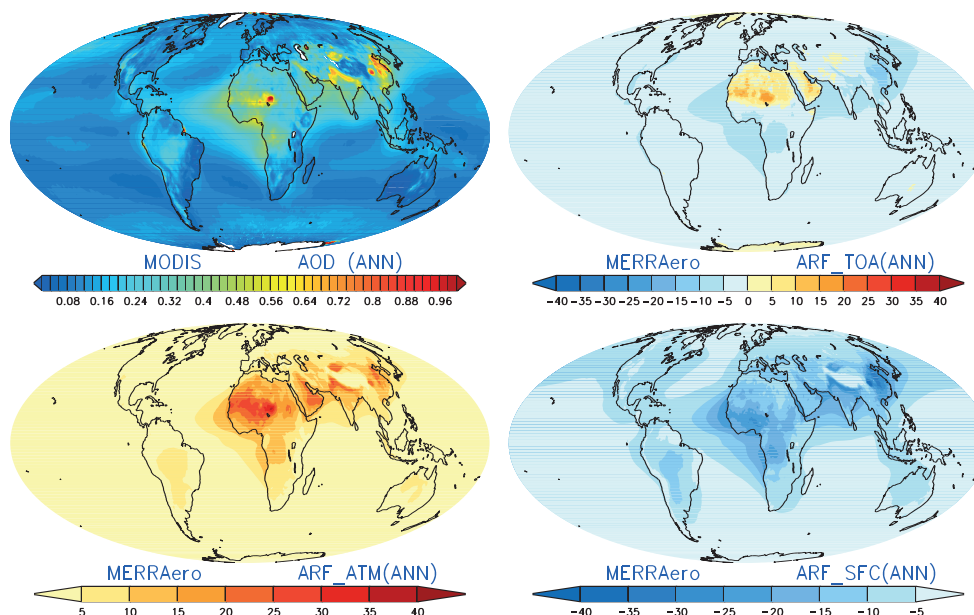
Figure 6. Annual Global distribution of (a) AOD from MODIS and aerosol radiative forcing for (b) top of the atmosphere, (c) atmospheric column, and (d) the surface, based on MERRAero reanalysis. The MODIS AOD is the mean climatology for 2003–2011 based on Terra and Aqua Collection 5.1 merged products. The units of AOD are nondimensional, while aerosol radiative forcing is in units of W m^{-2}. From *Lau and Kim* [2014].

in addition, some precipitation also evaporates before reaching the ground. In the evaporation process, aerosol particles inside the cloud or precipitation droplets that reenter the atmosphere are more internally mixed and are usually larger in size than before cloud processing [*Pruppacher and Klett*, 1997; *Hoose et al.*, 2008]. Enhanced aerosol number concentrations of ultrafine particles have been observed in the vicinity of clouds, suggesting that new particle formation occurs that is a function of precursor gas (e.g., SO_2) concentrations and ambient relative humidity ($>70\%$) [*Hegg*, 1990, 1991; *Radke and Hobbs*, 1991]. Another study suggested that the new particle formation in clouds is from nucleation of water insoluble trace gases, which survive the deep convective updraft and produce new particles at low temperatures [*Kulmala et al.*, 2006].

2.5. Regional Scales
2.5.1. Satellite Observations Provide Global Aerosol Amount and Type Constraints
Satellite detection of aerosol types and amounts is useful for constraining IN and CCN activity. The advent of the NASA and ESA Earth Observing System (EOS) satellites operating since the mid-1990s has heralded in an era of unprecedented global aerosol, cloud, and precipitation measurements, spawning new discoveries of many aspects of aerosol-cloud-precipitation interactions. A major achievement of the EOS satellite observations is the availability of almost two decades of continuous global estimates of AOD, as obtained by a number of satellites, shown in Figure 6. Seventeen years of coverage (1995–2012) is provided by ESA's Along-Track Scanning Radiometer-2 (ATSR-2) and Advanced ATSR (AATSR) instruments; this series will be extended after the launch of Sentinel 3, expected in 2015 by the Sea and Land Surface Temperature Radiometer (SLSTR). Over 14 years of observations, beginning in 2000, are available from NASA's MODerate resolution Imaging Spectroradiometer (MODIS) and Multiangle Imaging SpectroRadiometer (MISR). These AOD maps reveal the global nature of aerosol distribution, with regions of high AOD, hereinafter referred to as "hot spots," covering large areas downwind of major desert, wildfire, volcanic, and pollution sources. Specifically, these hot spots include not only major anthropogenic sources over East Asia, the Indo-Gangetic Plain of northern India, biomass burning over the Amazon, South Africa, and Southeast Asia but also natural sources such as desert dusts from the Middle East and northern Africa (Figure 6a). More than 8 years (since 2006) of space-based Cloud-Aerosol Lidar with Orthogonal Polarization (CALIOP) (on the CALIPSO spacecraft) backscatter and depolarization profiles have provided important constraints on vertical aerosol distribution. Another major milestone of the EOS satellite era is that similar to other physical and dynamical quantities,

aerosol optical depth is now being assimilated into global forecast and climate models, providing global aerosol reanalysis products that are more consistent with the physics and dynamics of the earth climate system [e.g., *Zhang et al.,* 2008]. This has led to better understanding and modest improvement in representation of aerosol-cloud interactions in climate models. With some limitations due to uncertainties in available aerosol and surface property constraints, such as particle single-scattering albedo and hygroscopicity, surface albedo, and the occurrence of aerosol below clouds, the aerosol reanalysis [e.g., *Benedetti et al.,* 2009; *Morcrette et al.,* 2009] enables the global-scale estimation of aerosol radiative effects (Figures 6b–6d). Globally, at the top of the atmosphere (TOA), with the exception of bright desert surfaces over the Sahara and the Middle East and ice sheets of Greenland and Antarctica where multiple scattering and absorption of solar radiation may occur, the aerosol radiative forcing produces a slight net cooling of the atmosphere-Earth surface system of some 3–10 W m^{-2} (Figure 6b). The redistribution of radiative energy between the atmosphere and Earth's surface by aerosols can be of greater magnitude and can regionally dominate climate forcing and feedbacks [e.g., *Ramanathan et al.,* 2001]. This redistribution is manifested in the form of substantial heating (10–40 Wm^{-2}) of the atmospheric column (Figure 6c) and a nearly equal amount of cooling of the Earth's surface (Figure 6d) over the low-latitude aerosol hotspots and nearby areas. This redistribution is likely to alter atmospheric stability and convective potential, as well as to induce atmospheric dynamical feedbacks producing regional changes in clouds and precipitation, in comparison to an otherwise pristine or less polluted world.

A sizable absorption in the atmosphere, and subsequently a difference between surface and top-of-atmosphere ARE, mainly results from the absorption of sunlight by aerosols (direct effect). For aerosol-cloud interactions, to a good approximation, the forcing at the solar wavelengths is the same at the surface and at the top of the atmosphere.

2.5.2. Aerosol-Water Cycle Interaction

Up to now, most of the fundamental work on aerosol-cloud-precipitation interactions has been derived from local concepts of direct, semidirect, and indirect (microphysics) effects for individual rain cloud clusters as described in other sections of this review. The studies of aerosol impacts on the water cycle involving large-scale dynamical feedback effects are just beginning. Multiple factors other than aerosols, e.g., local and remote sea surface temperature changes associated with El Niño–Southern Oscillation (ENSO), land use change, and warming by greenhouse gases, are well known to have strong control on regional water cycle variability. Up to now, most studies on aerosol-water cycle interactions are based on coupled model perturbation experiments, with various assumptions on aerosol properties, distributions, and forcing, superimposed on top of the aforementioned strong controls and feedback processes. However, model results are highly dependent on the representation of aerosol processes, which in state-of-the-art climate models are in the early stages of development and have large uncertainties. In addition, the lack of reliable long-term data for aerosol 3-D distribution, types, and optical properties has made the task of validating model assumptions and results very challenging. As a result, there are diverse results and views (see sections 2.5.3–2.6) regarding how the aerosol-water cycle feedback may operate on regional and global scales.

To synthesize current results from models and observations, some basic principles of aerosol-water cycle interactions need to be stressed. On regional and global scales, the impacts of aerosols on precipitation involve atmospheric systems with spatial scales of hundreds to thousands of kilometers, and time scales up to seasonal to interannual and beyond, much longer than those for the life cycles of clouds and synoptic weather systems. Over these scales, the atmospheric large-scale circulation plays an important role in the formation of rain and the emission and transport of aerosols. Consequently, responses of regional water cycles to aerosol forcing are often nonlocal in nature involving atmosphere feedback processes that could give rise to maximum response in rainfall, winds, and temperature far away from the aerosol source region. Furthermore, the feedback processes may also change surface energy and moisture fluxes, affecting soil wetness and sea surface temperature, which have longer memory compared to the atmosphere. Hence responses to aerosol forcing may also be time-lagged with respect to the maximum aerosol forcing [*Lau et al.,* 2008; *Lau and Kim,* 2011].

2.5.3. Rainfall and Diabatic Heating Feedback Induced by Aerosols

This section focuses on aerosol-induced feedback processes over the Asian monsoon regions, where major aerosol hot spots are located (Figure 6a). In these regions, there is an abundant supply of atmospheric moisture, and the atmosphere is conditionally unstable. The interaction between aerosols and the regional water cycle can be extremely complex, involving the interplay among aerosol local forcing from direct (radiative) and

indirect (microphysics) effects, as well as feedback processes involving changes in monsoon wind, transport of aerosol and moisture, vertical stability, and latent heating from redistribution of rainfall and convection.

2.5.3.1. Direct Effects

The large negative surface aerosol radiative forcing (Figure 6d) and small thermal capacity over Asian monsoon land regions compared to the Indian Ocean cool the land faster than the ocean. This could result in reduced surface evaporation, reduced rainfall, and diminished latent heating over land, leading to a slowing down of the local Hadley circulation and subsequently a weakening of the monsoon circulation [*Liepert et al.,* 2004; *Ramanathan et al.,* 2005; *Wild and Liepert,* 2010; *Bollasina et al.,* 2012; *Cherian et al.,* 2013]. For the South Asian monsoon, BC has been proposed as the key species of aerosol that could induce regional climate change [*Ramanathan and Carmichael,* 2008], but there are uncertainties regarding both BC's source strength and the way the associated climate impacts are represented in models [e.g., *Bond et al.,* 2011, 2013; *Andreae and Ramanathan,* 2013]. Studies have also shown that desert dusts may have strong impacts on monsoon rainfall variability and change [*Lau et al.,* 2006a, 2006b; *Lau and Kim,* 2006a, 2006b; *Vinoj et al.,* 2014] Atmospheric heating by absorbing aerosols (BC and dust) can induce a water cycle feedback through the so-called Elevated Heat Pump (EHP) effect [*Lau et al.,* 2006a, 2006b]. The EHP postulates that during the premonsoon and early monsoon season, from April to June, the absorption of solar radiation by thick layers of dust and BC accumulated over the Indo-Gangetic Plain (IGP) and central India warms the upper part of the aerosol layer, enhances rising motion and increases the advection of moisture to northern India and the Himalaya foothills. The increased moisture enhances convective instability and increases rainfall over the Himalaya foothills and Bay of Bengal region downwind of the southwesterly monsoon flow. The latent heat from increased rainfall further warms the atmosphere above the aerosol layer and draws in more low-level monsoon moisture initiating a positive feedback that results in a northward shift of rainfall from central India to the Himalaya foothills. Since southern India and the Indian Ocean are relatively clean compared to the IGP and northern India, the EHP-induced tropospheric heating effectively speeds up and amplifies the seasonal progression of the monsoon by increasing the upper tropospheric meridional temperature gradient between northern India and regions to the south [*Yanai et al.,* 1992], leading to an advance of the rainy season in northern India and the Himalaya foothills. The increase in clouds and rainfall in the early season reduces surface solar radiation and increases soil moisture, causing anomalous cooling of the land regions over northern and central India. These may sow the seeds for reduced rainfall in July–August or early termination of the Indian monsoon [*Meehl et al.,* 2008]. Analyses of satellite observations of AOD distributions from Total Ozone Mapping Spectrometer (TOMS) and MODIS, midtropospheric temperature from Microwave Sounding Unit (MSU), and satellite-derived Global Precipitation Climatology Project (GPCP) rainfall data together with station rainfall, and reanalyses of wind data have provided preliminary results supporting aspects of the EHP hypothesis [*Lau and Kim,* 2006a, 2006b; *Gautam et al.,* 2009a, 2009b, 2010].

The efficiency of the dynamic feedback induced by absorbing aerosols depends on the vertical profile of the aerosols and the location of the maximum induced heating. Here, CALIOP backscatter and depolarization profiles have provided a key piece of information in support of the EHP; i.e., desert dust transported into northern India during May–June is carried by the large-scale vertical motion and convection to great heights (~5 km) over the IGP against the Himalaya foothills [*Gautam et al.,* 2010]. Furthermore, dust particles become more absorbing, by being swept over industrial cities and coated with fine BC particles. This means that more absorbing aerosol accumulates over the IGP from surface to higher elevations, thus increasing the feedback efficiency via the EHP effect [*Lau et al.,* 2009a, 2009b].

Variations of the EHP effect have been suggested by several general circulation model (GCM) experiments, generally indicating that heating due to BC aerosol may increase monsoon rainfall in spring, but reduce rainfall during the peak summer monsoon season [*Meehl et al.,* 2008; *Collier and Zhang,* 2009; *Randles and Ramaswamy,* 2008; *Mahmood and Li,* 2012]. Some aspects of the EHP remain controversial, especially regarding the local versus nonlocal responses [*Nigam and Bollasina,* 2010; *Lau and Kim,* 2011]. For example, observations from CALIPSO satellite data have shown that radiative heating by aerosols over the Tibetan Plateau is small, leading some authors to question the validity of the EHP [*Kuhlmann and Quaas,* 2010]. It is important to recognize that the presence of aerosol and aerosol radiative heating over the Tibetan Plateau is not necessary for the EHP and related dynamic feedback mechanisms. Model results have shown that the anomalous warming over the Tibetan Plateau is due to the nonlocal effect of circulation change, i.e., adiabatic warming from compensating descent over the Tibetan Plateau in association with the aerosol-induced ascent

over the Himalaya foothills [*Lau and Kim*, 2010]. The northward shift of the summer monsoon rainfall may also be related to the increase in low-level moist static energy over northern India, due to advection of moisture from the Arabian Sea induced by BC heating over the Indo-Gangetic plain [*Wang et al.*, 2009]. Large-scale overturning circulation induced by atmospheric heating by aerosol over the Arabian Sea may also have an impact on winter monsoon rainfall over the Bay of Bengal [*Krishnamurti et al.*, 2009].

The possible impact of aerosols on the East Asian monsoon is even more complex compared to the South Asian monsoon, because of the multiple natural and anthropogenic aerosol sources and the much larger spatial scales of the East Asian monsoon system. Compounding these issues is the strong downstream influence from the South Asian monsoon and lateral forcing from Eurasia and the North Pacific. Numerous studies have claimed attributions of various aspects of rainfall and wind changes in different regions of East Asia to aerosol forcing, but validation has been a major challenge. At this time, there are diverse views, but no consensus on dominant forcing and feedback pathways attributed to aerosols that can explain the observed East Asia monsoon rainfall anomalies, such as the well-known North-dry South-wet pattern over East Asia [*Wang and Zhou*, 2005].

GCM experiments have shown various possible impacts of aerosol particles on East Asian monsoon climate dynamics. An increased aerosol loading in China may cause a significant increase in precipitation in the southern part of China in July due to the induced surface cooling in midlatitudes that leads to the strengthening of the Hadley circulation [*Gu et al.*, 2006]. The dimming effect of sulfate aerosol can reduce atmospheric baroclinicity, decelerate the East Asia jet stream, and consequently reduce rainfall over East Asia in late spring and early summer [*Kim et al.*, 2007]. In one study, the combined effects of BC and sulfate aerosols were found to be largely dominated by sulfates in producing a weakened East Asian monsoon for both summer and winter season [*Liu et al.*, 2009]. Another GCM experiment has found that through the semidirect effect, BC aerosols can cause a reduction in cloud and rainfall in Southern China and India, while increasing rainfall over northern China through increased moisture transport by the West Pacific Subtropical High [*Zhang et al.*, 2009a, 2009b]. However, this modeling result is contrary to the observed long-term North-dry and South-wet pattern in recent decades [*Wang and Zhou*, 2005].

2.5.3.2. Indirect Effects

The aerosol indirect effect on the monsoon water cycle is still in an early stage of research. Evidence of reduction in cloud effective radius as a function of increasing AOD in northern India, consistent with the albedo effect [*Twomey*, 1977], has been found from MODIS and Aerosol Robotic Network (AERONET) data [*Abish and Mohanakumar*, 2011; *Tripathi et al.*, 2007; *Panicker et al.*, 2010; *Cherian et al.*, 2013]. Analysis of the microphysical structure of deep convective clouds over the Indian Peninsular region observed during the Cloud Aerosol Interaction and Precipitation Enhancement Experiment (CAIPEEX) showed that polluted clouds had larger concentrations of smaller drops. These clouds had to grow to a greater depth before rain could be initiated [*Konwar et al.*, 2012; *Khain et al.*, 2013]. From CALIPSO and CAIPEEX data, it was found that during relatively lightly polluted conditions over the IGP, there was a frequent generation of small droplets above the height of precipitation initiation due to in-cloud nucleation [*Prabha et al.*, 2011]. However, the specific effects of aerosol microphysics effects on system-wide monsoon rainfall and winds are still unknown.

For the East Asian monsoon, coupled chemistry-aerosol climate model experiments have shown that the first indirect effect for the most part reduces surface solar radiation and surface temperature, while the aerosol cloud lifetime effect can significantly suppress rainfall during fall and winter over the East Asian mainland [*Huang et al.*, 2006, 2007]. However, the results are sensitive to the autoconversion (the process of conversion of cloud to rain water) scheme used. These studies also found that the combined direct and indirect effects can lead to increased cloudiness and cloud liquid water, which generates a substantial increase in downward long wave radiation to the surface. This could lead to an increase in nighttime surface air temperature in winter and a reduction of the diurnal temperature range over the industrial part of China. Observations from GPCP and station rainfall data and numerical simulations have shown that there is a decreased frequency of light rain over China and suppressed rain over the East China Sea in the last 50 years, attributable in part to the reduced rate of collision and coalescence of cloud drops by aerosols [*Qian et al.*, 2009; *Bennartz et al.*, 2011]. Another possible impact of aerosol indirect effects on the water cycle is the invigoration of deep convection through delayed ice nucleation and increased latent heating from ice-phase rain at higher levels [*Rosenfeld et al.*, 2008a, 2008b, 2008c]. Simulations with high-resolution cloud resolving models have indicated that aerosol-invigorated convection can enhance moisture convergence and warming of the upper troposphere locally [*Koren et al.*, 2010a, 2010b; *Fan et al.*, 2012b]. However, evidence of invigoration of deep

convection systems by aerosols in the Asian monsoon region is lacking. Impacts by indirect effects on the overall monsoon water cycle remain unclear and may be difficult to separate from aerosol radiative and dynamical feedback effects.

In summary, models have played an important role in advancing the understanding of aerosol-monsoon water cycle interactions. However, due to the lack of observational data for validation, especially on aerosol and cloud properties, the skill of current model simulations of the regional water cycle interaction with aerosol emission, transport, and aerosol-cloud microphysical processes cannot be ascertained. This skill is likely to not be very high, however, considering the poor model representations of aerosol and cloud processes. To better understand the impacts of aerosols on regional water cycles, more work is needed in the areas of improving the representation of aerosol physics in climate models, particularly the optical and physical properties of aerosols and their role in hydrometeor activation in both the liquid and ice phases. Satellite observations and derived quantities related to aerosols, such as the global aerosol radiative forcing (Figure 6) described here, have been instrumental in providing the global perspective and the basic framework for aerosol-water cycle feedback studies as discussed in the beginning of this section (see Figure 1). Without this global perspective, aerosol-cloud-rainfall studies would have remained at the local process level, and aerosol connections to large-scale dynamics would not have been explored. Most importantly, observations (both satellite and ground-based) regarding microphysical properties of aerosols and clouds on regional scales are largely missing. Field observations and future satellite missions with focus on aerosol microphysical and optical properties, types, and vertical distributions will be key to constraining model results to observations, thus reducing uncertainties in future model simulations.

2.6. Global-Scale Aerosol Impacts

The Madden-Julian Oscillations (MJO) and the El Niño–Southern Oscillation (ENSO) are two of the most dominant natural oscillations of the tropical atmosphere-ocean system on intra-seasonal and inter-annual time scales, affecting a wide range of weather and climate events in the tropics and mid-latitudes [*Lau and Waliser*, 2012]. There is now a growing body of evidence, mostly from satellite observations, of global signatures of aerosol properties, emission and transport associated with MJO and ENSO.

2.6.1. MJO and Aerosols

The MJO is an intrinsic tropical atmospheric oscillation manifested as a planetary-scale eastward propagating coherent structure of winds, temperature, water vapor, clouds, and precipitation on a time scale of 30–60 days, across the tropical belt spanning the equatorial Indian and Western Pacific Oceans, South America, and the Atlantic Ocean. The influence of the MJO is not limited to the tropics but also extends to the extratropics, through moisture surges and energy propagation via preferred regions in the seasonally varying basic flow of the atmosphere. As the MJO circumnavigates the tropics, it passes over aerosol sources and outflow regions and exerts influences on aerosol emission and distribution. Global satellite data have made it possible for correlative studies of MJO and aerosols. Using the TOMS aerosol index (AI) and MODIS/AVHRR (Advanced Very High Resolution Radiometer) AOD and the MJO index derived from AVHRR outgoing long-wave radiation, *Tian et al.* [2008] showed a strong correlation of AOD with MJO, with high (low) aerosol concentration during dry (wet) phase of the MJO. Following *Wheeler and Hendon* [2004], *Tian et al.* [2011] and *Guo et al.* [2013] divided a full cycle of MJO oscillation into eight phases and found negative correlation between MODIS dust AOD over the Atlantic and low-level zonal wind anomalies, with the former lagging the latter by about one MJO phase (about 6 days). This indicates that transport of Saharan dust occurs mostly in association with easterly low-level flow of the MJO. These results are expected, given that MJOs are generally associated with strong winds and rainfall oscillations that affect aerosol transport and wet deposition processes. However, how aerosol processes may affect the dynamics and evolution of the MJO is still an open question. Recently, a small but growing number of studies have indicated possible impacts of aerosols in affecting MJO-related intra-seasonal oscillations in monsoon regions. *Manoj et al.* [2010] found from observations obtained using CAIPEEX and TOMS ozone data that the heating by absorbing aerosols and invigorated convection could play a role in the transition of the Indian monsoon breaks to active spells. *Hazra et al.* [2013] showed from model simulations a coupled dynamical feedback pathway involving aerosol direct heating, cloud microphysics, and large-scale dynamics that could affect monsoon intra-seasonal variability and predictability. More recently, *Vinoj et al.* [2014] have found from MODIS and MISR observations, and confirmed with numerical experiments, that anomalous dust accumulation over the Arabians Sea can increase monsoon rainfall over

northern/central India on time scales of days to weeks through fast nonlocal feedback processes involving aerosol radiative heating and induced changes in monsoon winds, moisture, and convergence. *Lau* [2014] has suggested that these fast feedback processes, which are induced by absorbing aerosols (dust and BC), could play an important role in the response of the Asian monsoon water cycle to global warming.

2.6.2. ENSO and Aerosols

The positive phase of the ENSO, i.e., El Niño, is well known to be associated with increased sea surface temperature over the tropical eastern Pacific and a weakening of the Walker circulation, characterized by anomalous large-scale rising motion over the central and eastern Pacific and subsidence over the western Pacific. Based on tropospheric ozone and CO measurements from the Ozone Measuring Instrument (OMI), the Microwave Limb Sounder (MLS) on the Aura satellite, and numerical simulations using the Global Model Initiative Chemistry Transport Model (GMI CTM), studies have found that the anomalous subsidence motion over the Western Pacific intensifies and prolongs the biomass burning season over the Maritime Continent and northern Australia [*Chandra et al.,* 2009a, 2009b; *Ziemke and Chandra*, 2003; *Logan et al.,* 2008]. Analyses of MODIS and MISR data from the Aqua/Terra satellite have found reductions in aerosol size over the western Pacific/Maritime Continent during El Niño, indicating dominance of fine particles from biomass burning and urban pollution, in association with drier and more stable atmospheric conditions. During La Niña, aerosol size increases over the same region, indicating more coarse particles such as dust and sea salt, in association with stronger winds and aerosol remote transport. Enhanced forest fire activities over the northern part of South America during the 2006 El Niño have also been reported [*Le Page et al.*, 2008]. The increase in biomass burning produces more absorbing carbonaceous aerosols. Biomass burning emissions over the Maritime Continent of Southeast Asia during El Niño, which corresponds to local drought conditions, have been estimated to lead to an increase by more than 30 times of the aerosol loading compared to La Niña, suggesting a possible feedback between drought conditions and biomass burning [*van der Werf et al.,* 2008]. Enhanced forest fire activities over the northern part of South America during El Niño have also been identified from ATSR and AATSR satellite observations [*Le Page et al.*, 2008]. GCM experiments with interactive sea surface temperature (SST) have shown that increased carbonaceous aerosols from biomass burning in the maritime continent during El Niño can lead to increased atmospheric heating by shortwave absorption and SST cooling through reduction of net radiation at the surface. The combined effects lead to increased atmospheric stability and colder SST, further suppressing rainfall and enhancing the drought conditions [*Tosca et al.,* 2010]. Besides biomass burning, increased desert dust loading during El Niño detected over Barbados has been linked to droughts in West Africa [*Prospero and Lamb*, 2003]. Increased dust emission over the deserts of Australia may be associated with drought conditions induced by El Niño [*Mitchell et al.,* 2010].

2.6.3. Intertropical Convergence Zone and Aerosols

The Intertropical Convergence Zone (ITCZ) is a narrow region of active deep convection in the near-equatorial region of the Pacific and the Atlantic, where the southeast and northeast trade winds meet. It coincides with the rising branch of the Hadley circulation, which is a key component of the atmospheric general circulation. This subsection highlights recent work on attribution of aerosol effects to changes in the ITCZ and related climate anomalies in the twentieth century. These works are mostly exploratory and based on numerical simulations but represent an area of growing interest, as climate scientists are beginning to pay attention to the possibilities that aerosol may have already impacted major climate anomalies such as the Sahel droughts during the 1950–1980s. Climate model experiments have suggested that both radiative (direct) and cloud-mediated (indirect) effects of sulfate aerosols could have impacted tropical SST, which could in turn change circulation and rainfall in tropical regions. Specifically, stronger cooling of the Northern Hemisphere SST compared to the Southern Hemisphere by anthropogenic sulfate aerosols in the Atlantic may have caused the equator-ward shift of the Atlantic ITCZ and the West African monsoon rain band. This shift could have suppressed rainfall over the Sahel region, thus causing the long-term Sahel drought in 1950–1980 [*Rotstayn and Lohmann*, 2002; *Biasutti and Giannini*, 2006]. On the other hand, a modeling study [*Lau et al.,* 2009a, 2009b] has shown that atmospheric heating induced by increased dust loading during Saharan dust outbreaks over the North Atlantic could, through the EHP effect, induce enhanced convection at the northern flank of the Atlantic ITCZ, abutting the southern edge of the Saharan dust layer. The increased convection is associated with a stronger African easterly low level jet and enhanced dust transport from the Sahara [*Kim et al.,* 2010]. These results are consistent with observations from MODIS and TRMM and from the Africa Monsoon Multiscale Analysis (AMMA) field campaign [*Jenkins et al.,* 2008; *Wilcox et al.,* 2009]. Additionally, Saharan dust aerosols have been suggested as a possible mechanism in

influencing tropical cyclogeneses of African easterly waves along the Atlantic ITCZ, affecting long-term trends of Atlantic hurricanes through induced SST changes and associated changes in the large scale tropical circulation [*Evan et al.,* 2006; *Lau and Kim*, 2007a, 2007b; *Reale et al.,* 2014].

Coupled-model twentieth century simulations including cross-hemispheric transport of anthropogenic aerosols from Asia to Australia have shown increased rainfall and cloudiness over much of Australia during 1951–1996 in agreement with observed trends. The strong impact of aerosols is primarily due to the massive Asian aerosol haze, which alters the meridional SST and surface temperature and pressure gradients over the tropical Indian Ocean (warmer in the south, colder in the north), thereby keeping the ITCZ in the Southern Hemisphere and increasing the tendency of monsoonal winds to flow toward Australia [*Rotstayn et al.,* 2007]. On an even more profound level, based on the results of coupled model simulations, *Booth et al.* [2013] have suggested that aerosols from fossil fuel and biomass burning, as well as volcanic eruptions, had been a prime driver of North Atlantic climate variability, including the decadal shift in the Atlantic ITCZ in the twentieth century. This result is controversial, given that multidecadal variability in Atlantic SST has long been thought to be governed by internal ocean dynamics [*Mehta and Delworth*, 1995].

The long-term (multidecadal and longer) changes due to aerosols are likely the results of cumulative effects of responses to relatively small aerosol perturbation forcing, amplified through a chain of dynamical feedback processes in coupled ocean-atmosphere models as described in sections 2.5–2.6. These feedback processes highly depend on the model representation of aerosol physics and ocean-atmosphere dynamics. Initial biases may be amplified resulting in large uncertainties. Thus, attributions of aerosol impacts for twentieth century climate anomalies to aerosols have to be treated with extreme caution. Up to now, most numerical experiments on aerosol impacts and interaction with the water cycle were carried out independently by modeling groups, with vastly different assumptions, initial and boundary controls, time period of integration, and experimental design. These make it very difficult to compare results among models and with observations. Future work needs to focus on intercomparison of multimodel simulations based on common model assumptions and experimental designs, using consistent datasets for aerosol emissions and validating basic model assumptions and climatology based on reliable observations.

3. The Challenge and Methods of Global Measurements of CCN and IN

3.1. The Importance of CCN in Determination of Cloud Properties

Two basic properties govern aerosol particles' ACPC interactions: the extent to which they scatter and absorb light and their potential to nucleate cloud droplets or ice crystals under specific conditions of supersaturation. This section focuses on the role aerosols play as cloud condensation nuclei. To emphasize that the number of nuclei depends on the water vapor supersaturation (S), we will use the expression CCN(S) to represent that fraction of the aerosol population that can nucleate cloud droplets at a specified value of S. Since the particles' composition determines both their radiative properties and their CCN ability, aerosol composition will also be discussed. Issues related to ice crystal nucleation are addressed in the subsequent section.

As described in section 2.1, the initial microphysical properties of a water cloud are to a large extent determined by the supersaturation and the number concentration of CCN(S) at the value of S in the cloud base region. As the cloud evolves, its microphysical properties depend on the evolution of S within the cloud, the interstitial CCN(S) population present, and the CCN(S) population in air that is entrained into the cloud at its margins, as well as on interactions between droplets. Therefore, a realistic simulation of cloud behavior at the microphysical scale depends on having accurate knowledge of the spatial and temporal distribution of CCN(S) at highly resolved spatial and temporal scales (centimeters to kilometers, seconds to hours).

3.2. The Importance and Required Accuracy of CCN Measurements at Local to Global Scales

The previous sections (especially sections 2.5 and 2.6) have shown the profound impacts of CCN, due to their influence on cloud and precipitation properties, on the energy budget, hydrological cycle, and atmospheric circulations at regional and global scales. This underlines the importance of global measurements of these aerosols at all scales.

When going from the cloud scale to regional and global scales in weather and climate models, the spatial resolution requirements for CCN(S) fields can be relaxed, as long as valid parameterizations exist, since the spatial variability of aerosols is small compared to the spatial variability of humidity, which dominates cloud

heterogeneity [e.g., *Anderson et al.,* 2003; *Quaas,* 2012]. In absolute terms, the CCN spatial variability can still be rather high. Then, however, regional or global coverage becomes essential. A similar problem exists at longer time scales: To determine secular trends in ACPC forcings, we need large-scale coverage over time spans of years to decades. These requirements cannot be met by direct (in situ) measurements, because the much shorter lifetime of atmospheric aerosol particles with respect to greenhouse gases implies large spatial and temporal variability. This makes global coverage by in situ measurements impossible and hides secular trends behind short-term variability. The microphysical processes relevant for ACPC act on time scales of the order of 10^2 to 10^3 s. Snapshot observations from diverse meteorological situations are thus excellent bases for statistical analysis, and the global coverage of satellite data is in principle able to deliver the relevant quantities for all weather regimes occurring around the globe. This has been shown previously for several aspects of cloud physics [e.g., *Doutriaux-Boucher and Quaas,* 2004; *Lohmann et al.,* 2007].

An urgent need for global observations of CCN(S) by remote sensing follows from these considerations. Because the microphysical and radiative effects of aerosols act simultaneously on a given cloud population and change the thermodynamic environment of cloud formation and the microphysical processes of the cloud development [*Rosenfeld et al.,* 2008a], the CCN(S) field should be observed simultaneously with aerosol light scattering and absorption properties. Since the effects of light scattering (cooling of the ground surface) and absorption (cooling at the ground combined with heating aloft) have different impacts on atmospheric stability, they must be observed independently. Here, quantitative measures of absorption are especially important.

The required accuracy of the measurements is determined by the amount of change in CCN that would make a significant difference to the microphysical behavior of a cloud. Because the cloud response to CCN is logarithmic, the magnitude of this change depends on the CCN reference level. At low CCN concentrations and in CCN-limited regimes, the large fractional change due to small absolute differences in CCN is important, and the most cloud-significant changes are at the low end of the concentration range. There, space-borne aerosol remote-sensing techniques have a signal-to-noise problem. In contrast, at large CCN concentrations or perturbations—for instance, if we want to distinguish between clouds growing over the clean and smoky Amazon—larger uncertainties, up to a factor of 3 or even an order of magnitude, may be acceptable. The analysis by *Reutter et al.* [2009] showed that in an updraft-limited-regime, it would not make much difference if we have 10,000 or 100,000 cm^{-3} CCN. However, at low CCN concentrations and in the CCN-limited regime, small differences will be important.

3.3. What Do Current Satellite Sensor Data Offer?

There are no effective remote sensing methods for directly measuring the small-size part of the typical CCN distribution, as particles of 0.05 to 0.1 μm in diameter, which often make up a significant fraction of the CCN number concentration, are indistinguishable from atmospheric gas molecules with these methods. Consequently, indirect remote-sensing methods for deducing the CCN distribution have been developed that rely on in situ observations from aircraft or ground to provide the required detail, with very limited coverage, combined with larger-scale satellite proxy observations [e.g., *Andreae,* 2009b]. A very different approach that might eventually provide better retrievals is described in section 3.5.

The classical "direct" passive remote sensing techniques (e.g., AVHRR, ATSR-2, AATSR, or MODIS) yield aerosol spatial distribution data only for aerosol load via column integrated extinction (the sum of scattering and absorption, given as AOD, aerosol optical depth) and for general information on aerosol size (via AOD spectral dependence at solar wavelengths). Remote-sensing observations that include multiangle and/or polarization measurements in addition to the multispectral measurements (e.g., AATSR, MISR, or POLDER) can provide qualitative constraints on column-effective particle size, shape, and single-scattering albedo, but only when the midvisible (500 nm) AOD exceeds about 0.15 to 0.2 and not for particles smaller than about 0.1 μm, which typically comprise the smaller-sized part of the CCN size distribution. This is valuable but not sufficient. Because the ratio of aerosol light scattering to absorption is closely connected to the aerosol sources and atmospheric history, it is likely that data-model-fusion in the form of remote sensing combined with an aerosol chemistry-transport model could substantially improve the interpretation of remote-sensing observations [*Kahn,* 2012; *Yu et al.,* 2013]. Further, remote-sensing techniques cannot detect aerosol below optically thick cloud, another area where model-data fusion holds promise. And it goes without saying that for the observation of secular aerosol trends, including aerosol proxies for the CCN distribution, well calibrated, traceable, and accurate sensors must be kept in orbit.

3.3.1. Aerosol Optical Depth

AOD and its wavelength-dependence, usually expressed as the Ångström exponent (negative log of the AOD spectral slope), can be retrieved from many passive satellite sensors observing backscattered solar radiation such as AVHRR, AATSR, MISR, MERIS (MEdium Resolution Imaging Spectrometer), and MODIS. Algorithm descriptions and validation are provided in many references [e.g., *Nakajima and Higurashi*, 1998; *Veefkind et al.*, 1998; *Mishchenko et al.*, 1999; *North*, 2002; *Martonchik et al.*, 2009; *Kahn et al.*, 2010; *Remer et al.*, 2005; *Levy et al.*, 2010, and references therein; see also *Kokhanovsky and de Leeuw*, 2009 and *de Leeuw et al.*, 2011 for an overview]. A table summarizing the major, currently available satellite tropospheric aerosol data products is given in *Kahn* [2012]. The regional variability of AOD broadly corresponds to that of CCN [*Andreae*, 2009b]. To enhance the suitability of retrieved AOD as a CCN proxy, it has been suggested to calculate the product of the AOD and the Ångström exponent, the so-called aerosol index, AI [*Deuzé et al.*, 2001; *Nakajima et al.*, 2001]. This idea makes use of the fact that usually the majority of CCN are fine-mode aerosols, which produce larger Ångström exponents (all other factors being equal), so qualitatively, substituting AI for AOD has the correct sign, though not necessarily the correct magnitude. As was shown by *Kapustin et al.* [2006], the relationship between AI and CCN depends critically on the details of the aerosol size distribution and composition and on the ambient relative humidity. Also, currently available Ångström exponent products derived from satellite data amount to classifications in about three-to-five bins for multiangle instruments such as MISR [e.g., *Kahn et al.*, 2010], and over land, aerosol properties are assumed for single-view instruments such as MODIS [*Levy et al.*, 2010]. So AI can be used as a qualitative indicator of CCN occurrence, but quantitative constraints on CCN distribution would require in situ sampling, or some other proxy, in most cases.

3.3.2. Vertical Profiles of Aerosol Extinction

Another important property of atmospheric aerosols (and also CCN) is their vertical distribution. Altitude information can be mapped from multiangle passive instruments like MISR using tomographic techniques for clouds and for aerosols near sources, where plume features can be identified in multiple angular views, with vertical resolution between about 0.3 and 0.5 km [*Muller et al.*, 2002; *Moroney et al.*, 2002; *Seiz and Davies*, 2006; *Kahn et al.*, 2007; *Nelson et al.*, 2013]. Information on aerosol layer height can be derived from passive UV-absorption methods even for subvisible layers, e.g., with OMI instrument data, provided the aerosol extinction and absorption properties are adequately known [*Satheesh et al.*, 2009].

Far from aerosol sources, where visible plume structure is lacking but aerosol layers are more spatially extensive, detailed aerosol vertical distribution can be obtained from active sensors [*Winker et al.*, 2009, 2010, 2012], nicely complementing the multiangle techniques [*Kahn et al.*, 2008]. Since 2006, lidar observations in space are available from the CALIPSO mission. The CALIOP instrument onboard the CALIPSO satellite measures the backscattered lidar signal at two wavelengths and two polarization states. Important advantages of CALIPSO observations are that aerosol properties can be retrieved with similar sensitivity over land, ocean, and even snow, as well as during the day and at night. Also, aerosol observations above thick clouds and even below thin cloud layers are possible with lidar. The CALIOP observations are available during day and night (with lower signal to noise ratio during the day due to interference with the solar radiation). From CALIOP observations, not only information on the vertical extinction profile but also some constraints on aerosol type can be obtained from the observed degree of depolarization, and ratios of extinction and backscatter [*Cattrall et al.*, 2005; *Omar et al.*, 2009]. However, as for the passive sensors, the combined use of the observed aerosol spectral extinction and backscatter to estimate the CCN abundance depends strongly on the details of the aerosol size distribution. Also, unlike the passive imager data, the width of the satellite footprint at the surface for active sensors is very limited; for CALIPSO it is only 70 m. Thus, the probability that a specific scene is observed by CALIPSO is very low (4 orders of magnitude lower than for passive satellite instruments, ~2000 km versus ~70 m), although extended aerosol plumes are observed frequently.

3.3.3. Aerosol Absorption

Information on aerosol absorption is routinely derived in the ultraviolet (UV) spectral range using the UV aerosol index (UVAI), which is a measure of spectral contrast (usually referred to as the residue) between two selected UV wavelengths. The positive part of the residual (the so-called aerosol absorbing index, AAI) was originally developed for Total Ozone Mapping Spectrometer (TOMS) observations to correct ozone retrievals in the presence of strongly absorbing aerosols. However, it turned out that the AAI is also a very useful quantity in itself for detecting absorbing aerosols (mainly desert dust and biomass burning aerosols) [e.g., *Hsu et al.*, 1996; *Herman et al.*, 1997; *Gleason et al.*, 1998; *Chiapello et al.*, 1999; *Torres et al.*, 2002]. Recently it

was also shown that the negative part of the residual contains useful information on (mainly) scattering aerosols [*Penning de Vries et al.,* 2009; *Penning de Vries and Wagner*, 2011].

Important advantages of the UVAI are that this parameter can be retrieved above clouds and that it is only weakly dependent on surface type (because of the small surface albedo and large atmospheric gas opacity in the UV). The most important limitation of the UVAI, on the other hand, is that it is only a qualitative indicator of the presence of UV absorbing or scattering aerosols. The difficulty in retrieving aerosol absorption quantitatively arises from the fact that the UVAI also depends strongly on AOD, single scattering albedo, and aerosol layer height. Moreover, although the UVAI can be retrieved above clouds and to some extent within and below thin clouds, a strong cloud effect on the UVAI still exists, which further hinders its quantitative interpretation [e.g., *Penning de Vries and Wagner*, 2011]. The footprint of current satellite instruments from which the UVAI can be retrieved is rather coarse, ranging from $12 \times 26 \, km^2$ for OMI to $40 \times 320 \, km^2$ for GOME, which exacerbates cloud heterogeneity issues within retrieval regions. Unfortunately, to date, imaging satellite sensors usually have little or no coverage of the UV spectral range.

Currently available instruments can also measure aerosol absorption in the visible and near infrared (IR) spectral range, where the aerosol contribution to radiative forcing is maximal, under good retrieval conditions (e.g., sufficiently high AOD). At longer wavelengths, aerosol absorption can be constrained by combining multiangle, multispectral, and if available, polarization data, using approaches that rely on scattering rather than absorption of background Rayleigh UV radiation. With these techniques, surface albedo must also be taken into account. Qualitative constraints on aerosol single-scattering albedo (SSA) in the visible can be derived from MISR, in approximately two to four bins over the natural range of SSA, provided the mid-visible AOD exceeds about 0.15 or 0.2, and the algorithm climatology options include particles having about the right size and SSA [e.g., *Kahn et al.,* 2009; *Kahn and Limbacher*, 2012]. With the addition of polarization, somewhat greater sensitivity to particle absorption can be achieved [e.g., *Hasekamp*, 2010], as has been demonstrated with POLDER [*Waquet et al.,* 2014]. A next-generation satellite instrument would exploit the full potential of retrieving aerosol absorption in the visible and near IR from space, by providing UV, visible, and NIR channels, with both multiangle and polarization sensitivity.

3.3.4. Satellite Observations of Tropospheric Trace Gases as Proxies for CCN

During recent years, several nadir-looking satellite instruments sensing at high spectral resolution were launched, from which the abundances of tropospheric trace gases can be determined. Some of these observations might be useful as CCN proxies, at least in certain situations. From observations in the UV, visible and near IR spectral range [e.g., from GOME-1, SCIAMACHY, OMI, or GOME-2, see *Burrows et al.,* 1999; *Bovensmann et al.,* 1999; *Levelt and Noordhoek*, 2002; *EUMETSAT*, 2005] trace gases such as NO_2, HCHO, CO, CHOCHO, or SO_2 can be analyzed. Observations in these spectral ranges are typically sensitive to the entire tropospheric column including the near-surface layers (for cloud-free cases). From observations in the thermal IR (e.g., from MOPITT, TES, IASI, and AIRS) CO can be retrieved most easily. Observations made from high spectral resolution instruments (e.g., IASI) can also provide information about several other trace gases, which might also be studied as possible CCN proxies (e.g., NH_3, CH_3OH, and C_2H_4) [see *Coheur et al.,* 2009].

3.3.5. Relations Between Trace Gases, UVAI, and AOD as CCN Indicators

Some initial studies have been performed investigating the relationship between simultaneous satellite observations of AOD and tropospheric trace gas column densities: *Veefkind et al.* [2011] found a significant correlation between MODIS AOD and OMI trace gas columns for various regions in the world. This study, however, is not based on the correlation of individual observations but on monthly or seasonal means. In addition, in other cases such correlations could not be found, because they depend on the specific mixture and properties of emission sources and the meteorological conditions at a given location. For instance, satellite observations over Paris or Johannesburg show clearly enhanced concentrations of NO_2, but AOD is not evidently higher over the same area [*Sundström et al.,* 2013]. The use of trace gases as proxies for new particle formation, also using AOD and UV radiation from satellites, has been proposed by *Kulmala et al.* [2011].

Recently, *Wagner et al.* [2013] investigated correlations between measurements of AOD and trace gases for selected biomass burning regions based on daily observations. Over the investigated regions [Abracos Hill in the Amazon (-10.75°S, 62.35°W), Mongu in Zambia (15.25°S, 23.15°E), and Bac Giang in Vietnam (21.28°N, 106.22°E)] enhanced concentrations of CO, NO_2, HCHO, and CHOCHO were often found during the biomass burning seasons (see also Figure 7). However, large differences in the relationship between the different quantities were found for different locations indicating differences in fire types and chemical transformations.
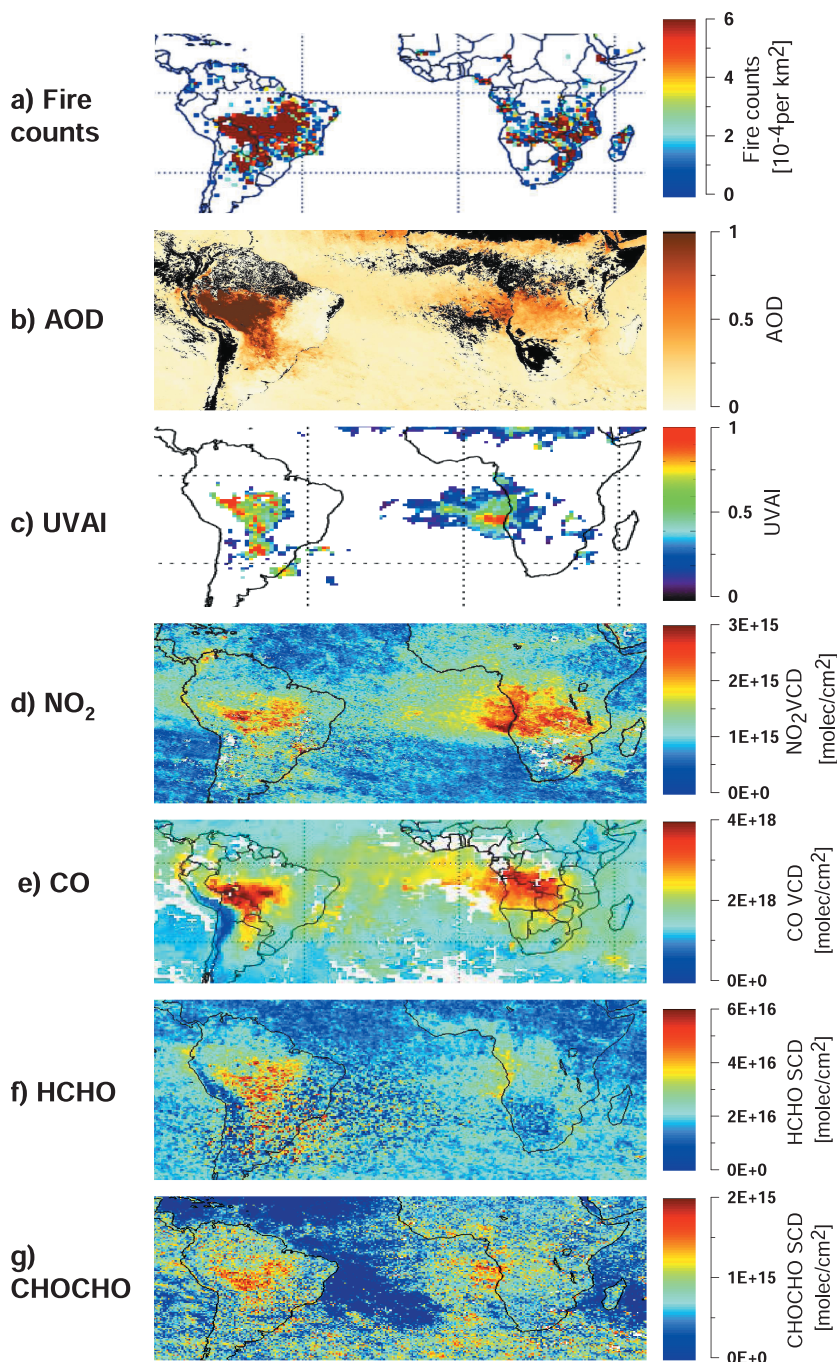
Figure 7. Monthly averages (September 2004) for different quantities retrieved from satellite observations over biomass burning regions. (a) Fire counts derived from AATSR (obtained from ESA, http://shark1.esrin.esa.it/ionia/FIRE/), (b) AOD retrieved from MODIS (http://neo.sci.gsfc.nasa.gov), (c) UVAI retrieved from SCIAMACHY (http://www.temis.nl), (d) NO_2 tropospheric vertical column density (VCD) retrieved from SCIAMACHY, (e) CO VCD retrieved from MOPITT for clear sky conditions (obtained from the NASA Langley Research Center Atmospheric Science Data Center, http://eosweb.larc.nasa.gov/PRODOCS/mopitt/table_mopitt.html), (f) HCHO Slant Column Density (SCD) retrieved from SCIAMACHY, and (g) CHOCHO SCD retrieved from SCIAMACHY. Observations from SCIAMACHY (UVAI, NO_2, HCHO, and CHOCHO) are averaged for clear and cloudy sky observations. NO_2, HCHO, and CHOCHO are from retrievals of the Max Planck Institute for Chemistry Mainz (from *Wagner et al.* [2013]).

An important advantage of many of these proxies is that they can be measured from satellite even in the presence of clouds. For the locations investigated in the study, satellite observations of NO_2, HCHO, CHOCHO, and the UVAI were typically available for twice the number of days compared to AERONET observations. Besides possible instrumental problems, this difference is mainly related to the presence of clouds. However, not all satellite observations of trace gases and UVAI made in the presence of clouds yield useful information.

Correlation studies between satellite observations of trace gases (CO, NO_2, HCHO, and CHOCHO), UVAI, and AOD over biomass burning regions indicate that the selected satellite quantities could in principle be used as proxies for the presence of aerosols and possibly also for CCN, because the emissions of these gases are correlated with the emissions of the aerosols. However, at least to date, the derived correlations are not specific enough, too weak, and/or too dependent on other environmental factors to allow an accurate estimate of the CCN abundance. The correlation analyses were carried out with respect to AOD measurements and not in situ CCN data.

In summary, satellite observations of various CCN proxies might have the potential to provide valuable information on atmospheric CCN abundance. In contrast to AOD observations, they can often be performed in the presence of clouds, taking into account the cloud height and coverage. Because the gas measurements as proxies for AOD are not very accurate, however, and the step of translating from AOD to CCN would result in even greater uncertainty, the usefulness of trace gases as a direct proxy for CCN is not yet known.

It is expected that future satellite observations of trace gases will be improved compared to existing sensors, especially with respect to spatial resolution, signal-to-noise ratio, and temporal sampling (e.g., using geostationary orbits). For satellite observations of aerosol extinction profiles and aerosol absorption (including the visible and near IR spectral range), improvements can be expected from combined multiangle viewing and polarization-sensitive instruments. Imaging instruments would need to include two or more UV wavelengths to allow the retrieval of UVAI at high spatial resolution. Finally, carrying out correlation studies of satellite CCN proxies with coincident in situ CCN observations on a global scale would make it possible to investigate further the suitability of the various satellite CCN proxies.

3.3.6. Satellite Aerosol Classification

Aerosol type information can potentially be used to identify anthropogenic aerosols, but currently, there still are limitations regarding the type of information available from satellite observations. For example, the fine mode fraction has been used as a proxy for urban-industrial pollution [e.g., *Bellouin et al.,* 2005, 2008; *Kaufman et al.,* 2005b], though many assumptions are involved with this approach and significant biases can occur where natural aerosols are present. Type-specific optical properties are required to determine the associated top-of-atmosphere, in-layer, and surface forcing. To better partition these three terms in the future, the most important parameters are single scattering albedo and, to a lesser degree, the first moment of the scattering phase function (asymmetry parameter). Multiangle observations by MISR provide perhaps the most successful approach so far to retrieve aerosol type globally. The MISR product yields qualitative constraints on aerosol size, shape, and single scattering albedo under good retrieval conditions (e.g., midvisible AOD greater than about 0.15 or 0.2) [*Kahn and Limbacher*, 2012]. To date, MISR provides a limited but near-global data set of aerosol type constraints for an extended period of time [*Kahn et al.,* 2010]; complementary work using multiangle, multiwavelength, and polarization information from PARASOL is under way [*Dubovik et al.,* 2011]. In addition, the depolarization and color ratios from lidar provide qualitative classification of particle type as well [e.g., *Omar et al.,* 2009]. Polarized, multiangle, multispectral observations with passive instruments (such as the PARASOL and APS satellite instruments, and the RSP, MSPI, and PACS airborne imagers that are aimed at testing concepts for future satellite missions, and the planned 3M imager) combine the strengths of multiple instruments currently in space, aimed at providing tighter constraints on aerosol type and optical properties [*Mishchenko et al.,* 2007; *Hasekamp,* 2010; *Diner et al.,* 2010]. The spectral resolution in the thermal infrared channels offered by IASI has successfully been explored by *Clarisse et al.* [2013] to provide aerosol type information. Also, the spectral resolution offered by instruments such as GOME, SCIAMACHY, and GOME-2 is used in a synergistic approach together with radiometers to obtain aerosol type information [*Holzer-Popp et al.,* 2008]. As the experience from MISR [e.g., *Kahn et al.,* 2010], MODIS [e.g., *Levy et al.,* 2010; *Remer et al.,* 2005], and AATSR [*Holzer-Popp et al.,* 2013; *de Leeuw et al.,* 2013] has shown, it is essential to compare global data sets from any technique to the "ground truth." AERONET has proven extremely useful to provide not only optical thickness data but also constraints on size distribution and to some extent asymmetry parameters, single scattering albedo, and type [e.g., *Holben et al.,* 2006; *Eck et al.,* 2010]. Satellite AOD sensitivity varies with retrieval
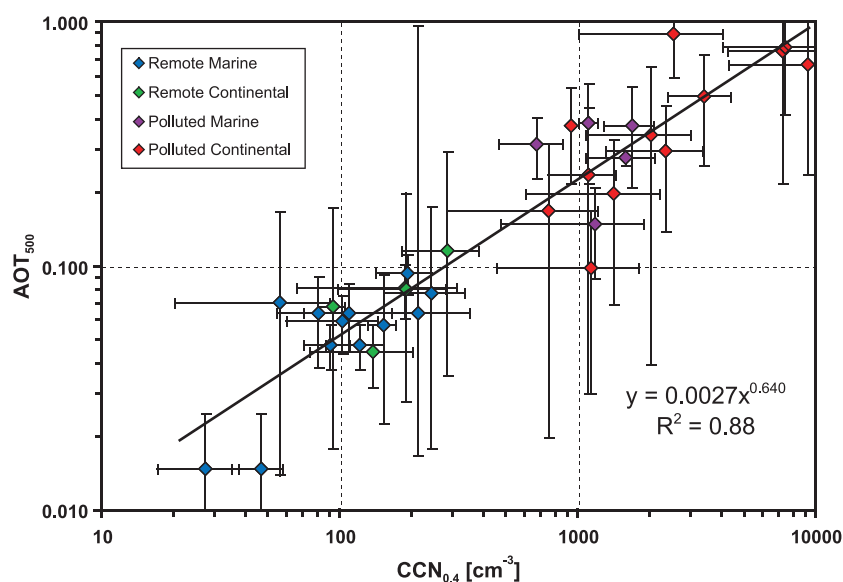
Figure 8. Relations between AOD at 500 nm and CCN at supersaturation of 0.4% for aerosols, excluding sea spray and dust. From *Andreae* [2009b].

conditions; based on AERONET comparisons, MODIS retrieves midvisible AOD to within 0.05 or ±20% AOD over dark, vegetated land and 0.03 or ±5% over dark water [*Levy et al.*, 2010; *Remer et al.*, 2005], while MISR retrieves AOD to within 0.05 or 20% and even better over dark water [*Kahn et al.*, 2010].

Aside from surface-based remote sensing, aircraft field campaigns staged around the world provide measurements that go beyond the validation of satellite retrievals, as described below, adding correlative information about CCN and satellite observables that can be used to improve the translation between global-scale proxies retrieved from space and the particles that effect cloud formation and mediate their evolution.

3.4. Are There Acceptable Simplifications and Assumptions?

We move from these more general considerations to the particular problem of observing CCN(S). The ability of aerosols to act as CCN is determined to a first approximation by a combination of particle size and hygroscopicity parameter, κ [*Petters and Kreidenweis*, 2007]. Therefore, to determine the column burden of CCN(S), one would need to know the detailed aerosol size distribution, ($N(d)$), throughout the column and the aerosol composition-dependent value of κ. To complicate matters, aerosol size distribution and composition (κ) typically vary with altitude. These requirements make the characterization of CCN(S) distributions by remote sensing, and especially the variability of CCN(S) with height, appear quite challenging. However, a new conceptual approach that uses clouds as natural CCN chambers might be able to overcome this challenge, as shown in section 3.5.

3.4.1. Relationships Between AOD, Aerosol Composition, and CCN

It is not easy to determine size distributions in the CCN-relevant size range (80–400 nm diameter) from radiometric measurements, because of a lack of sensitivity to sizes smaller than about 150 nm in diameter and difficulties in extracting size-distribution details. Furthermore, remote observations of κ are not possible, because they require details of the aerosol composition for CCN-relevant sizes. Fortunately, atmospheric aging over hours to days results in a significant convergence of aerosol properties ($N(d)$; κ) [e.g., *Andreae*, 2009a; *Jimenez et al.*, 2009; *Dusek et al.*, 2006; *Kammermann et al.*, 2010; *Levin et al.*, 2012]. Since regionally the shape of the size distribution and the mean effective κ of most aged aerosol populations vary only over a limited range, there are tighter relationships than might otherwise be expected between fine-mode AOD (diameters smaller than 1000 nm) and CCN(S) concentration (which is dominated by particles in the 100–200 nm diameter range), as shown in Figure 8 [*Andreae*, 2009b]. The empirically observed correlations between column-integrated fine-mode AOD and surface CCN(S) measurements also indicate that surface concentrations are often correlated with column burden. This requires a well-mixed boundary layer with no disconnected layers above (i.e., it may depend on the time of day and meteorological situation). However, such relationships would not exist when there is significant transported aerosol (e.g., elevated dust or smoke layers) above the boundary layer. At least for regions

where correlations are observed, rough estimates of CCN(S) abundances from radiometric measurements seem possible. It must be noted, however, that the CCN-AOD relationship shown in Figure 8 was meant to be a proof of principle and that the value of CCN(0.4) for a given AOD varies within a factor of about three. Consequently, this relationship is too coarse to be useful as a predictive parameterization for most applications.

A more detailed study using collocated optical and CCN measurements at selected sites shows similar relationships [*Liu and Li*, 2014]. Whereas the study of *Andreae* [2009b] used (fine-mode dominated) AOD at 500 nm observed from the ground as a measure of column aerosol burden, *Liu and Li* [2014] explored the use of a range of wavelengths and the influence of other variables, such as relative humidity and single scattering albedo. They showed that some improvement is possible by using AOD at shorter wavelengths to represent the CCN-relevant fine mode. Based on a data set acquired at a continental site, they proposed a parameterization for converting AOD to CCN using the aerosol index (i.e., the product of the AOD and the Ångström exponent), which also can be observed from space. However, the retrieval accuracy of the Ångström exponent also has large uncertainty (section 3.3.1 above). Their results showed that in the absence of dominating signals from desert dust, sea salt, or black carbon, the relative estimation error (RE) of their parameterization is 96%. The RE is defined as (estimated-measured)/measured CCN concentrations at a supersaturation of 0.4%. Limiting the relationship to relative humidity values of <80% improved the RE to 85%. Although the paper of *Liu and Li* [2014] does not provide enough detail to allow a clear statistical evaluation of their stated uncertainty, it is likely that their parameterization is also uncertain to a factor of 2 or more, which limits its predictive usefulness.

Given the rapidly increasing availability of CCN(S) measurements worldwide, further investigations like those of *Andreae* [2009b] and *Liu and Li* [2014], linking ground data to column data at a wider range of sites, are encouraged. These should include measurements of CCN(S), scattering coefficient, Ångström exponent, single scatter albedo, humid growth factor, and size distribution, and ideally also vertical distributions from lidar or aircraft. Such studies could yield a more representative assessment of the conditions under which the resulting estimates of CCN(S) are good enough for aerosol-cloud-interaction studies.

Improved algorithms have been proposed, which take into account the effects of aerosol size, composition, and relative humidity [*Gasso and Hegg*, 2003; *Kapustin et al.,* 2006], but no quantitative assessment of the improvement due to these additional physical considerations is yet available. MODIS provides fine-mode particle concentration over the ocean from remote sensing measurements, for the size range of 0.03–0.1 µm, called PSML003-Ocean. It was developed with the intention to estimate CCN concentrations, but it was never validated. Recent work has shown that there are relationships between chemical and optical properties of aerosols (i.e., between the wavelength dependence of extinction and the organic mass fraction, which in turn is correlated with the hygroscopicity factor) that may be useful in the remote detection of the CCN properties of aerosols, provided data specific to aerosol type are available [*Shinozuka et al.,* 2009].

3.4.2. Synergetic Approaches Involving Ground-Data/In Situ Data and Modeling

Passive radiometric measurements will at best provide column-integrated burdens of a proxy for CCN(S), and the lack of vertical information limits the usefulness of this information for modeling of ACPC interactions. Active remote sensing with multiwavelength Raman or multiwavelength high spectral resolution lidars (HSRL) provide vertically resolved aerosol size distribution data that might offer insights [*de Graaf et al.,* 2013; *Veselovskii et al.,* 2004], even though the gap between ground and the lowest detection altitude would need to be closed (e.g., by in situ profiling). In a complementary sense, observational data and model fusion can extend these samples to provide reasonable estimates of aerosol vertical distributions over larger areas. Another complementary element will be space-borne HSRL lidar data offered by the upcoming EarthCare mission [*Donovan et al.,* 2013].

An additional difficulty is the swelling of aerosols due to the increased relative humidity near clouds that enhances the AOD, which may cause false positive relationships between AOD and the inferred CCN with cloud cover [*Myhre et al.,* 2007]. Therefore, aircraft field validation campaigns are needed to test the limits of this approach and to help refine the interpretation of remote sensing data for this application, as appropriate. More accurate knowledge of the relative humidity and composition of the aerosols could help improve the conversion between AOD and CCN. For example, *Zieger et al.* [2011] used combined simulations and observations around the Cabauw measurement site in the central Netherlands to show the shift of aerosol equilibrium size due to changing relative humidity with height.
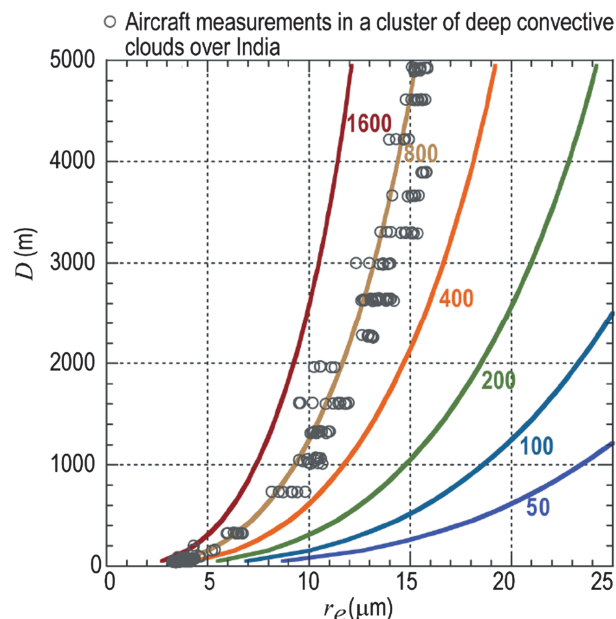
Figure 9. The adiabatic effective radius as a function of height above cloud base (D) for clouds with various number of cloud drop concentrations at their base, for cloud base at a height of 2 km and temperature of 15℃. Actual aircraft measurements of 1 s r_e are shown for a cloud that had 610 drops cm^{-3} at its base. From *Rosenfeld et al.* [2012c].

3.5. Satellite Inference of CCN by Retrieved Cloud Properties

As discussed above, the conversion of the optically measured aerosol properties into CCN is rather inaccurate and has many limitations, especially in the vicinity of clouds. However, measuring CCN near the clouds that interact with them is essential for understanding cloud aerosol interactions and aerosol cloud-mediated forcing. Furthermore, an obvious problem in measuring CCN interactions with clouds from space is the fact that they are obscured from the satellite view by the very clouds that ingest these CCN from the boundary layer.

An alternative approach that can overcome these problems has been proposed, which in effect uses clouds as CCN counters [*Rosenfeld et al.*, 2012c; *Rennó et al.*, 2013]. In a laboratory CCN chamber, a set of known vapor supersaturations with respect to water is applied to an air sample containing aerosol. The number concentrations of nucleated cloud drops are counted, and the CCN(S) spectrum is obtained.

Ideally, simultaneous observations of cloud droplet effective radii and updraft velocities near cloud base can yield classical CCN spectra (i.e., N_{CCN} versus S) in a fashion analogous to a laboratory CCN chamber. With values of κ based on assumed fine-mode composition adopted from global air chemistry and aerosol modeling, these CCN-spectra can be inverted to derive rough size distributions. Conversely, if the cloud drop number concentration ($N(d)$) near its base is known or assumed, κ of the aerosols in the boundary layer can be derived.

To use naturally occurring clouds as CCN chambers, it is necessary to be able to retrieve the number of aerosol particles that nucleate into cloud drops at cloud base, N_a, and the cloud-base updraft, W_b. A method for doing this from space was recently introduced by *Rosenfeld et al.* [2012c], and a satellite mission aimed at acquiring the necessary data was proposed [*Rennó et al.*, 2013].

The satellite retrieval of N_a for convective clouds assumes that all cloud drops are nucleated at cloud base and that the cloud drops continue to grow with height by condensation as in an adiabatic parcel, without significant coalescence or evaporation due to mixing with the ambient air outside of the cloud. It is also assumed that the boundary layer is well mixed, so that all clouds in a viewing area several tens of kilometers in size have the same base height and ingest the same aerosols. Under these conditions, the retrieved vertical evolution of cloud-top effective radius, r_e, can be uniquely related to N_a for a given cloud base pressure and temperature, as illustrated in Figure 9. Fortunately, the deviations of the actual r_e from its adiabatic value in convective clouds are small for the lower parts of the clouds, because the mixing process is close to inhomogeneous. Inhomogeneous mixing occurs when the rate of evaporation of small cloud drops is much larger than the rate of ambient air entrainment, so that the drops that border the entrained air parcel evaporate completely, while leaving the other drops away from the mixing front little affected and hence retaining their r_e. *Freud and Rosenfeld* [2012] have shown that observed clouds exhibit similar behavior above their bases up to the height when coalescence becomes significant, i.e., when r_e exceeds about 14 μm. The average deviation between calculated N_a based on the r_e vertical profile and N_a actually measured at cloud base was an overestimate of about 30%, due to the deviation of the real clouds from the adiabatic assumption. *Freud and Rosenfeld* [2012] showed how to correct for this bias if the relative humidity outside the clouds is known. The updraft velocity, W_b, can be retrieved by high-resolution multiple stereoscopic

views that allow tracking of the vertical evolution of the cloud surface. The value of W_b can then be calculated based on the assumption that the airflow is continuous between the rising cloud envelope and the cloud base.

The high spatial resolution of the recently launched NPP/VIIRS (375 m) allows the retrieval of N_a for boundary layer clouds, but W_b has to be estimated by properties such as the surface sensible heat flux and relative humidity [*Williams and Stanfill*, 2002]. A proof of concept for retrieving CCN using clouds as CCN chambers was demonstrated in boundary layer convective clouds over the Southern Great Plains super site in Oklahoma [*Rosenfeld et al.*, 2014]. N_a was retrieved from the NPP/VIIRS using the method shown in Figure 9. The cloud-base height and W_b were measured by vertically pointing ground-based radar. The supersaturation was obtained by the expression, $S = c \, W_b^{3/4} N_a^{1/2}$ [*Pinsky et al.*, 2012], where c is a coefficient that depends on cloud-base temperature and pressure. The satellite-retrieved N_a is in fact CCN(S), as calculated by this expression. It was validated favorably against surface measurements of CCN under well-mixed boundary layer conditions.

The next step toward demonstrating satellite CCN retrieval is deriving cloud base pressure and temperature, which are required for the calculation of N_a and S. This was achieved from the high-resolution NPP/VIIRS data and validated against lidar measurements of cloud base with an accuracy of about 1°C and 100 m [*Zhu et al.*, 2014]. The last piece of the derivation would be retrieving W_b directly by the satellite. The retrieval is based on the difference between surface air and skin temperatures, cloud base height, and horizontal wind speed.

The error propagation in this method was calculated and presented in *Rosenfeld et al.* [2012c]. A retrieval error of underestimating $r_e = 16\,\mu m$ by $1\,\mu m$ (a factor of 1.067) corresponds to an overestimation of N_a by a factor of 1.21. Another 20% error can be added due to the uncertainty in the mixing mode of the cloud drops with the ambient air, bringing the error in retrieving N_a to a factor of 1.45. An uncertainty of 20% in W_b causes S to be biased by 12% in the same direction. A 45% bias in N_a causes S to be biased by 14% in the opposite direction. Combining the errors results in an overall error estimate of 25% in S.

By measuring the cloud updraft and the vertical profiles of microstructure and precipitation-forming processes independently (section 2.1.3), this method can measure the aerosol-cloud interactions in the most direct and accurate way and can disentangle the aerosol effects from the dynamical effects on the clouds and precipitation-forming processes. This would allow disentangling the effects of aerosols from the effects of cloud-base updraft, and thus meteorology, on boundary layer clouds. Measuring the updrafts at greater heights would require development of a suitable satellite, such as proposed by *Rennó et al.* [2013].

3.6. The Importance and Challenge of Measuring Ice Nuclei From Space
3.6.1. The Knowledge Gap in Aerosol Ice Nucleating Activity

A major gap in current knowledge is that of aerosol ice-nucleating properties and number concentrations as a function of ice super saturation and temperature, at appropriate spatial resolution. This is a key limitation in observing the relationship between aerosol IN properties and their impact on supercooled and ice clouds. The gap also makes it impossible to account for IN activity realistically in simulations at all scales. As for the CCN, filling the IN gap is an essential prerequisite for including ACPC interactions in climate models and for validating aerosol model simulations.

One difficulty in observing IN aerosols from space is that they are masked by the vast majority of aerosols, which are not IN. There is roughly one IN for about every 10^5 CCN aerosols. However, there are some useful indicators for observing IN aerosols from space.

3.6.2. What Aerosol Types Can Serve as IN?

It is commonly accepted that mineral dust aerosols can serve as IN at modestly low temperatures and low ice supersaturations. When present in high concentrations, desert dust can be detected reasonably well from satellites. In addition, heavy urban and industrial air pollution over China was reported to exhibit IN activity similar to that of desert dust [*Rosenfeld et al.*, 2011]. However, there is no agreement on the IN activity of carbonaceous aerosols [*Hoose and Möhler*, 2012]. Some terrestrial biogenic aerosols such as pollen can serve as IN under low supercooling conditions. Furthermore, particular kinds of bacteria can serve as IN at relatively warm temperatures of only a few degrees below 0°C [*Hoose et al.*, 2010], but there is presently no ability to detect them by remote sensing.

The finding that the concentration of aerosol particles with a diameter greater than 0.5 μm can explain a large fraction of the variability in IN concentrations [*DeMott et al.,* 2010] can be addressed with satellite remote sensing. There is still large variability in the IN activity of different types of aerosols with particle size greater than 0.5 μm. The only exception is desert dust, which is readily detectable by satellites and serves as good IN. Again, the essential question is under what conditions is this approach to interpreting the remotely sensed data adequate for constraining aerosol-cloud interaction models? We conclude that except for desert dust, the prospects of detecting IN from satellite are not very good.

4. The Challenge of Observing Cloud-Mediated Aerosol Radiative Effects

4.1. The Challenge

The processes by which aerosols can modulate cloud radiative effects at various scales have been discussed in previous sections. In summary, in terms of aerosol radiative impacts on clouds, both the albedo and cloud-lifetime or cloud-cover effects were the first to be widely recognized. In addition, a large variety of other microphysical effects have been identified such as the invigoration of water [*Koren et al.,* 2014] and mixed phase [*Rosenfeld et al.,* 2008a] clouds, and the "cloud-burning effect" [*Ackerman et al.,* 2000; *Johnson et al.,* 2004; *Kaufman et al.,* 2005a]. All these aerosol cloud-mediated effects have been broadly accepted as a collection of concepts for distinguishing different processes. But although cloud-aerosol interactions can sometimes be very apparent in small-scale observations (for example, in ship tracks as seen from space if conditions are suitable), *Stevens and Feingold* [2009] caution that correlations between observed cloud and aerosol properties cannot always be used to identify cause and effect. It might be necessary to also consider intrinsic buffering mechanisms in the cloud-aerosol system that may modulate or counteract the traditional cloud-aerosol effects [*Feingold et al.,* 2010] as well as to consider the impact of the observational scale [*McComiskey and Feingold,* 2012]. Moreover, the meteorological context needs to be taken into account [e.g., *Loeb and Schuster,* 2008], where the direction of aerosol influences can depend on the regime under consideration (positive and negative semidirect effect [*Johnson et al.,* 2004]; aerosol-precipitation [*Rosenfeld et al.,* 2008a]). Despite these challenges, *Stevens and Feingold* [2009] suggest studying these regimes one by one. The challenges here are measuring these components and disentangling them by remote sensing, especially from the vantage of global coverage that satellites can provide.

However, before the above challenges can be properly addressed, we have to overcome the low skill of current satellite sensors in observing cloud and aerosol properties simultaneously, as well as deal with aerosol retrieval artifacts in the vicinity of clouds [*Várnai and Marshak,* 2009; *Várnai et al.,* 2012]. Swelling of aerosols due to higher relative humidity in the vicinity of clouds increases their AOD and AI [*Loeb and Schuster,* 2008]. Apparent AOD increases further in association with the clouds due to cloud contamination [*Koren et al.,* 2008b] and thickening of the boundary layer near more-developed convective clouds. This association of greater AOD in the vicinity of clouds might explain at least part of the reported increase in cloud cover with greater AOD and AI [*Sekiguchi et al.,* 2003; *Kaufman et al.,* 2005a; *Kaufman and Koren,* 2006; *Loeb and Schuster,* 2008; *Koren et al.,* 2008a; *Dey et al.,* 2011; *Small et al.,* 2011]. A physically based positive correlation exists between larger cloud fraction and deeper clouds, especially in convective cloud regimes. *Gryspeerdt et al.* [2014] demonstrated that this often explains a substantial part of the indicated decrease in cloud-top pressure in association with greater AOD, which has been ascribed to aerosol cloud invigoration [*Koren et al.,* 2005, 2010a, 2010b, 2012; *Yuan et al.,* 2011a, 2011b; *Niu and Li,* 2012; *Koren et al.,* 2014]. Therefore, reliable documentation of the effects of aerosols on cloud cover and invigoration cannot be based on comparisons with AOD and AI exclusively.

The objective here is to move the discussion toward relating retrieved cloud-aerosol interactions to the energy budgets and to the question where in the atmosphere (or at the surface) the energy is deposited. Understanding the relationship between the microphysical, macrophysical, and optical cloud-aerosol parameters on the one hand, and the associated fluxes and heating rates on the other, is essential not only to attributing budget terms to atmospheric constituents but also to understanding atmospheric dynamics and radiation-related aerosol-cloud feedbacks and buffering mechanisms directly from observations, rather than relying solely on model simulations.

4.2. Limitations of Space-Borne Remote Sensing:
4.2.1. Limitations in Measuring Aerosols in the Vicinity of Clouds

Current studies of aerosol radiative impacts on clouds (and of cloud processing of aerosol particles) from space are based on separate retrievals of aerosol and cloud parameters in (usually disjoint) satellite pixels. For *spatially homogeneous clouds*, the optical thickness of an overlying aerosol layer has been retrieved from space-borne lidar observations [*Chand et al.,* 2008] without relying on assumptions about the lidar ratio as had been done in previous studies. *Waquet et al.* [2009] published the first retrieval of aerosol optical thickness above or within clouds from passive spectral imagery of POLDER, followed by *Torres and Bhartia* [2012], who used OMI. However, both studies assumed fixed aerosol optical properties (single scattering albedo and scattering phase function). Furthermore, they sensed aerosols only above the clouds, whereas it is also necessary to measure the aerosols that are ingested into the clouds from the boundary layer. *Waquet et al.* [2013] used multiangle and multispectral polarized reflectance from a POLDER "hyper-pixel" (coarsened data) to retrieve cloud and aerosol properties separately but point out that their method is not very sensitive for deriving aerosol single-scattering albedo.

The modeling study by *Hasekamp* [2010] argues that multiangle polarized reflectance observations have an advantage over single-view nonpolarized passive imagery in providing accurate retrievals of multiple aerosol and cloud parameters with low dependence on a priori information about, e.g., aerosol type and scattering properties. For example, the single scattering albedo, index of refraction, and information about aerosol size can be retrieved by such methods. The index of refraction can be used for estimating the amount of absorbed water in the aerosols, which reflects their swelling in high relative humidity [*Kapustin et al.,* 2006], provided the retrieval constraints are sufficiently tight, and some independent information about particle composition is available. The value of the combination of multiangle polarized reflectance measurements for aerosol retrieval has been demonstrated by application to PARASOL [*Dubovik et al.,* 2011; *Waquet et al.,* 2014]. The October 2012 PACE (Pre-Aerosol, Clouds, and ocean Ecosystem) science definition team report [*Del Castilo et al.,* 2012] discusses the advantages and drawbacks of the various flavors of a "3 M" (multidirectional, multipolarization, and multispectral) imager concept as currently developed at ESA. Aircraft experiments such as the Polarimeter Definition Experiment (PODEX, conducted in early 2013 with the NASA's ER-2 high altitude aircraft) provide a test bed for airborne proxy instruments, making it possible to test various options for future satellite instruments and to validate retrieval techniques with experimental data.

Overall, ACPC requires constraints on CCN size distribution, hygroscopicity, and concentration in the cloud-droplet-formation region near cloud base, which are best determined with in situ measurements, but can be inferred from remotely sensed CCN proxies combined with aerosol transport modeling. (An early example of this approach is *Schwartz et al.* [2002].) Aerosols adjacent to clouds, in particle detrainment regions, can be probed with lidar [*Tackett and Di Girolamo*, 2009].

In the top-of-atmosphere upwelling irradiance data as derived from Earth Radiation Budget (ERB)-type broadband instruments such as CERES, aerosol-induced changes to the cloud radiative budget cannot be isolated. Perhaps the most direct space-borne observation of the aerosol radiative effect above or within clouds is the study by *de Graaf et al.* [2012], which uses spectrally resolved reflectance observations by SCIAMACHY. From the measured spectrum, two shortwave infrared wavelengths (only marginally affected by aerosol absorption) are used to retrieve cloud optical thickness and effective radius, which is then used to parameterize the spectral reflectance under unpolluted conditions. The difference between the observed and parameterized (unpolluted reference) reflectance can be converted into the radiative flux that is absorbed by the aerosol layer above the cloud. *de Graaf et al.* [2012] use this method to constrain the direct radiative effect of absorbing aerosols over clouds in the South Atlantic Ocean west of Africa for the month of August 2006 ($23 \pm 8 \, \mathrm{W \, m^{-2}}$, with a variation of $22 \, \mathrm{W \, m^{-2}}$). This shows the potential and importance of spectrally resolved and contiguous observations.

4.2.2. The Vertical Dependence of Cloud-Mediated Aerosol Radiative Effects

The vertical structure of a cloud-aerosol scene is of fundamental importance for the correct vertical partitioning of the global energy budget [*Trenberth et al.,* 2009]. Correct knowledge of the vertical distribution of radiative and of latent heating in the atmosphere and at the surface is key to a better understanding of the role of dynamics in aerosol-cloud interactions. Unfortunately, surface forcing by cloud-aerosol fields is even less well understood than that at the top of the atmosphere [e.g., *Wild*, 2005; *Wild et al.,* 2013], let alone the vertically resolved atmospheric absorption and heating rates. Active remote sensing can

measure the vertical profiles and constrain the composition of aerosols. This allows for studying the effect of aerosol layers above a cloud field on the combined aerosol-cloud radiative properties [*Costantino and Bréon*, 2010]. *Chand et al.* [2009] used CALIPSO observations to retrieve aerosol optical thickness above cloud layers and to calculate top-of-atmosphere forcing (aerosol direct effect above clouds). They also derived the absorption in the atmosphere as a function of the underlying cloud fraction and cloud albedo and determined the critical cloud properties beyond which top-of-atmosphere cooling by the overlying aerosol layer turns into warming. This is similar to the effect of surface albedo on aerosol forcing [*Russell et al.,* 2002]. The caveat in any such studies is that the critical cloud fraction or surface albedo depends on the aerosol single scattering albedo, which is difficult to measure from space.

Wilcox [2012] quantified observationally a small negative semidirect effect caused by thickening clouds in response to an overlying but vertically separated absorbing aerosol layer; this differs from the classical semidirect effect, where the cloud is immersed or is in direct contact with an absorbing aerosol layer, leading to cloud thinning. The study uses a combination of AMSR-E microwave-derived liquid water path and the OMI aerosol index for detecting aerosol layers, in conjunction with CERES-derived cloud-aerosol albedo, and MODIS to screen for overcast conditions. Although it does not rely on active remote sensing, it is one of the few studies that utilize observations to show the importance of vertical structure when assessing the magnitude and even the sign of aerosol radiative effects on clouds.

4.2.3. Complications due to Cloud Heterogeneity and 3-D Effects

Heterogeneous cloud-aerosol fields represent a great challenge to space-borne remote sensing because the signal measured by passive imagers carries not only information about the diverse atmospheric constituents and surface properties within the pixel itself but is also superimposed with the radiative signatures of nearby cloud and aerosol particles, gases, and the surface. Even distant clouds can bias the retrieval of aerosol properties [*Zhang et al.,* 2005] due to radiation scattered into the pixel of interest. *Marshak et al.* [2008] showed that this effect is not spectrally neutral, but results in an enhancement of reflectance at shorter wavelengths (bluing), because secondary scattering by atmospheric molecules, which affects the shortest wavelengths most, is superimposed on the observed signal. On the other hand, *Redemann et al.* [2009] showed by comparison with sun photometer measurements that near-cloud aerosol optical thickness retrievals from MODIS might have a bias that does not depend on wavelength. In addition to aerosol-induced biases in cloud retrievals, aerosol particles above or around clouds also produce biases in retrieved cloud properties, especially when they are absorbing. *Haywood et al.* [2004] showed that an absorbing aerosol layer above clouds can mimic an aerosol indirect effect in imager-derived cloud properties; *Meyer et al.* [2013] introduce an algorithm that corrects this effect in MODIS cloud retrievals.

Because clouds and aerosols are so difficult to distinguish in many circumstances, *Charlson et al.* [2007] and *Koren et al.* [2007] have emphasized the need to study them as a system rather than separating them artificially. *Koren et al.* [2008b] found that unresolved clouds within the pixel of an imager lead to an overestimation in the satellite-derived aerosol layer reflectance that grows with coarser resolution, and *McComiskey and Feingold* [2012] point out that the assessment of aerosol indirect effects depends on the resolution of the data used.

It is generally assumed that retrievals based on polarized reflectance are less affected by cloud heterogeneity because the radiative transfer tends to be dominated by single scattering. The limits of this assumption are currently being explored with observations (see *Alexandrov et al.* [2012] for cloud retrievals). Space-based lidar techniques do not suffer as much from multiple scattering effects. *Tackett and Di Girolamo* [2009] used CALIPSO data to show that aerosols in the immediate vicinity of tropical trade wind clouds actually had reduced droplet number concentration, larger size, and narrower size distribution than cloud particles farther away. *Várnai et al.* [2012] used CALIPSO and MODIS observations to quantify the MODIS overestimation of aerosol optical thickness as a function of the distance to the nearest cloud. However, it is still unclear to what extent the near-cloud effects in apparent aerosol optical thickness in general are caused by retrieval artefacts and changes in particle size and/or number concentration.

4.2.4. Assessing the Diurnal Cycle of Radiative Budget Terms

The state-of-the art NASA EOS satellite observations have morning and afternoon overpass times, providing two snapshots per day (approximately 10:30 AM and 1:30 PM) of the relationship between cloud or aerosol retrievals on the one hand and the associated upwelling irradiance on the other. However, to follow the temporal evolution of aerosol-cloud interactions over the course of the day, it is necessary to determine local

diurnal patterns for scenarios of interest. Geostationary satellites currently provide cloud retrievals that can be traced throughout the day, but their spectral bands do not allow the accuracy of aerosol retrievals that is obtained from the polar orbiting satellites. *Zhang et al.* [2011] used a multiangle approach to obtain aerosol retrievals from geostationary data, based on *Lyapustin et al.* [2011]. This work may help to better define the requirements for aerosol retrievals from geostationary orbits.

4.3. Aircraft Measurements
4.3.1. Aircraft Simulators for Spacecraft Instruments
Most space-borne sensors to date have aircraft prototype instruments that are tested during spacecraft instrument development, e.g., on the high-altitude ER-2, which serves as a NASA spacecraft simulator. This allows the validation of retrieval techniques before the instruments are launched into space. Once a satellite instrument is operational, aircraft measurements are conducted for validation and vicarious calibration. For example, MODIS observations of clouds are validated with MAS or MASTER measurements on the ER-2 [*King et al.,* 2010], and CALIPSO aerosol retrieval products are regularly validated with HSRL on the NASA King Air [*Hair et al.,* 2008]. In addition, the AERONET ground-based network has proven highly successful in validating space-based aerosol products worldwide.

4.3.2. Advantage of Aircraft in Resolving Vertical and Horizontal Cloud-Aerosol Scenes
The different observational perspectives from aircraft and ground stations (generally, suborbital observations) make it possible to go beyond the information that is available about cloud-aerosol layers from space-borne sensors and to examine the relationship between cloud-aerosol properties and their effect on the shortwave energy budget. In particular, the absorption of atmospheric layers, and the surface forcing, can be better constrained from aircraft and from the surface than from space. To date, only a few studies have used sub-orbital measurements to investigate the aerosol direct, indirect, and semidirect effect.

4.4. Summary of Available and Conceptual Remote Sensing Approaches for Studying Aerosol Cloud Radiative Effects
4.4.1. Passive Imagers
Passive imagers are still the workhorses of atmospheric remote sensing and, in combination with scanning (ERB-like) radiometers, will remain the most important tools for probing the radiative energy budget from space.

Advantages Extensive spatial coverage and frequent repeat cycle; provide top-of-atmosphere radiances, which is the most important quantity for deriving irradiance; long time-series are already available; retrievals of a large variety of cloud microphysical parameters are possible.

Drawbacks Limited retrieval capabilities; little or no skill in retrieving vertically resolved cloud and aerosol properties; not possible to retrieve aerosol and cloud properties within single pixels; retrieval artifacts in cloud/aerosol properties due to aerosols/clouds nearby; usually low spectral resolution with only a few bands, or broadband observations.

Possible advancements Higher spectral resolution and wider spectral coverage by multispectral imagers would increase retrieval capabilities and might increase the accuracy in energy budget estimations, especially in conditions when aerosols and clouds occur in the same pixel. Multidirectional and multiviews offer data on altitude and possibly on cloud dynamics. Adding polarization to the multidirectional views can add information on aerosol and cloud properties in new ways. Specifically, the Aerosol Polarimetry Sensor [*Mishchenko et al.,* 2007] was developed for the GLORY satellite mission, but unfortunately its launch on 2011 failed and no replacement is secured yet. Also, multiple instruments in different orbits could provide better diurnal and generally greater overall coverage.

4.4.2. Active Techniques
From space, CALIPSO has allowed the detection of aerosol layer height and at least some information about aerosol optical properties. Aircraft HSRL systems allow the retrieval of vertically resolved extinction and some aerosol type differentiation [*Burton et al.,* 2014]. The next generation of space-borne active instruments will probably inherit many of the advancements that were made with aircraft instruments over the last 10 years. For example, the satellite EarthCare mission is planned to carry an HSRL.

Advantages Accurate vertical information; aerosol retrievals in the vicinity of clouds with minimal cloud-related artefacts; radar allows for a good characterization of precipitation flux.

Drawbacks The small spatial coverage makes it possible to achieve global coverage only in the statistical sense (a "slice" of the globe), depending on the orbit. Another problem is that of validation: Whereas MODIS aerosol products can be widely validated with AERONET data, the narrow swath width of CALIOP does not cover sufficient surface stations to allow statistically sound validation.

Possible advancements A space-borne high-spectral-resolution lidar (HSRL) would provide layer-resolved aerosol type information, and a scanning lidar in space might increase the spatial coverage of lidar-based retrievals. However, the technology for achieving this reliably is still immature.

4.4.3. Multiple Viewing-Angle and Polarized Observations

Observations using multiple viewing angles provide the best currently available global-scale retrievals of aerosol type and even qualitative constraints on SSA. They allow substantially better separation of the surface and atmospheric signals than single-view imagers and, by way of determining SSA from space, allow limited vertical partitioning of budget terms (surface, layer, top-of-atmosphere forcing). Additional, polarimetric capabilities are available for PARASOL and are currently being added to multiangle imaging instruments (e.g., in the Multiangle SpectroPolarimetric Imager, MSPI, PACS, and 3MI), which will improve the retrieval of aerosol optical properties and provide frequent, global coverage. Fully polarized, multiangle, multispectral observations promise the most detailed aerosol type differentiation and most accurate optical property retrieval that can be achieved with passive remote sensing from space [*Hasekamp*, 2010; *Dubovik et al.*, 2012]. They allow one to distinguish aerosols from clouds, provide enhanced aerosol type information for identifying and at least to some extent quantifying anthropogenic effects in the climate system. The relative independence from surface effects on aerosol retrievals might significantly increase retrieval accuracy in clear-sky scenes compared to nonpolarized techniques. Multiangle measurements can also be used for obtaining the vertical structure and motions of clouds [*Moroney et al.*, 2002; *Seiz and Davies*, 2006; *Martins et al.*, 2011].

4.4.4. Remarks and Suggestions

Given the limitations of the above-mentioned approaches for aerosol-cloud remote sensing, it is obvious that no single instrument can close all the gaps in our knowledge. Therefore, a plan to match observations from several satellites has emerged over the past few years, combined with data assimilation approaches in numerical weather predictions where raw data (e.g., radiances) are directly ingested into a model by Kalman filtering. This direct way to connect models to satellite data is realized by so-called instrument simulators, which provide synthetic measurements that can be compared with the observations. Such model runs are termed Observing System Simulation Experiments (OSSEs) and have their origins in numerical weather simulation. Although the results of an OSSE are no substitute for actual measurements, due to whatever limitations there are in the model physical parameterizations as well as any spatial and/or temporal resolution mismatch, they offer a powerful way to test the model physics and the consistency of the measurements [*Wind et al.*, 2013].

To improve the measurement of budget terms from space, it may be advantageous to consider a satellite having complete solar and terrestrial spectrum coverage in a sun-asynchronous orbit, such as a precessing orbit, to better capture the diurnal pattern (currently, it is only observed twice a day, at fixed local solar times). Also, a better knowledge of aerosol single scattering albedo (and the asymmetry parameter) and vertical distribution will be crucial for partitioning energy budget terms vertically, which might be achieved by multiangle, polarized measurements.

The A-Train is a constellation of early afternoon, sun synchronous polar orbiting satellites, which were designed for exploiting the synergy between the sensors on the various satellites. This should be used as a model for future satellite combinations, possibly with a better overlap of footprints, and/or with pointing capabilities. The surface budget should be tied better to top-of-atmosphere observations by extending surface-based observations.

Beyond the synergistic application of current and incrementally advanced measurement and modeling techniques, the combined retrieval of cloud and CCN properties in the same cloudy area, using a methodology such as that described in section 3.5, might provide a significant advance in the field. The retrieved CCN as well as the response of cloud properties can be assimilated into model simulations to improve the weather forecasting and constrain GCMs. Having simultaneous CCN, cloud microstructure and dynamical properties will make it possible to disentangle the aerosol and meteorological effects on the cloud systems. It would require a specially designed satellite, such as the instrument proposed by *Rennó et al.* [2013].

4.5. Loss of Old Satellites and Their Replacements

The past decade has been an unusually fruitful period in terms of remote-sensing observations of aerosols and clouds, leading to major advances in observation technology, retrieval techniques, climate-quality data sets, and understanding of underlying aerosol-cloud-precipitation processes. A summary table of major currently available satellite instruments used for tropospheric aerosol data products is given in *Kahn* [2012]. The value of these data, especially for climate studies, rests heavily upon having multidecadal observations with at least the accuracy and richness of the data currently being acquired, to identify trends, isolate mechanisms by stratifying on multiple parameters, and validate retrievals from continuing, coincident suborbital measurements. Yet the resources needed to maintain, and certainly to advance, current capabilities have been difficult to obtain. There are no follow-on instruments scheduled to carry forward the observations of relevant NASA EOS satellite capabilities, such as those of CLOUDSAT, CALIPSO, and MISR, which were launched between 1999 and 2006, and are already functioning well beyond their design lives. Likewise, the loss of ESA's ENVISAT in April 2012 has caused a gap in the observations of SCIAMACHY, MERIS, and AATSR. However, after successful launches of the EUMETSAT/ESA Sentinels, relevant data will become available from SLSTR and OLCI on Sentinel-3, expected launch in 2015. Sentinel 1 was already launched in April 2014; SLSTR and OLCI are similar to AATSR and MERIS, respectively, but with extended capabilities. The PARASOL mission terminated in 2013, but multiviewing, multichannel, multipolarization information will become available from 3 M on Sentinel-5, planned for launch in 2020. Data from the Ultraviolet Visible Near-infrared (UVN) spectrometer and from Eumetsat's thermal InfraRed Sounder (IRS), both embarked on the MTG-Sounder (MTG-S) satellite, will also become available around the same time; a Sentinel-5 precursor with spectrometer in the UV, visible and solar IR bands (TROPOMI) is scheduled for launch in 2015. The GPM, a TRMM follow-on mission, was launched in 2014. The ESA/JAXA Earth Clouds and Aerosol Explorer Mission (EarthCARE) [*Donovan et al.,* 2013], with expected launch in late 2016, will replace CLOUDSAT and CALIPSO with expanded capabilities for measuring aerosols using the HSRL technique and cloud vertical motions with its Doppler radar.

The new NPP/VIIRS imager, a MODIS follow-on instrument, is capable of providing imagery that can be used for retrieving aerosol and cloud properties at a resolution of 375 m. Retrieving cloud and aerosol properties from geostationary satellites will get a substantial boost from the improved spatial and spectral resolution. The GOES-R satellite will have a nominal resolution of 2 km for cloud properties, which is an improvement on the present 3 km resolution of the METEOSAT Second Generation. The METEOSAT Third Generation, which may be available starting in 2020, will provide imagery with capability of retrieving cloud properties at a nominal resolution of 0.5 to 1 km.

5. Disentangling the Aerosol Effects on Earth's Energy Budget in All Its Forms

5.1. The Challenge

In this review, we have shown that aerosols and their interactions with clouds affect, sometimes substantially, Earth's energy budgets in all their forms. This constitutes their importance to the climate systems and the need to quantify all the resulting energy transformations in the context of a GCM. Aerosols affect Earth's energy flows in many ways, including the following:

1. Aerosol scattering reflects solar energy back to space while cooling the surface.
2. Aerosols absorb solar radiation and heat the layer in which the aerosols reside.
3. Absorbing aerosols, by warming a cloudy air layer, "burns" the clouds, which then reflects less solar radiation back to space.
4. Scattering and absorbing aerosols, by cooling the surface, delay or prevent convection and thus prevent the formation of clouds that would reflect more solar radiation to space.
5. CCN aerosols, by nucleating more numerous smaller cloud drops, brighten clouds by the Twomey effect and reflect more solar radiation back to space while cooling the layer below cloud tops.
6. In a very pristine atmosphere, where large S can exist, adding CCN leads to reduced S, additional condensation, and invigoration of shallow water clouds, which then reflect more solar energy to space.
7. CCN, by suppressing precipitation in marine Sc, allow the existence of a full cloud cover, along with a very large ($>100\,W\,m^{-2}$) increase in the reflected solar radiation.
8. In deeper clouds, CCN suppressing warm rain causes invigoration by the mechanism of added release of latent heat, accompanied by greater melting and evaporation cooling at low level. This leads to deeper

convective overturning, stronger vertical and horizontal winds, and stronger rain intensities, followed by longer periods to recover from the instability.

9. The deep cloud invigoration redistributes precipitation in time and space, followed by changes in air temperature and moisture.

10. The changes in temperature due to the differences in latent heating lead to changing of air circulation systems and weather patterns.

11. The deep cloud invigoration causes greater reflectance of solar radiation, which is countered to unknown extent by reduction in the thermal radiative cooling from the colder and more expansive cloud tops.

12. The deep cloud invigoration detrains more vapor into the upper troposphere, which serves there as a potent greenhouse gas.

13. Ice nuclei aerosols glaciate supercooled cloud water faster and enhance precipitation in the case of otherwise long-lived water clouds.

14. Ice nuclei, by glaciating supercooled layer clouds, which are abundant in the polar regions but can occur even in the tropics at heights above 5 km, cause their dissipation. This creates a negative forcing during daylight, but a positive forcing at night.

Accounting for all these aerosol effects requires accounting for the energy budget. This implies that doing so correctly should result in a closure of all the aerosol effects and other components of the energy budget, along with documenting the physical processes as listed here. This can be best done in the form of a box closure experiment, which is described in the next sections.

5.2. A Box Experiment for Representing All Fluxes In and Out of a Cube Within a GCM

The essence of a GCM is the calculation of all the fluxes of energy and mass in all their forms between adjacent grid boxes. The TOA energy balance is the net radiative energy flux through the top of the model, and in its global integrated form over time and space, it represents the global heat change. When accounting for the heat that is getting stored in the system in the form of change in ocean heat storage and melted ice, it is possible to obtain the global surface temperature change. Fluxes of mass at the surface include emission sources and some of the sinks for aerosols, vapor, and trace gases that occur there.

The ideal field experiment that would constrain a GCM is one that can determine all the fluxes within a 3-D domain, of several hundreds of kilometers on the side, inside a GCM. The regions of greatest interest, where aerosols have the greatest impact, are described in sections 2.5 and 2.6. The aerosol-dependent interactions of the processes within the cloud system at the regional scale and beyond can be quantified by the measured fluxes through the box boundaries. The fluxes of mass include air flow, water in all its forms in the air, at the surface, underground, and in the seas and oceans. The fluxes also include relevant trace constituents, such as aerosols and their precursors. The fluxes of energy include solar and thermal radiation, sensible heat in the atmosphere and oceans, and latent heat in the form of phase changes of the water substance.

5.3. The Scale of the Box Experiment

Clouds play a major role in modulating the energy and mass fluxes in all their forms. Therefore, the domain of the box closure experiment should contain the scale of a full lifecycle of a typically deep convective cloud system which is driven by the diurnal heating cycle. This is necessary for encompassing most of the buffering effects that may produce systematic and opposite responses of perturbations at different parts and/or different stages in the lifecycle of the cloud systems. For example, added aerosols may initially suppress rain but increase it later in the lifecycle of a convective rain cloud system. This implies a required domain size of about 5 × 5 degrees of latitude and longitude for the box experiment and a time scale of the full lifecycle of the convective system, which is at least 24 h.

5.4. The Design of the Measurements in the Box Experiment

Major issues in the design of such an experiment are the required accuracy for the various flux parameters, the kind of measurements, their point accuracy, and the spatial density that are required to achieve it. Different treatment is needed for the random and bias components of the measurement errors. Therefore, these two components have to be defined independently.

The estimation of the required temporal and spatial density of the various measurements can be done by a high-resolution simulation that includes the domain of the box, sampling the data from the sampling times

and locations, adding to them the instrument measurement errors, and calculating the fluxes at the box boundaries based on these sampled data. The error can be obtained by comparison of the calculated fluxes with the "true" simulated fluxes, as calculated based on the full simulated data. This is an essential step in the design of such an experiment. These calculations will quantify the frequency in space and time of the measurement means, as shown in Table 1. Their results may also change the priorities of the measurements, as estimated now and marked in Table 1.

Execution of such a box closure experiment requires a major effort of highly coordinated international cooperation, as it is beyond the possibility of any single research entity. Integration of such an effort is highly desirable, because the overall result goes much further than the sum of its components. The experiment that came closest to this goal was GATE [*Frank*, 1978], which measured the air and vapor mass flux that is consistent with the observed amounts of tropical rainfall, using a network of ship-borne radars and radiosondes at the equatorial Eastern Atlantic Ocean.

5.5. The Constituents of a Box Closure Experiment

Major components of a box closure are as follows:

1. Radiation: Surface and top of atmosphere solar and thermal radiative fluxes, partitioned according to the contributions from aerosols, clouds, water vapor, and other greenhouse gases

   a. Satellite measurements of TOA radiation, separated into cloud-free and cloudy conditions
   b. Surface downwelling radiation measurements during cloud-free and cloudy conditions
   c. Satellite measurements of precipitable water vapor
   d. Satellite measurements of upper tropospheric water vapor that is detrained from anvils
   e. Satellite measurements of CO_2 and other greenhouse gases
   f. Satellite measurements of cloud top temperatures, albedo, and emissivity

2. Nonradiative heat transfer: Surface sensible and latent heat fluxes; atmospheric and oceanic heat storage and transport; atmospheric vertical profiles of latent heating

   a. Measurements of surface energy budgets in different types of environments, such as forest, pasture, and water bodies
   b. Calculation of heat advection, based on the atmospheric motions and soundings, and accounting for latent heating

3. Air motions: The changes in air mass fluxes at the lateral boundaries determine the forcing of circulation systems. This requires the documentation of lateral mass and latent and sensible energy fluxes

   a. Radiosonde network enclosing the box area, complemented, and interpolated by satellite soundings
   b. Satellite-retrieved winds at various heights, based on tracking clouds and moisture features (Atmospheric Motion Vectors)
   c. Doppler S-Band radar measurements

4. Hydrological cycle: Precipitation measurements are required for obtaining a vertical profile of the latent heat and moisture fluxes

   a. 3-D coverage of Doppler and polarimetric measurements for measuring the dynamics of the precipitation systems and their hydrometeor types
   b. Correction for drop size and attenuation by polarimetric measurements
   c. Validation by rain gauge and disdrometer networks
   d. Separation into convective and stratiform components
   e. Hydrologic measurements of soil moisture, runoff, and stream flows
   f. Measurements of evaporation and evapotranspiration
   g. Atmospheric height-dependent moisture convergence, as measured by the sounding network and satellite measurements of moisture soundings

5. Aerosols and their precursors: The aerosol direct and cloud-mediated effects on the radiative and latent heat budget of the atmosphere, and the resultant changes in the atmospheric motions that feed back to the clouds, precipitation, and aerosols

   a. Surface measurements of precursor trace gases and aerosol size-dependent chemistry, hygroscopicity, and CCN activity

Table 1. The Measured Parameters, Measuring Instruments, and Achievable Accuracy for the Box Experiments[a]

Parameter	Marine Sc	Trade Wind Cumuli	Deep Convective	Achievable Accuracy	Instrument	Platform
Radiation						
Satellite measurements of TOA radiation, separated to cloud-free and cloudy conditions	H	H	H	2 W m^{-2} for SW instantaneous grid point measurement; 3.7 W m^{-2} for LW [Loeb et al., 2009 JC]	MODIS, CERES	Satellite
Surface downwelling radiation measurements during cloud-free and cloudy conditions	H	H	H	LW: 1%; SW: 2% (daily) [Wild et al., 2013] +3 W/m² representativeness error of a point observation for regional (1°) means [Hakuba et al., 2013]	Pyranometer (SW total), Pyrheliometer (SW direct), Pyrgeometer (LW)	Surface
Satellite measurements of water vapor, with emphasis on upper tropospheric vapor that is detrained from anvils.	L	L	H	10–30% [Hegglin et al., 2008; Stiller et al., 2012 and references therein]	ACE-FTS, MIPAS, AURA-MLS, AIRS	Satellite
Satellite measurements of CO_2 and CH_4 (near-surface-sensitive column-averaged dry air mole fractions)	M	M	M	CO_2 0.5–1%, CH4 1% [Buchwitz et al., 2014]	CO_2, CH_4: SCIAMACHY, GOSAT	Satellite
Tropospheric ozone: Tropospheric column or layer averaged mixing ratio				Tropospheric ozone: 10–20% [Zhang et al., 2010; Boynard et al., 2009]	Tropospheric ozone: TES, OMI, IASI	
Satellite measurements of cloud top temperatures, albedo and emissivity.	H	H	H	Temperature: ~ ±5 K for optically thin clouds ±1 K for optically thick clouds	AIRS and TOVS (T and Emissivity)	EOS Aqua (AIRS)
				Emissivity: ±0.05 for effective emissivity > 0.50; ±0.15 for emissivity < 0.50	CERES (Albedo)	Various NOAA polar-orbiting satellites (TOVS)
				Albedo: No absolute uncertainty reported; Stability better than 1%/year	MISR-MODIS-CERES (TOA Flux)	EOS Terra and Aqua (MODIS, CERES)
				SW TOA Flux: ~ 4% for all-sky, 2–3% over thick cloud		EOS Terra (MISR)
Nonradiative heat transfer:						
Surface sensible and latent heat fluxes. Atmospheric and oceanic heat storage and transport; atmospheric vertical profiles of latent heating.	H	H	H	Sensible and latent heat fluxes: ~15–20% half-hourly (~5% daily) random error, order of 10–20% surface energy balance closure deficit [Kessomkiat et al., 2013]	Sonic anemometer for fluxes	
Calculation of heat advection, based on the atmospheric motions and soundings, and accounting for the latent heating.	H	H	H	0.25 K d^{-1} of atmospheric heating		Soundings and satellites, aircraft
Air motions:						
Air motions: The changes in air mass fluxes at the lateral boundaries determine the forcing of circulation systems. This requires the documentation of lateral mass and latent and sensible energy fluxes.	H	H	H	Divergence of 0.01 kg m^{-3} h^{-1}		Soundings and satellites, aircraft
	M	M	M	5 m/s, 30 km		Satellite

Table 1. (continued)

Parameter	Marine Sc	Trade Wind Cumuli	Deep Convective	Achievable Accuracy	Instrument	Platform
Satellite-retrieved winds at various heights, based on tracking clouds and moisture features (Atmospheric Motion Vectors). Hydrological cycle	H	H	H			
Doppler S-Band radar measurements (clear air motions)	H	H	H	1 km, 1 m/s		Surface radars
Precipitation measurements are required for obtaining a vertical profile of the latent heat and moisture fluxes.	H	H	H	10% of the rainfall accumulation	Polarimetric Radar and rain gauges	Surface and satellite radars
3D coverage of Doppler and polarimetric hydrometeor type and size measurements	M	M	H	20% of MVD	Polarimetric radar	Surface radar
3D evolution of drizzle in MSC, with a cloud radar	H	M	M	Sensitivity of −15 dBZ	Cloud radars	Surface and satellite radars
Separate to convective and stratiform components	—	—	H	10% of the rainfall accumulation	Radar data analysis	
Hydrologic measurements of soil moisture, runoff, and stream flows.	NA	NA	M	10%	Stream flows	
Measurements of evaporation and evapotranspiration.	H	H	H	see latent heat flux: ~15–20% half-hourly (~5% daily) random error) [Kessomkiat et al., 2013]	Link to latent heat	
Atmospheric height-dependent moisture convergence, as measured by the sounding network and satellite measurements of moisture soundings.	H	H	H	0.0001 kg m^{-3} h^{-1}	Link to soundings lateral fluxes	
Aerosols and their precursors:						
Measurements of precursor gases	M	M	M	For most inorganic precursors gasses typically better than 5%: e.g., 1% or 0.2 ppb for SO$_2$	Monitor instruments	Airplane, surface
Aerosol size distribution	H	H	H	±10% in number size distribution in submicron ranges from 20 to 200 nm [Wiedensohler et al., 2012], decreasing accuracy (±30%) at higher particle sizes. Total particle number concentrations better than ±5%.	SMPS or DMPS APS, PCASP (supermicron)	Airplane, lidar, surface
Measurements of size-resolved aerosol chemistry	M	M	M	At best 0.1 µg/m^3 for size specific speciation, 25% for PM1 [Canagaratna et al., 2007]. Lower detection limit varying with species, 0.03 µg m^{-3} (nitrate, sulfate, and chloride) up to 0.5 µg m^{-3} (organics) [Drewnick et al., 2009]	AMS, time of flight mass spectrometer	Airplane, surface
Measurements of aerosol hygroscopicity and CCN-activity	M	M	M	Better than ±20% in hygroscopicity parameter [Su et al., 2010]. For hygroscopic growth factor, typically ±0.05 [Swietlicki et al., 2008]. For hygroscopic growth factor, typically ±0.05 [Swietlicki et al., 2008]	CCNC, HTDMA	Airplane, surface
CCN activation spectra including giant CCN	H	H	H	Similar to aerosol hygroscopicity, above	DMPS, SMPS, CCNC, PCASP	Airplane, surface
Ice nucleating activity of the aerosols	N/A	N/A	H	Better than order of magnitude in the activated fraction [Jones et al., 2011],	INC	Airplane, surface

Table 1. (continued)

Parameter	Marine Sc	Trade Wind Cumuli	Deep Convective	Achievable Accuracy	Instrument	Platform
Surface sun photometers (spectral AOD)	M	M	M	14% for activated fraction in deposition freezing [Kanji et al., 2013] Cimel 0.01 [Eck et al., 2010], Microtops 0.02 [Ichoku et al., 2002]	sun photometers (Cimel)	Airplane, surface
Satellite measurements of aerosol parameters: AOD, SSA, spectral AOD, depolarization ratio, UVAAI.	H	H	H	AOD: The larger of 0.05 or 20% over land; the larger of 0.03 or 10% over dark water. SSA—qualitative two-to-four bins between very absorbing and nonabsorbing. Particle size—qualitative fine/coarse ratio over water from MODIS; qualitative, three-to-five size bins from MISR UVAI—Precision of 0.1 for AI > 0.8 over ocean, and for AI > 0.5 over land. from OMI [Torres et al., 2013]		Satellite
Cloud-aerosol interactions The aerosol direct and cloud-mediated effects on the radiative and latent heat budget of the atmosphere, and the resultant changes in the atmospheric motions that feed back to the clouds, precipitation and aerosols. The great challenge here is disentangling the aerosols from meteorological effects on clouds and their radiative effects.						
Cloud cover, optical depth, albedo and radiative effects under different aerosol conditions in as similar meteorology as possible. Study of adjacent clouds in and out of aerosol plumes can be effective.	H	H	H	LWP, r_e, N_d, cloud optical depth for convective and layer clouds	Data processing	
For layer clouds: satellite retrieved cloud top effective radius, liquid water path and cloud drop concentrations. Validation with aircraft measurements and cloud radar	H	H	H	LWP, r_e, N_d, cloud optical depth for convective and layer clouds	Data processing	
For convective clouds: satellite-retrieved vertical profiles of cloud particle effective radius and thermodynamic phase. Validation with aircraft measurements.	H	H	H	10% of the effective radius	Data processing	
Cloud base updraft spectra, by vertically pointing radar and lidar, and by aircraft and UAVs.	H	H	H	On the order of 0.1 m s^{-1}	Radar, lidar	Surface and aircraft
Cloud base CCN, as obtained from cloud base updrafts and drop number concentrations.	H	H	H	30% of drop concentrations at cloud base	Data processing	
Secondary activation of aerosols in deep convective clouds. This can be inferred by the satellite retrieved vertical profiles of cloud particle effective radius, and validated in more detailed by aircraft.	N/A	M	M	30% of small drop and ice concentrations at any level	Data processing	

Table 1. (continued)

Parameter	Marine Sc	Trade Wind Cumuli	Deep Convective	Achievable Accuracy	Instrument	Platform
New particle formation	M	M	M	Qualitative in smallest sizes (diameter < 3 nm), similar to particle number size distribution measurements in larger sizes (Kulmala et al., 2012] 20% of MVD	AIS, NAIS, DMPS, PSM	Surface and aircraft
Vertical profile of hydrometeor types, concentrations and sizes, by surface and space borne radars.	M	M	H		link to polarimetric radar measurements	
Detrained aerosols from the clouds at various heights, as measured by aircraft.	M	M	M	Similar to the size distribution measurements (above)	SMPS, PCASP	aircraft
Scales						
Horizontal along wind	1500 km	500 km	500 km			
Horizontal across wind	200 km	200 km	500 km?			
Vertical resolution	50 m	100 m	100..400 m			
Horizontal resolution	50 m	100 m	1000 m			
Temporal scale	3 days	1 day	1 day			
Potential locations	Offshore California, Offshore Chile, Canary Islands or Cape Verde	South China Sea, Gulf of Mexico	Indonesia, Amazonas, Congo			

[a]The importance codes in columns 2–4 are as follows: High (essential, must be included), M (important to be included), L (low priority). Instrument names are as follows: AIS, Aerosol and Air Ion Spectrometer; AMS, Aerosol Mass Spectrometer; CCNC,Cloud Condensation Nuclei Counter; Cimel, Sun photometer; DMPS, Differential Mobility Particle Sizer; HTDMA, Hygroscopic Tandem Differential Mobility Analyzer; INC, Ice Nuclei Counter; NAIS, Nanometer aerosol and Air Ion Spectrometer; PCASP, Passive Cavity Aerosol Spectrometer Probe; PSM, Particle Size Magnifier; SMPS, Scanning Mobility Particle Sizer.

b. Ice nucleating activity of the aerosols

c. Airborne measurements of the same parameters, and spectral scattering and absorption coefficients throughout the vertical profile; airborne lidar

d. Surface sun photometers

e. Satellite measurements of aerosol parameters: AOD, SSA, Ångström exponent, depolarization ratio. Aerosol types can be retrieved based on these and on multi-angle measurements, as described in section 3.3.6

6. Cloud-aerosol interactions: The aerosol direct and cloud-mediated effects on the radiative and latent heat budget of the atmosphere, and the resultant changes in the atmospheric motions that feed back to the clouds, precipitation, and aerosols. The great challenge here is disentangling the effects of aerosols from meteorological effects on clouds and their radiative effects

a. Cloud cover, optical depth, albedo, and radiative effects under different aerosol conditions in as similar meteorology as possible; study of adjacent clouds in and out of aerosol plumes can be effective

b. For layer clouds: satellite retrieved cloud top effective radius, liquid water path and cloud drop concentrations; validation with aircraft measurements

c. For convective clouds: satellite-retrieved vertical profiles of cloud particle effective radius and thermodynamic phase; validation with aircraft measurements

d. Cloud base updraft spectra, by vertically pointing radar and lidar, and by aircraft and unmanned aerial vehicles (UAVs)

e. Cloud base CCN, as obtained from cloud base updrafts and drop number concentrations

f. Secondary nucleation of aerosols in deep convective clouds; this can be inferred by the satellite-retrieved vertical profiles of cloud particle effective radius and validated more detail by aircraft

g. Vertical profile of hydrometeor types, concentrations, and sizes, by surface and space borne radars

h. Detrained aerosols from the clouds at various heights, as measured by aircraft

i. Composition and longevity of supercooled layer clouds, and their dependence on CCN and IN, as measured by aircraft, lidar, radar, and satellites

j. Cirrus microstructure, radiative effects and their dependence on CCN and IN, as measured by aircraft, lidar, radar, and satellites

5.6. Recommended Cloud Regimes and Locations for the Box Experiment

The criteria for the selection of the cloud regimes and sites for box experiments are as follows: (1) cloud regimes that cover a large fraction of the world, (2) cloud regimes that are known or suspected to be susceptible to aerosol effects, (3) regimes where the clouds are not dominated by

synoptic forcing, and (4) regions that experience large variability of aerosols for the same cloud and meteorological conditions.

The cloud regimes and the geographic areas that best satisfy these conditions are as follows:

1. Marine stratocumulus
   a. Off the coast of Chile
   b. Off the coast of California
   c. The Canary Islands or Cape Verde
2. Trade wind cumulus
   a. Southwest China Sea off the coast of Vietnam in winter
   b. The western Gulf of Mexico in winter
3. Deep tropical convection
   a. Indonesia
   b. The Amazon
   c. Congo

5.7. Process Studies

In addition to the box experiment, process studies are also needed, as the model simulations are lacking much knowledge of the processes involved.

Process studies of high priority, addressing major gaps of knowledge, include the following:

1. Ice forming processes, both primary and secondary.
2. The nature of mixing of convective clouds—homogeneous versus inhomogeneous. This has major implications for the ability to retrieve N_a from satellites.
3. Secondary activation well above cloud base.
4. Environmental controls of cloud base updraft.
5. Impact of chemical composition of aerosols on their CCN activity.

These topics are already well recognized and the subject of current research. Numerical experiments might highlight missing physics not yet recognized and being researched.

5.8. Global Experiments

The results of the box experiment are configured for constraining the parameterization of the global models. The improvements in the global models and in the satellite retrievals will be implemented and applied to regional and global scales. Then the model simulations and satellite retrievals at these larger scales will be checked for consistency.

5.9. Recommendations

Our overall objective is to facilitate the understanding of the role of ACPC in climate forcing, which leads to reducing the uncertainties of the aerosol effects and its anthropogenic forcing component. Here we present recommendations for the ways to reach this goal. There are two levels of experiments: (1) case study process experiments and (2) box closure experiments.

The essence of a GCM is the calculation of fluxes of mass and energy between the adjacent grid cells and the upper and lower boundaries of the domain, i.e., surface and TOA. The box closure experiment measures the fluxes through the boundaries of a box that include several GCM grid cells to the extent possible. In order to reach physically meaningful closures, the box of the closure experiment must be at the minimum time and space scales of the lifecycle of the convective systems, which is about $5 \times 5°$ and 24 h. This has to be repeated for a large number of convective events. In addition, in order to reach the necessary accuracy of the calculated fluxes, the box experiment needs to have a "critical mass" with respect to the measurements that need to be made in order to be effective. There are incremental steps that can be taken before the larger box experiment is performed. Such steps include the following: (1) perform closure studies of clouds and CCN, using satellite, airborne, and surface measurements that constrain numerical simulations; (2) use a combination of measurements and models for disentangling meteorology and aerosol microphysical effects on clouds on a case study basis; and (3) 3-D combined retrievals of cloud and nearby aerosol properties.

Design box closure experiments, separately for marine Sc, trade winds, and tropical deep convective clouds. The focus of these experiments will be on quantifying to the extent possible the fluxes of energy and mass in all their forms at the boundaries of the box. This includes radiation budgets at the surface and TOA. The design of the box experiment can be made along the following outline:(a) running the numerical simulations for the design and evaluation of the scales and magnitudes of the various terms and measurables, (b) compare the results with existing measurements and identify discrepancies and gaps, (c) identify smaller scale studies that can address the gaps without the need for the whole box experiment, (d) evaluate the needed accuracy and spatial and temporal sampling strategy for the various measurements, and (e) identify the appropriate instruments and their platforms for the required measurements.

The expected outcomes of the box experiments are as follows: (1) improved interpretation of satellite measurements of cloud-aerosol interactions; (2) improved constraints on the aerosol indirect effects for the marine Sc, trade wind and deep convective clouds systems, which in combination represent most of the Earth's atmosphere; (3) improved parameterization of cloud-aerosol interactions for simulations at scales from cloud-resolving to global; and (4) reduction of the uncertainty in the aerosol effects on earth energy budget and the anthropogenic forcing component.

As the scale of these box experiments is larger than any single entity can support, large-scale international cooperation and coordination for realizing this vision will be required.

6. Summary

An overarching goal of the research on ACPC interactions is the ability to realistically represent them in numerical weather prediction and climate models. In numerical weather predictions, the goal is to enable a realistic representation of precipitation characteristics, including extreme events, along with generally more realistic weather forecasts. In climate prediction, ACPC research aims at a realistic representation of the radiative forcing by anthropogenic aerosols and of cloud- and aerosol-related feedbacks in the climate system.

The processes of ACPC originate at the microphysical scale. For many of these processes, theories and fundamental understanding are available (e.g., droplet activation and generation of warm rain (section 2.1) or aerosol scavenging (section 2.4). For others, fundamental knowledge is scarce and science relies on empirical studies (e.g., ice nucleation and precipitation formation in mixed-phase clouds). How these microphysical processes translate into macrophysical processes such as precipitation fluxes at the surface, latent heating of the atmosphere, or radiation fluxes depends on cloud dynamics and differs between aerosol-cloud regimes due to a large variety of feedbacks, sometimes enhancing, sometimes "buffering" initial perturbations (section 2.2). Finally, effects of aerosols on large-scale climate phenomena are difficult to analyze from observations alone. Such studies have to rely on a model-data combination, applying models that represent the relevant ACPC interactions as realistically as possible and as comprehensively as necessary (sections 2.5 and 2.6).

In consequence, the challenge is twofold, namely, to empirically develop an understanding of (1) how microphysical and cloud-dynamical processes of ACPC function (a process-scale understanding) and (2) how the ACPC interplay affects the energy and water cycle, specifically how it affects diabatic heating, at a cloud-system scale; i.e., how it can be parameterized at horizontal scales from 1 km to 100 km for numerical weather predictions and GCMs (a statistical understanding).

The latter approach needs to rely on simplifications, and such assumptions can be validated at least for specific aerosol-cloud regimes (section 2.1).

Since model parameterizations have to apply to all weather situations, observations need to cover all relevant aerosol-cloud regimes. Satellite data covering the global scale and long time series have proven to be of outstanding relevance to ACPC research.

Satellite observations available today offer a tremendous wealth of data, covering several decades of basic aerosol and cloud retrievals and covering several years of comprehensive aerosol, cloud, precipitation, and radiation retrievals (section 3.3). Metrics to quantify aerosol-cloud-precipitation interactions have been defined based on available satellite retrievals (section 2.3) and have proven very useful for evaluating models.

However, the very quantities necessary to assess the effect of aerosol on clouds, the cloud condensation nuclei (CCN) and ice nuclei (IN) concentrations, are not available from current retrievals (sections 3.1, 3.2, and 3.6). Indeed, current satellites do not allow the retrieval of aerosol properties in situations with clouds or precipitation present, and thus, ACPC studies based on satellite data, in any case, cannot rely directly on satellite retrievals without assumptions or additional information (sections 4.2 and 4.5). But present retrievals of cloud properties are inadequate in several regards: For liquid clouds, droplet number concentration retrievals rely on many assumptions, and for ice clouds, information on crystal number concentrations, shapes, and orientations is unavailable or very uncertain.

One option to improve the situation for CCN retrievals may be to apply a new concept for a future satellite mission, using clouds in the atmosphere as a "natural cloud chamber" (section 3.5). Another option is to advance methods for aircraft observations (sections 4.3 and 4.4).

For a breakthrough in scientific research on ACPC, however, this study argues that a coordinated effort using observations and models from process to large scales is necessary. Such a "box experiment" would actually need to address not just one, but ideally all relevant aerosol-cloud regimes, and cover at least the scale of several general circulation model grid boxes.

Notation

AAI	aerosol absorbing index
AATSR	Advanced Along Track Scanning Radiometer
ACE/FTS	Atmospheric Chemistry Experiment/Fourier transform spectrometer
ACI	Aerosol Cloud Interactions effect
ACPC	aerosol-cloud-precipitation-climate interactions
AERONET	Aerosol Robotic Network
AI	aerosol index
AIRS	Atmospheric Infrared Sounder
AMMA	Africa Monsoon Multiscale Analysis
AMSR-E	Advanced Microwave Scanning Radiometer - EOS
AOD	aerosol optical depth
APS	Aerosol Polarimetry Sensor/Aerosol Particle Sizer
ARE	Aerosol Radiative Effects
ATSR	Along Track Scanning Radiometer
AURA-MLS	Microwave Limb Sounder onboard AURA satellite
AVHRR	Advanced Very High Resolution Radiometer
BC	black carbon
BRDF	bidirectional reflectance distribution function
CAIPEEX	Cloud Aerosol Interaction and Precipitation Enhancement Experiment
CALIOP	Cloud-Aerosol Lidar with Orthogonal Polarization
CALIPSO	Cloud-Aerosol Lidar and Infrared Pathfinder Satellite Observation
CCI	Aerosol Climate Change Initiative
CCN	(number concentration of) cloud condensation nuclei
CERES	Clouds and Earth's Radiant Energy System
CHASER	Clouds, Hazards, and Aerosols Survey for Earth Researchers
d	aerosol or cloud drop diameter
D^*	cloud depth for reaching r_e^* and initiation of rain
EarthCARE	Earth Clouds, Aerosols and Radiation Explorer
EHP	Elevated Heat Pump
ENSO	El Niño–Southern Oscillation
ENVISAT	environmental satellite
EOS	Earth Observing System
ERB	Earth Radiation Budget
ESA	European Space Agency
f	fractional cloud cover

GCM	global circulation model
GERB	Geostationary Earth Radiation Budget
GEWEX	Global Energy and Water Cycle Experiment
GMI CTM	Global Model Initiative Chemistry Transport Model
GOES-R	Geostationary Operational Environmental Satellite - R
GOME	Global Ozone Monitoring Experiment
GOSAT	Greenhouse Gases Observing Satellite
GPCP	Global Precipitation Climatology Project
GPM	Global Precipitation Mission
HIAPER	High-performance Instrumented Airborne Platform for Environmental Research
HIPPO	HIAPER Pole-to-Pole
HSRL	high spectral resolution lidar
IASI	Infrared Atmospheric Sounding Interferometer
IGAC	International Global Atmospheric Chemistry
IGBP	International Geosphere–Biosphere Programme
IGP	Indo-Gangetic Plain
iLEAPS	Integrated Land Ecosystem–Atmosphere Processes Study
IPCC	Intergovernmental Panel of Climate Change
IN	ice nuclei
IR	infrared radiation
IRS	InfraRed Sounder
ISSI	International Space Science Institute
ITCZ	Intertropical Convergence Zone
JAXA	National Space Development Agency of Japan
κ	aerosol hygroscopicity parameter
LIDAR	laser imaging, detection and ranging
LW	longwave radiation
LWP	liquid water path
MAS	MODIS airborne simulator
MASTER	MODIS/ASTER airborne simulator
MERIS	Medium Resolution Imaging Spectrometer
MIPAS	Michaelson Interferometer for Passive Atmospheric Sounding
MISR	Multiangle Imaging SpectroRadiometer
MJO	Madden-Julian Oscillations
MLS	Microwave Limb Sounder
MODIS	Moderate-Resolution Imaging Spectroradiometer
MOPITT	Measurements Of Pollution In The Troposphere
MSG	METEOSAT Second Generation
MSPI	Multiangle SpectroPolarimetric Imager
MTG	METEOSAT Third Generation
MTG-S	MTG-sounder
MVD	Median Volume Diameter
N_a	number of activated cloud drops at cloud base
N_{ccn}	number concentration of CCN
N_d	cloud drop number concentration
N_{IN}	number concentration of IN
NASA	National Aeronautics and Space Agency
NIR	near-infrared
NPP/VIIRS	Suomi National Polar-orbiting Partnership/ Visible Infrared Imaging Radiometer Suite
OLCI	Ocean Land Color Instrument
OMI	Ozone Monitoring Instrument
OSSEs	Observing System Simulation Experiments
PACS	Passive Aerosol and Cloud Suite

PARASOL	Polarization & Anisotropy of Reflectances for Atmospheric Sciences coupled with Observations from a Lidar
PODEX	Polarimeter Definition Experiment
POLDER	Polarization and Directionality of the Earth's Reflectances
r_e	cloud drop effective radius
$r_{e,crit}$	critical r_e for initiation of rain
S	water vapor supersaturation
SAT-ACPC	Remote Sensing of Aerosol-Cloud-Precipitation-Climate interactions
Sc	Stratocumulus clouds
SCD	Slant Column Density
SCIAMACHY	Scanning Imaging Absorption Spectrometer for Atmospheric Chartography
SLSTR	Sea and Land Surface Temperature Radiometer
SOA	secondary organic aerosol
SSA	single-scattering albedo
SST	sea surface temperature
SW	shortwave radiation
T	cloud-top temperature
T_g	glaciation temperature
TES	Tropospheric Emission Spectrometer
TOA	top of the atmosphere
TOMS	Total Ozone Mapping Spectrometer
TOVS	TIROS Operational Vertical Sounder
TP	tropopause
TRMM	Tropical Rainfall Measuring Mission
TRMM-LIS	Lightning Imaging Sensor onboard the Tropical Rainfall Measuring Mission satellite
TROPOMI	TROPOspheric Monitoring Instrument
τ	cloud optical thickness
UAV	unmanned aerial vehicle
UTC	coordinated universal time
UTLS	upper troposphere and lower stratosphere.
UV	ultra violet radiation
UVAI	ultra violet aerosol index
UVD	ultraviolet visible near-infrared spectral range
VCD	Vertical Column Density
VOC	volatile organic compounds
W_b	cloud base updraft
WCRP	World Climate Research Program
3MI	multiviewing, multichannel, multipolarization imaging mission

References

Abish, B., and K. Mohanakumar (2011), Role of fine mode aerosols in modulating cloud properties over industrial locations in north India, *Ann. Geophys.*, *20*, 1605–1612, doi:10.5194/angeo-29-1605-2011.

Ackerman, A. S., O. B. Toon, and P. V. Hobbs (1993), Dissipation of marine stratiform clouds and collapse of the marine boundary layer due to the depletion of cloud condensation nuclei by clouds, *Science*, *262*, 226–229.

Ackerman, A. S., O. B. Toon, D. E. Stevens, A. J. Heymsfield, V. Ramanathan, and E. J. Welton (2000), Reduction of tropical cloudiness by soot, *Science*, *288*, 1042–1047.

Ackerman, A. S., M. P. Kirkpatrick, D. E. Stevens, and O. B. Toon (2004), The impact of humidity above stratiform clouds on indirect aerosol climate forcing, *Nature*, *432*, 1014–1017.

Alexandrov, M. D., B. Cairns, C. Emde, A. S. Ackerman, and B. van Diedenhoven (2012), Accuracy assessments of cloud droplet size retrievals from polarized reflectance measurements by the research scanning polarimeter, *Remote Sens. Environ.*, *125*, 92–111, doi:10.1016/j.rse.2012.07.012.

Anderson, T. L., R. J. Charlson, D. M. Winker, J. A. Ogren, and K. Holmen (2003), Mesoscale variations of tropospheric aerosols, *J. Atmos. Sci.*, *60*, 119–136.

Andreae, M. O. (2007), Aerosols before pollution, *Science*, *315*, 50–51.

Andreae, M. O. (2009a), A new look at aging aerosols, *Science*, *326*, 1493–1494.

Andreae, M. O. (2009b), Correlation between cloud condensation nuclei concentration and aerosol optical thickness in remote and polluted regions, *Atmos. Chem. Phys.*, *9*, 543–556.

Andreae, M. O., and V. Ramanathan (2013), Climate's dark forcings, *Science*, *340*(6130), 280–281.

Andreae, M. O., and D. Rosenfeld (2008), Aerosol–cloud–precipitation interactions. Part 1. The nature and sources of cloud-active aerosols, *Earth Sci. Rev.*, *89*, 13–41.

Andreae, M. O., B. Stevens, G. Feingold, S. Fuzzi, M. Kulmala, W. K. Lau, U. Lohmann, D. Rosenfeld, and P. Siebesma (2009), Aerosols, Clouds, Precipitation and Climate (ACPC): Science Plan & Implementation Strategy, Melbourne, August 2009. [Available at http://www.gewex.org/ssg-22/ACPC_SciencePlan_FINAL.pdf.]

Atlas, D., and C. R. Williams (2003), The anatomy of a continental tropical convective storm, *J. Atmos. Sci.*, *60*, 3–15, doi:10.1175/1520-0469(2003)060<0003:TAOACT>2.0.CO;2.

Balkanski, Y. J., D. J. Jacob, G. M. Gardner, W. C. Graustein, and K. K. Turekian (1993), Transport and residence times of tropospheric aerosols inferred from a global three-dimensional simulation of ^{210}Pb, *J. Geophys. Res.*, *98*, 20,573–20,586, doi:10.1029/93JD02456.

Barth, M., P. Rasch, J. T. Kiehl, C. M. Benkovitz, and S. E. Schwartz (2000), Sulfur chemistry in the National Center for Atmospheric Research Community Climate Model: Description, evaluation, features and sensitivity to aqueous chemistry, *J. Geophys. Res.*, *105*, 1387–1415, doi:10.1029/1999JD900773.

Bell, T. L., D. Rosenfeld, K.-M. Kim, J.-M. Yoo, M.-I. Lee, and M. Hahnenberger (2008), Midweek increase in U.S. summer rain and storm heights suggests air pollution invigorates rainstorms, *J. Geophys. Res.*, *113*, D02209, doi:10.1029/2007JD008623.

Bell, T. L., D. Rosenfeld, and K.-M. Kim (2009), Weekly cycle of lightning: Evidence of storm invigoration by pollution, *Geophys. Res. Lett.*, *36*, L23805, doi:10.1029/2009GL040915.

Bellouin, N., O. Boucher, J. Haywood, and M. S. Reddy (2005), Global estimate of aerosol direct radiative forcing from satellite measurements, *Nature*, *438*, 1138–1141.

Bellouin, N., A. Jones, J. Haywood, and S. A. Christopher (2008), Updated estimate of aerosol direct radiative forcing from satellite observations and comparison against the Hadley Centre climate model, *J. Geophys. Res.*, *113*, D10205, doi:10.1029/2007JD009385.

Benedetti, A., et al. (2009), Aerosol analysis and forecast in the European Centre for medium-range weather forecasts Integrated Forecast System: 2. Data assimilation, *J. Geophys. Res.*, *114*, D13205, doi:10.1029/2008JD011115.

Bennartz, R., J. Fan, J. Rausch, L. Y. R. Leung, and A. K. Heidinger (2011), Pollution from China increases cloud droplet number, suppresses rain over the East China Sea, *Geophys. Res. Lett.*, *38*, L09704, doi:10.1029/2011GL047235.

Biasutti, M., and A. Giannini (2006), Robust Sahel drying in response to late 20th century forcings, *Geophys. Res. Lett.*, *33*, L11706, doi:10.1029/2006GL026067.

Bister, M., and M. Kulmala (2011), Anthropogenic aerosols may have increased upper tropospheric humidity in the 20th century, *Atmos. Chem. Phys.*, *11*, 4577–4586, doi:10.5194/acp-11-4577-2011.

Bollasina, M. A., Y. Ming, and V. Ramaswamy (2012), Anthropogenic aerosols and the weakening of the South Asian summer monsoon, *Science*, *334*, 502–505.

Bond, T. C., C. Zarzycki, M. G. Flanner, and D. M. Koch (2011), Quantifying immediate radiative forcing by black carbon and organic matter with the Specific Forcing Pulse, *Atmos. Chem. Phys.*, *11*, 1505–1525, doi:10.5194/acp-11-1505-2011.

Bond, T. C., et al. (2013), Bounding the role of black carbon in the climate system: A scientific assessment, *J. Geophys. Res. Atmos.*, *118*, 5380–5552, doi:10.1002/jgrd.50171.

Booth, B. B., B. Dunstone, N. J. Halloran, P. R. Andrews, and T. B. Nicolas (2013), Aerosols implicated as a prime driver of twentieth-century North Atlantic climate variability, *Nature*, *484*, 228–232, doi:10.1038/nature10946.

Bovensmann, H., J. P. Burrows, M. Buchwitz, J. Frerick, S. Noël, V. V. Rozanov, K. V. Chance, and A. P. H. Goede (1999), SCIAMACHY: Mission objectives and measurements modes, *J. Atmos. Sci.*, *56*, 127–150.

Boynard, A., C. Clerbaux, P.-F. Coheur, D. Hurtmans, S. Turquety, M. George, J. Hadji-Lazaro, C. Keim, and J. Meyer-Arnek (2009), Measurements of total and tropospheric ozone from IASI: Comparison with correlative satellite, ground-based and ozonesonde observations, *Atmos. Chem. Phys.*, *9*, 6255–6271, doi:10.5194/acp-9-6255-2009.

Brenguier, J. L., H. Pawlowska, L. Schüller, R. Preusker, J. Fischer, and Y. Fouquart (2000), Radiative properties of boundary layer clouds: Droplet effective radius versus number concentration, *J. Atmos. Sci.*, *57*, 803–821.

Bretherton, C. S., P. N. Blossey, and J. Uchida (2007), Cloud droplet sedimentation, entrainment efficiency, and subtropical stratocumulus albedo, *Geophys. Res. Lett.*, *34*, L03813, doi:10.1029/2006GL027648.

Buchwitz, M., et al. (2014), The Greenhouse Gas Climate Change Initiative (GHG-CCI): Comparison and quality assessment of near-surface-sensitive satellite-derived CO_2 and CH_4 global data sets, *Remote Sens. Environ.*, doi:10.1016/j.rse.2013.04.024, in press.

Burrows, J. P., et al. (1999), The Global Ozone Monitoring Experiment (GOME): Mission concept and first scientific results, *J. Atmos. Sci.*, *56*, 151–175.

Burton, S. P., M. A. Vaughan, R. A. Ferrare, and C. A. Hoststler (2014), Separating mixtures of aerosol types in airborne High Spectral Resolution Lidar data, *Atmos. Meas. Tech.*, *7*, 419–436, doi:10.5194/amt-7-419-2014.

Cai, W., T. Cowan, A. Sullivan, J. Ribbe, and G. Shi (2010), Are anthropogenic aerosols responsible for the northwest Australia summer rainfall increase? A CMIP3 perspective and implications, *J. Clim.*, *24*, 2556–2564, doi:10.1175/2010JCLI3832.1.

Canagaratna, M. R., et al. (2007), Chemical and microphysical characterization of ambient aerosols with the aerodyne aerosol mass spectrometer, *Mass Spectrom. Rev.*, *26*(2), 185–222.

Carrió, G. G., and W. R. Cotton (2011), Investigations of aerosol impacts on hurricanes: Virtual seeding flights, *Atmos. Chem. Phys.*, *11*, 2557–2567.

Carslaw, K. S., et al. (2013), Large contribution of natural aerosols to uncertainty in indirect forcing, *Nature*, *503*, 67–71.

Cattrall, C., J. Reagan, K. Thome, and O. Dubovik (2005), Variability of aerosol and spectral lidar and backscatter and extinction ratios of key aerosol types derived from selected Aerosol Robotic Network locations, *J. Geophys. Res.*, *110*, D10S11, doi:10.1029/2004JD005124.

Chameides, W. L. (1986), Possible role of NO_3 in the nighttime chemistry of a cloud, *J. Geophys. Res.*, *91*, 5331–5337, doi:10.1029/JD091iD05p05331.

Chand, D., T. L. Anderson, R. Wood, R. J. Charlson, Y. Hu, Z. Liu, and M. Vaughan (2008), Quantifying above-cloud aerosol using spaceborne lidar for improved understanding of cloudy-sky direct climate forcing, *J. Geophys. Res.*, *113*, D13206, doi:10.1029/2007JD009433.

Chand, D., R. Wood, T. L. Anderson, S. K. Satheesh, and R. J. Charlson (2009), Satellite-derived direct radiative effect of aerosols dependent on cloud cover, *Nat. Geosci.*, *2*, 181–184.

Chandra, S., et al. (2009a), Tropical tropospheric ozone: Implications for dynamics and biomass burning, *Atmos. Chem. Phys.*, *9*, 4239–4249, doi:10.5194/acp-9-4239-2009.

Chandra, S., J. R. Ziemke, B. N. Duncan, T. L. Diehl, N. J. Livesey, and L. Froidevaux (2009b), Effects of the 2006 El Niño on tropospheric ozone and carbon monoxide: Implications for dynamics and biomass burning, *Atmos. Chem. Phys.*, *9*, 4239–4249, doi:10.5194/acp-9-4239-2009.

Charlson, R. J., J. H. Seinfeld, A. Nenes, M. Kulmala, A. Laaksonen, and M. C. Facchini (2001), Reshaping the theory of cloud formation, *Science*, *292*, 2026–2027.

Charlson, R., A. Ackerman, F.-M. Bender, T. Anderson, and Z. Liu (2007), On the climate forcing consequences of the albedo continuum between cloudy and clear air, *Tellus B*, *59*, 715–727, doi:10.1111/j.1600-0889.2007.00297.x.

Chen, B., and Y. Yin (2011), Modeling the impact of aerosols on tropical overshooting thunderstorms and stratospheric water vapor, *J. Geophys. Res.*, *116*, D19203, doi:10.1029/2011JD015591.

Chen, Y.-C., M. W. Christensen, L. Xue, A. Sorooshian, G. L. Stephens, R. M. Rasmussen, and J. H. Seinfeld (2012), Occurrence of lower cloud albedo in ship tracks, *Atmos. Chem. Phys.*, *12*, 8223–8235, doi:10.5194/acp-12-8223-2012.

Cherian, R., C. Venkataraman, J. Quaas, and S. Ramachandran (2013), GCM simulations of aerosol extinction, heating and effects on precipitation over India, *J. Geophys. Res. Atmos.*, *118*, 2938–2955, doi:10.1002/jgrd.50298.

Chiapello, I., J. M. Prospero, J. R. Herman, and N. C. Hsu (1999), Detection of mineral dust over the North Atlantic Ocean and Africa with the Nimbus 7 TOMS, *J. Geophys. Res.*, *104*(D8), 9277–9291, doi:10.1029/1998JD200083.

Chin, M., D. J. Jacob, G. M. Gardner, M. S. Foreman Fowler, P. A. Spiro, and D. L. Savoie (1996), A global three dimensional model of tropospheric sulfate, *J. Geophys. Res.*, *101*, 18,667–18,690, doi:10.1029/96JD01221.

Chin, M., R. B. Rood, S.-J. Lin, J.-F. Müller, and A. M. Thompson (2000), Atmospheric sulfur cycle simulated in the global model GOCART: Model description and global properties, *J. Geophys. Res.*, *105*, 24,671–24,687, doi:10.1029/2000JD900384.

Chin, M., P. Ginoux, S. Kinne, O. Torres, B. N. Holben, B. N. Duncan, R. V. Martin, J. A. Logan, A. Higurashi, and T. Nakajima (2002), Tropospheric aerosol optical thickness from the GOCART model and comparisons with satellite and sunphotometer measurements, *J. Atmos. Sci.*, *59*, 461–483.

Clarisse, L., P.-F. Coheur, F. Prata, J. Hadji-Lazaro, D. Hurtmans, and C. Clerbaux (2013), A unified approach to infrared aerosol remote sensing and type specification, *Atmos. Chem. Phys.*, *13*, 2195–2221, doi:10.5194/acp-13-2195-2013.

Coheur, P.-F., L. Clarisse, S. Turquety, D. Hurtmans, and C. Clerbaux (2009), IASI measurements of reactive trace species in biomass burning plumes, *Atmos. Chem. Phys.*, *9*, 5655–5667, doi:10.5194/acp-9-5655-2009.

Collier, J. C., and G. J. Zhang (2009), Aerosol direct forcing of Indian summer monsoon as simulated by NCAR CAM3, *Clim. Dyn.*, *32*, 313–332, doi:10.1007/s00382-008-0464-9.

Costantino, L., and F.-M. Bréon (2010), Analysis of aerosol-cloud interaction from multi-sensor satellite observations, *Geophys. Res. Lett.*, *37*, L11801, doi:10.1029/2009GL041828.

de Graaf, M., L. G. Tilstra, P. Wang, and P. Stammes (2012), Retrieval of the aerosol direct radiative effect over clouds from spaceborne spectrometry, *J. Geophys. Res.*, *117*, D07207, doi:10.1029/2011JD017160.

de Graaf, M., A. Apituley, and D. P. Donovan (2013), Feasibility study of integral property retrieval for tropospheric aerosol from Raman lidar data using principal component analysis, *Appl Opt.*, *52*(10), 2173–2186, doi:10.1364/AO.52.002173.

Del Castilo, A., et al. (2012), Pre-Aerosol, Clouds, and ocean Ecosystem (PACE) Mission Science Definition Team Report. [Available at http://dsm.gsfc.nasa.gov/pace_documentation/PACE_SDT_Report_final.pdf.]

de Leeuw, G., S. Kinne, J. F. Leon, J. Pelon, D. Rosenfeld, M. Schaap, P. J. Veefkind, B. Veihelmann, D. M. Winker, and W. von Hoyningen-Huene (2011), Retrieval of aerosol properties, in *The Remote Sensing of Tropospheric Composition From Space*, edited by J. P. Burrows, U. Platt, and P. Borrell, pp. 359–313, Springer, Berlin Heidelberg, doi:10.1007/978-3-642-14791-3.

de Leeuw, G., et al. (2013), Evaluation of seven European aerosol optical depth retrieval algorithms for climate analysis, *Remote Sens. Environ.*, doi:10.1016/j.rse.2013.04.023.

DeMott, P. J., A. J. Prenni, X. Liu, S. M. Kreidenweis, M. D. Petters, C. H. Twohy, M. S. Richardson, T. Eidhammer, and D. C. Rogers (2010), Predicting global atmospheric ice nuclei distributions and their impacts on climate, *Proc. Natl. Acad. Sci. U.S.A.*, *107*, 11,217–11,222.

Deuzé, J. L., et al. (2001), Remote sensing of aerosols over land surfaces from POLDER-ADEOS-1 polarized measurements, *J. Geophys. Res.*, *106*(D5), 4913–4926, doi:10.1029/2000JD900364.

Dey, S., G. L. Di, G. Zhao, A. L. Jones, and G. M. McFarquhar (2011), Satellite-observed relationships between aerosol and trade-wind cumulus cloud properties over the Indian Ocean, *Geophys. Res. Lett.*, *38*, L01804, doi:10.1029/2010GL045588.

Diner, D. J., et al. (2010), First results from a dual photoelastic-modulator-based polarimetric camera, *Appl. Opt.*, *49*, 2929–2946.

Donovan, D. P., H. W. Barker, R. J. Hogan, T. Wehr, M. Eisinger, D. Lajas, and A. Lefebvre (2013), Scientific aspects of the Earth clouds, Aerosols, and Radiation Explorer (EarthCARE) mission, *AIP Conference Proceedings*, *1531*, 444–447, doi:10.1063/1.4804802.

Doutriaux-Boucher, M., and J. Quaas (2004), Evaluation of cloud thermodynamic phase parameterizations in the LMDZ GCM by using POLDER satellite data, *Geophys. Res. Lett.*, *31*, L06126, doi:10.1029/2003GL019095.

Drewnick, F., S. S. Hings, M. R. Alfarra, A. S. H. Prevot, and S. Borrmann (2009), Aerosol quantification with the Aerodyne Aerosol Mass Spectrometer: Detection limits and ionizer background effects, *Atmos. Meas. Tech.*, *2*, 33–46, doi:10.5194/amt-2-33-2009.

Dubovik, O., M. Herman, A. Holdak, T. Lapyonok, D. Tanré, J. L. Deuzé, F. Ducos, A. Sinyuk, and A. Lopatin (2011), Statistically optimized inversion algorithm for enhanced retrieval of aerosol properties from spectral multi-angle polarimetric satellite observations, *Atmos. Meas. Tech.*, *4*, 975–1018, doi:10.5194/amt-4-975-2011.

Dubovik, O., T. Lapyonok, M. Herman, A. Lopatin, A. Holdak, P. Litvinov, D. Tanré, P. Goloub, and F. Ducos (2012), Development of unified retrieval algorithm for aerosol remote sensing, International Radiation Symposium 2012, Dahlem Cube, Berlin, Germany, 06–10 Aug.

Dusek, U., et al. (2006), Size matters more than chemistry for cloud nucleating ability of aerosol particles, *Science*, *312*, 1375–1378.

Eck, T. F., et al. (2010), Climatological aspects of the optical properties of fine/coarse mode aerosol mixtures, *J. Geophys. Res.*, *115*, D19205, doi:10.1029/2010JD014002.

Ervens, B., B. J. Turpin, and R. J. Weber (2011), Secondary organic aerosol formation in cloud droplets and aqueous particles (aqSOA): A review of laboratory, field and model studies, *Atmos. Chem. Phys.*, *11*, 11,069–11,102.

EUMETSAT (2005), GOME-2 Products Guide. [Available at http://www.eumetsat.int/en/area4/eps/product_guides/GOME-2/GOME2-PG.pdf.]

Evan, A. T., J. Dunion, J. A. Foley, A. K. Heidinger, and C. S. Velden (2006), New evidence for a relationship between Atlantic tropical cyclone activity and African dust outbreaks, *Geophys. Res. Lett.*, *33*, L19813, doi:10.1029/2006GL026408.

Fan, F., L. R. Leung, D. Rosenfeld, Q. Chen, Z. Li, J. Zhang, and H. Yan (2013), Microphysical effects determine macrophysical response for aerosol impact on deep convective clouds, *Proc. Nat. Acad. Sci. (PNAS)*, doi:10.1073/pnas.1316830110.

Fan, J., T. Yuan, J. M. Comstock, S. Ghan, A. Khain, L. R. Leung, Z. Li, V. J. Martins, and M. Ovchinnikov (2009), Dominant role by vertical wind shear in regulating aerosol effects on deep convective clouds, *J. Geophys. Res.*, *114*, D22206, doi:10.1029/2009JD012352.

Fan, J., L. R. Leung, Z. Li, H. Morrison, H. Chen, Y. Zhou, Y. Qian, and Y. Wang (2012a), Aerosol impacts on clouds and precipitation in eastern China: Results from bin and bulk microphysics, *J. Geophys. Res.*, *117*, D00K36, doi:10.1029/2011JD016537.

Fan, J., D. Rosenfeld, Y. Ding, L. R. Leung, and Z. Li (2012b), Potential aerosol indirect effects on atmospheric circulation and radiative forcing through deep convection, *Geophys. Res. Lett.*, L09806, doi:10.1029/2012GL051851.

Feingold, G., and I. Koren (2013), A model of coupled oscillators applied to the aerosol-cloud-precipitation system, *Nonlinear Processes Geophys.*, *20*(6), 1011–1021, doi:10.5194/npg-20-1011-2013.

Feingold, G., W. L. Eberhard, D. E. Veron, and M. Previdi (2003), First measurements of the Twomey indirect effect using ground-based remote sensors, *Geophys. Res. Lett.*, *30*(6), 1287, doi:10.1029/2002GL016633.

Feingold, G., H. L. Jiang, and J. Y. Harrington (2005), On smoke suppression of clouds in Amazonia, *Geophys. Res. Lett.*, *32*, L02804, doi:10.1029/2004GL021369.

Feingold, G., I. Koren, H. Wang, H. Xue, and W. A. Brewer (2010), Precipitation-generated oscillations in open cellular cloud fields, *Nature*, *466*, 849–52.

Feng, Y., and V. Ramanathan (2010), Investigation of aerosol-cloud interactions using a chemical transport model constrained by satellite observations, *Tellus*, *62B*, 69–86.

Frank, W. M. (1978), The life cycles of GATE convective systems, *JAS*, *35*, 1256–1264.

Freud, E., and D. Rosenfeld (2012), Linear relation between convective cloud drop number concentration and depth for rain initiation, *J. Geophys. Res.*, *117*, D02207, doi:10.1029/2011JD016457.

Freud, E., D. Rosenfeld, and J. R. Kulkarni (2011), Resolving both entrainment-mixing and number of activated CCN in deep convective clouds, *Atmos. Chem. Phys.*, *11*, 12,887–12,900, doi:10.5194/acp-11-12887-2011.

Gasso, S., and D. A. Hegg (2003), On the retrieval of columnar aerosol mass and CCN concentration by MODIS, *J. Geophys. Res.*, *108*(D1), 4010, doi:10.1029/2002JD002382.

Gautam, R., N. C. Hsu, K.-M. Lau, S.-C. Tsay, and M. Kafatos (2009a), Enhanced pre-monsoon warming over the Himalayan-Gangetic region from 1979 to 2007, *Geophys. Res. Lett.*, *36*, L07704, doi:10.1029/2009GL037641.

Gautam, R., C. Hsu, K. M. Lau, and M. Kafatos (2009b), Aerosol and rainfall variability over the Indian monsoon region: Distributions, trends and coupling, *Geophys, Annales*, *27*, 3691–3703. [Available at www.ann-geophys.net/27/3691/2009/.]

Gautam, R., C. Hsu, and K. M. Lau (2010), Pre-monsoon characterization and radiative effects over the Indo-Gangetic Plain: Implications for regional climate warming, *J. Geophys. Res.*, *115*, D17208, doi:10.1029/2010JD0.

George, R. C., R. Wood, C. S. Bretherton, and G. Painter (2013), Development and impact of hooks of high droplet concentration on remote southeast Pacific stratocumulus, *Atmos. Chem. Phys.*, *13*(13), 6305–6328.

Gerber, H. (1996), Microphysics of marine stratocumulus clouds with two drizzle modes, *J. Atmos. Sci.*, *53*(12), 1649–1662, doi:10.1175/1520-0469.

Giorgi, F., and W. L. Chameides (1986), Rainout lifetimes of highly soluble aerosols and gases as inferred from simulations with a general circulation model, *J. Geophys. Res.*, *91*(14), 367–14,376, doi:10.1029/JD091iD13p14367.

Gleason, J. F., N. C. Hsu, and O. Torres (1998), Biomass burning smoke measured using backscattered ultraviolet radiation: SCAR-B and Brazilian smoke interannual variability, *J. Geophys. Res.*, *103*(D24), 31,969–31,978, doi:10.1029/98JD00160.

Goren, T., and D. Rosenfeld (2012), Satellite observations of ship emission induced transitions from broken to closed cell marine stratocumulus over large areas, *J. Geophys. Res.*, *117*, D17206, doi:10.1029/2012JD017981.

Goren, T., and D. Rosenfeld (2013), Decomposing aerosol cloud radiative effects into cloud cover, liquid water path and Twomey components in Marine Stratocumulus, Accepted for Atmospheric Research.

Grabowski, W. W., and H. Morrison (2011), Indirect impact of atmospheric aerosols in idealized simulations of convective–radiative quasi equilibrium. Part II: Double-moment microphysics, *J. Clim.*, *24*, 1897–1912, doi:10.1175/2010JCLI3647.1.

Gryspeerdt, E., P. Stier, and B. S. Grandey (2014), Cloud fraction mediates the aerosol optical depth—Cloud top height relationship, *Geophys. Res. Lett.*, *41*, 3622–3627, doi:10.1002/2014GL059524.

Gu, Y., K. N. Liou, Y. Xue, C. R. Mechoso, W. Li, and Y. Luo (2006), Climatic effects of different aerosol types in China simulated by the UCLA general circulation model, *J. Geophys. Res.*, *111*, D15201, doi:10.1029/2005JD006312.

Guo, Y., B. Tian, R. A. Kahn, O. Kalashnikova, S. Wong, and D. E. Waliser (2013), Tropical Atlantic dust and smoke aerosol variations related to the Madden-Julian Oscillation in MODIS and MISR observations, *J. Geophys. Res. Atmos.*, *118*, 4947–4963, doi:10.1002/jgrd.50409.

Hair, J. W., C. A. Hostetler, A. L. Cook, D. B. Harper, R. A. Ferrare, T. L. Mack, W. Welch, L. R. Izquierdo, and F. E. Hovis (2008), Airborne high spectral resolution lidar for profiling aerosol optical properties, *Appl. Opt.*, *47*, 6734–6752.

Hakuba, M. Z., D. Folini, A. Sanchez-Lorenzo, and M. Wild (2013), Spatial representativeness of ground-based solar radiation measurements, *J. Geophys. Res. Atmos.*, *118*, 8585–8597, doi:10.1002/jgrd.50673.

Hasekamp, O. P. (2010), Capability of multi-viewing-angle photo-polarimetric measurements for the simultaneous retrieval of aerosol and cloud properties, *Atmos. Meas. Tech.*, *3*, 839–851, doi:10.5194/amt-3-839-2010.

Haywood, J. M., S. R. Osborne, and S. J. Abel (2004), The effect of overlying absorbing aerosol layers on remote sensing retrievals of cloud effective radius and cloud optical depth, *Q. J. R. Meteorol. Soc.*, *130*, 779–800.

Hazra, A., B. N. Goswami, and J.-P. Chen (2013), Role of Interactions between aerosol radiative effect, dynamics, and cloud microphysics on transitions of monsoon intraseasonal oscillations, *J. Atmos. Sci.*, *70*, 2073–2087, doi:10.1175/JAS-D-12-0179.1.

Hegg, D. A. (1990), Heterogeneous production of cloud condensation nuclei in the marine atmosphere, *Geophys. Res. Lett.*, *17*, 2165–2168, doi:10.1029/GL017i012p02165.

Hegg, D. A. (1991), Particle production in clouds, *Geophys. Res. Lett.*, *18*, 995–998, doi:10.1029/91GL01239.

Hegglin, M. I., D. D. Boone, G. L. Manney, T. G. Shepherd, K. A. Walker, P. F. Bernath, W. H. Daffer, P. Hoor, and C. Schiller (2008), Validation of ACE-FTS satellite data in the upper troposphere/lower stratosphere (UTLS) using non-coincident measurements, *Atmos. Chem. Phys.*, *8*, 1483–1499, doi:10.5194/acp-8-1483-2008.

Herman, J. R., P. K. Bhartia, O. Torres, C. Hsu, C. Seftor, and E. Celarier (1997), Global distribution of UV-absorbing aerosols from Nimbus 7/TOMS data, *J. Geophys. Res.*, *102*(D14), 16,911–16,922, doi:10.1029/96JD03065.

Heymsfield, A. J., P. C. Kennedy, S. Massie, C. Schmitt, Z. Wang, S. Haimov, and A. Rangno (2010), Aircraft-induced hole punch and canal clouds: Inadvertent cloud seeding, *Bull. Am. Meteor. Soc.*, *91*, 753–766, doi:10.1175/2009BAMS2905.1.

Hobbs, P. V. (2003), Aerosol-cloud interactions, Chapter 2, in *Aerosol-Cloud-Climate Interactions*, edited by P. V. Hobbs, pp. 33–73, Academic Press, Inc., San Diego, Calif.

Hoffmann, M. R., and J. G. Calvert (1985), *Chemical Transformation Modules for Eulerian Acid Deposition Models, Vol. 2, The Aqueous-Phase Chemistry*, EPA/600/3-85/017, U.S. EPA, Research Triangle Park, N. C.

Hoffmann, M. R., and J. O. Edwards (1975), Kinetics of oxidation of sulfite by hydrogen peroxide in acidic solution, *J. Phys. Chem.*, *79*, 2096–2098.

Holben, B. N., T. F. Eck, I. Slutsker, A. Smirnov, A. Sinyuk, J. Schafer, D. Giles, and O. Dubovik (2006), AERONET's version 2.0 quality assurance criteria, *IEEE Proc. of SPIE #6408*.

Holzer-Popp, T., M. Schroedter-Homscheidt, H. Breitkreuz, D. Martynenko, and L. Klüser (2008), Improvements of synergetic aerosol retrieval for ENVISAT, *Atmos. Chem. Phys.*, *8*, 76,551–7672.

Holzer-Popp, T., et al. (2013), Aerosol retrieval experiments in the ESA Aerosol_cci project, *Atmos. Meas. Tech.*, *6*, 1919–1957, doi:10.5194/amt-6-1919-2013.

Hoose, C., and O. Möhler (2012), Heterogeneous ice nucleation on atmospheric aerosols: A review of results from laboratory experiments, *Atmos. Chem. Phys.*, *12*, 9817–9854, doi:10.5194/acp-12-9817-2012.

Hoose, C., U. Lohmann, R. Bennartz, B. Croft, and G. Lesins (2008), Global simulations of aerosol processing in clouds, *Atmos. Chem. Phys.*, *8*, 6939–6963.

Hoose, C., J. E. Kristjánsson, and S. M. Burrows (2010), How important is biological ice nucleation in clouds on a global scale?, *Environ. Res. Lett.*, *5*, 024009, doi:10.1088/1748/9326/5/2/024009.

Hsu, N. C., J. R. Herman, P. K. Bhartia, C. J. Seftor, O. Torres, A. M. Thompson, J. F. Gleason, T. F. Eck, and B. N. Holben (1996), Detection of biomass burning smoke from TOMS measurements, *Geophys. Res. Lett.*, *23*(7), 745–748, doi:10.1029/96GL00455.

Huang, Y., R. E. Dickerson, and W. L. Chamedies (2006), Impact of aerosols indirect effect on surface temperature over East Asia, *Proceeding of Nat. Acad. Sci.* [Available at www.pnas.org/cgi/doi/10.1073/pnas.o504428103.]

Huang, Y., W. L. Chameides, and R. E. Dickenson (2007), Direct and indirect effects of anthropogenic aerosols on regional precipitation over East Asia, *J. Geophys. Res.*, *112*, D03211, doi:10.1029/2006/2006JD007114.

Ichoku, C., D. A. Chu, S. Mattoo, Y. J. Kaufman, L. A. Remer, D. Tanré, I. Slutsker, and B. N. Holben (2002), A spatio-temporal approach for global validation and analysis of MODIS aerosol products, *Geophys. Res. Lett.*, *29*(12), doi:10.1029/2001GL013206.

IPCC (2007), Summary for policymakers, in *Climate Change 2007: The Physical Science Basis*, Contribution of Working Group I to the Fourth Assessment Report of the Intergovernmental Panel on Climate Change, edited by S. Solomon, Cambridge Univ. Press, U. K.

Jacob, D. J. (1986), Chemistry of OH in remote clouds and its role in the production of formic acid and peroxymonosulfate, *J. Geophys. Res.*, *91*, 9807–9826, doi:10.1029/JD091iD09p09807.

Jenkins, G. S., A. S. Pratt, and A. Heymsfield (2008), Possible linkages between Saharan dust and tropical cyclone rain band invigoration in the eastern Atlantic during NAMMA-06, *Geophys. Res. Lett.*, *35*, L08815, doi:10.1029/2008GL034072.

Jiang, J. H., H. Su, S. T. Massie, P. R. Colarco, M. R. Schoeberl, and S. Platnick (2009), Aerosol-CO relationship and aerosol effect on ice cloud particle size: Analyses from Aura Microwave Limb Sounder and Aqua Moderate Resolution Imaging Spectroradiometer observations, *J. Geophys. Res.*, *114*, D20207, doi:10.1029/2009JD012421.

Jimenez, J. L., et al. (2009), Evolution of organic aerosols in the atmosphere, *Science*, *326*, 1525–529, doi:10.1126/science.1180353.

Johnson, B. T., K. P. Shine, and P. M. Forster (2004), The semi-direct aerosol effect: Impact of absorbing aerosols on marine stratocumulus, *Q. J. R. Meteorol. Soc.*, *130*, 1407–1422, doi:10.1256/qj.03.61.

Jones, H. M., M. J. Flynn, P. J. DeMott, and O. Möhler (2011), Manchester Ice Nucleus Counter (MINC) measurements from the 2007 International workshop on Comparing Ice nucleation Measuring Systems (ICIS-2007), *Atmos. Chem. Phys.*, *11*, 53–65, doi:10.5194/acp-11-53-2011.

Kahn, R., Y. Chen, D. L. Nelson, F.-Y. Leung, Q. Li, D. J. Diner, and J. A. Logan (2008), Wildfire smoke injection heights—Two perspectives from space, *Geophys. Res. Lett.*, *35*, L04809, doi:10.1029/2007GL032165.

Kahn, R., et al. (2009), Desert dust aerosol air mass mapping in the western Sahara, using particle properties derived from space-based multi-angle imaging, *Tellus*, *61B*, 239–251, doi:10.1111/j.1600-0889.2008.00398.x.

Kahn, R. A. (2012), Reducing the uncertainties in direct aerosol radiative forcing, *Surv. Geophys.*, *33*, 701–721, doi:10.1007/s10712-011-9153-z.

Kahn, R. A., and J. Limbacher (2012), Eyjafjallajökull volcano plume particle-type characterization from space-based multi-angle imaging, *Atmos. Chem. Phys.*, *12*, 9459–9477, doi:10.5194/acp-12-9459-2012.

Kahn, R. A., W.-H. Li, C. Moroney, D. J. Diner, J. V. Martonchik, and E. Fishbein (2007), Aerosol source plume physical characteristics from space-based multiangle imaging, *J. Geophys. Res.*, *112*, D11205, doi:10.1029/2006JD007647.

Kahn, R. A., B. J. Gaitley, M. J. Garay, D. J. Diner, T. Eck, A. Smirnov, and B. N. Holben (2010), Multiangle Imaging SpectroRadiometer global aerosol product assessment by comparison with the Aerosol Robotic Network, *J. Geophys. Res.*, *115*, D23209, doi:10.1029/2010JD014601.

Kammermann, L., M. Gysel, E. Weingartner, and U. Baltensperger (2010), 13-month climatology of the aerosol hygroscopicity at the free tropospheric site Jungfraujoch (3580 m a.s.l.), *Atmos. Chem. Phys.*, *10*, 10,717–10,732, doi:10.5194/acp-10-10717-2010.

Kanji, Z. A., A. Welti, C. Chou, O. Stetzer, and U. Lohmann (2013), Laboratory studies of immersion and deposition mode ice nucleation of ozone aged mineral dust particles, *Atmos. Chem. Phys. Discuss.*, *13*, 8701–8767, doi:10.5194/acpd-13-8701-2013.

Kapustin, V. N., A. D. Clarke, Y. Shinozuka, S. Howell, V. Brekhovskikh, T. Nakajima, and A. Higurashi (2006), On the determination of a cloud condensation nuclei from satellite: Challenges and possibilities, *J. Geophys. Res.*, *111*, D04202, doi:10.1029/2004JD005527.

Kaufman, Y. J., and I. Koren (2006), Smoke and pollution aerosol effect on cloud cover, *Science*, *313*, 655–658, doi:10.1126/science.1126232.

Kaufman, Y. J., I. Koren, L. A. Remer, D. Rosenfeld, and Y. Rudich (2005a), The effect of smoke, dust, and pollution aerosol on shallow cloud development over the Atlantic Ocean, *Proc. Natl. Acad. Sci. U.S.A.*, *102*, 11,207–11,212.

Kaufman, Y. J., O. Boucher, D. Tanre, M. Chin, L. A. Remer, and T. Takemura (2005b), Aerosol anthropogenic component estimated from satellite data, *Geophys. Res. Lett.*, *32*, L17804, doi:10.1029/2005GL023125.

Kessomkiat, W., H. J. Hendricks Franssen, A. Graf, and H. Vereecken (2013), Estimating random errors of eddy covariance data: An extended two-tower approach, *Agric. For. Meteorol.*, *171– 172*, 203–219.

Khain, A. P., M. Ovtchinnikov, M. Pinsky, A. Pokrovsky, and H. Krugliak (2000), Notes on the state-of-the-art numerical modeling of cloud microphysics, *Atmos. Res.*, *55*, 159–224, doi:10.1016/S0169-8095(00)00064-8.

Khain, A. P., D. Rosenfeld, and A. Pokrovsky (2005), Aerosol impact on the dynamics and microphysics of convective clouds, *Q. J. R. Meteor. Soc.*, *131*, 2639–2663.

Khain, A. P., N. Cohen, B. Lynn, and A. Pokrovsky (2008), Possible aerosol effects on lightning activity and structure of hurricanes, *J. Atmos. Sci.*, *65*, 3652–3677.

Khain, A., A. Pokrovsky, M. Pinsky, A. Seigert, and V. Phillips (2004), Simulation of effects of atmospheric aerosols on deep turbulent convective clouds using a spectral microphysics mixed-phase cumulus cloud model: Part I. Model description and possible applications, *J. Atmos. Sci.*, *61*, 2983–3001, doi:10.1175/JAS-3281.1.

Khain, A., D. Rosenfeld, A. Pokrovsky, U. Blahak, and A. Ryzhkov (2011), The role of CCN in precipitation and hail in a mid-latitude storm as seen in simulations using a spectral (bin) microphysics model in a 2D dynamic frame, *Atmos. Res.*, *99*, 129–146.

Khain, A., T. V. Prabha, N. Benmoshe, G. Pandithurai, and M. Ovchinnikov (2013), The mechanism of first raindrops formation in deep convective clouds, *J. Geophys. Res. Atmos.*, *118*, 9123–9140, doi:10.1002/jgrd.50641.

Kim, K. M., K. M. Lau, Y. Sud, and G. Walker (2010), Influence of aerosol-radiative forcing on the diurnal and seasonal cycles of rainfall over West Africa and the eastern Atlantic, from GCM simulations, *Clim. Dyn.*, doi:10.1007/s00382-010-0750-1.

Kim, M.-K., W. K. M. Lau, K.-M. Kim, and W.-S. Lee (2007), A GCM study of effects of radiative forcing of sulfate aerosol on large scale circulation and rainfall in East Asia during boreal spring, *Geophys. Res. Lett.*, *34*, L24701, doi:10.1029/2007GL031683.

King, M. D., S. Platnick, G. Wind, G. T. Arnold, and R. T. Dominguez (2010), Remote sensing of radiative and microphysical properties of clouds during TC4: Results from MAS, MASTER, MODIS, and MISR, *J. Geophys. Res.*, *115*, D00J07, doi:10.1029/2009JD013277.

Koch, D., D. Jacob, I. Tegen, D. Rind, and M. Chin (1999), Tropospheric sulfur simulation and sulfate direct radiative forcing in the GISS GCM, *J. Geophys. Res.*, *104*(23), 799–23,823, doi:10.1029/1999JD900248.

Kokhanovsky, A. A., and G. de Leeuw (Eds.) (2009), *Satellite Aerosol Remote Sensing Over Land*, 388 pp., Springer-Praxis, Berlin.

Konwar, M., R. S. Maheskumar, J. R. Kulkarni, E. Freud, B. N. Goswami, and D. Rosenfeld (2012), Aerosol control on depth of warm rain in convective clouds, *J. Geophys. Res.*, *117*, D13204, doi:10.1029/2012JD017585.

Koren, I., Y. Kaufman, L. Remer, and J. Martins (2004), Measurement of the effect of Amazon smoke on inhibition of cloud formation, *Science*, *303*, 1342–1345.

Koren, I., Y. J. Kaufman, D. Rosenfeld, L. A. Remer, and Y. Rudich (2005), Aerosol invigoration and restructuring of Atlantic convective clouds, *Geophys. Res. Lett.*, *32*, L14828, doi:10.1029/2005GL023187.

Koren, I., L. A. Remer, Y. J. Kaufman, Y. Rudich, and J. V. Martins (2007), On the twilight zone between clouds and aerosols, *Geophys. Res. Lett.*, *34*, L08805, doi:10.1029/2007GL029253.

Koren, I., J. V. Martins, L. A. Remer, and H. Afargan (2008a), Smoke invigoration versus inhibition of clouds over the Amazon, *Science*, *321*, 946–949.

Koren, I., L. Oreopoulos, G. Feingold, L. A. Remer, and O. Altaratz (2008b), How small is a small cloud?, *Atmos. Chem. Phys.*, *8*, 3855–3864, doi:10.5194/acp-8-3855-2008.

Koren, I., G. Feingold, and L. A. Remer (2010a), The invigoration of deep convective clouds over the Atlantic: Aerosol effect, meteorology or retrieval artifact?, *Atmos. Chem. Phys.*, *10*, 8855–8872.

Koren, I., L. A. Remer, O. Altaratz, J. V. Martins, and A. Davidi (2010b), Aerosol-induced changes of convective cloud anvils produce strong climate warming, *Atmos. Chem. Phys.*, *10*, 5001–5010, doi:10.5194/acp-10-5001-2010.

Koren, I., O. Altaratz, L. A. Remer, G. Feingold, J. V. Martins, and R. H. Heilblum (2012), Aerosol-induced intensification of rain from the tropics to the mid-latitudes, *Nat. Geosci.*, *5*, 118–122, doi:10.1038/ngeo1364.

Koren, I., G. Dagan, and O. Altaratz (2014), From aerosol-limited to invigoration of warm convective clouds, *Science*, *344*(6188), 1143–1146.

Krishnamurti, T. N., A. Chakraborty, A. Martin, W. K. Lau, K. Kim, Y. Sud, and G. Walker (2009), Impact of Arabian Sea pollution on the Bay of Bengal winter monsoon rains, *J. Geophys. Res.*, *114*, D06213, doi:10.1029/2008JD010679.

Kucienska, B., G. B. Raga, and R. Romero-Centeno (2012), High lightning activity in maritime clouds near Mexico, *Atmos. Chem. Phys.*, *12*, 8055–8072, doi:10.5194/acp-12-8055-2012.

Kuhlmann, J., and J. Quaas (2010), How can aerosols affect the Asian summer monsoon? Assessment during three consecutive pre-monsoon seasons from CALIPSO satellite data, *Atmos. Chem. Phys.*, *10*, 4673–4688.

Kulmala, M., A. Reissell, M. Sipilä, B. Bonn, T. M. Ruuskanen, K. E. J. Lehtinen, V. Kerminen, and J. Ström (2006), Deep convective clouds as aerosol production engines: Role of insoluble organics, *J. Geophys. Res.*, *111*, D17202, doi:10.1029/2005JD006963.

Kulmala, M., A. Arola, T. Nieminen, L. Riuttanen, L. Sogacheva, G. de Leeuw, V.-M. Kerminen, and K. E. J. Lehtinen (2011), The first estimates of global nucleation mode aerosol concentrations based on satellite measurements, *Atmos. Chem. Phys.*, *11*, 10,791–10,801, doi:10.5194/acp-11-10791-2011.

Kulmala, M., et al. (2012), Measurement of the nucleation of atmospheric aerosol particles, *Nat. Protoc.*, *7*, 1651–1667, doi:10.1038/nprot.2012.091.

Laakso, L., T. Grönholm, Ü. Rannik, M. Vehkamäki, M. Kosmale, V. Fiedler, and M. Kulmala (2003), Ultrafine particle scavenging coefficients calculated from six years field measurements, *Atmos. Environ.*, *37*, 3605–3613.

Laaksonen, A., P. Korhonen, M. Kulmala, and R. J. Charlson (1998), Modification of the Köhler equation to include soluble trace gases and slightly soluble substances, *J. Atmos. Sci.*, *55*(5), 853–862.

Langmuir, I. (1961), *Cloud Nucleation*, Collected Works of Langmuir, vol. 11, 619 pp., Pergamon Press.

Latham, J., et al. (2012), Marine cloud brightening, *Philos. Trans. R. Soc. A: Mathematical, Physical and Engineering Sciences*, *370*, 4217–4262.

Lau, K.-M., and K.-M. Kim (2006a), Observational relationships between aerosol and Asian monsoon rainfall, and circulation, *Geophys. Res. Lett.*, *33*, L21810, doi:10.1029/2006GL027546.

Lau, K.-M., and K.-M. Kim (2006b), Observational relationship between aerosol and Asian monsoon circulation rainfall, *Geophys. Res. Lett.*, *33*, L21810, doi:10.1029/2006GL027546.

Lau, K. M., and K. M. Kim (2007a), How Nature foiled the 2006 hurricane forecasts, *Eos Trans.*, *88*(9), 105–107.

Lau, K. M., and K. M. Kim (2007b), Cooling of the Atlantic by Saharan dust, *Geophys. Res. Lett.*, *34*, L23811, doi:10.1029/2007GL031538.

Lau, K. M., and K. M. Kim (2011), Comments on paper "Elevated Heat Pump hypothesis for the aerosol-hydroclimate link: 'Grounded' in observations? by Nigam and Bollasina", *J. Geophys. Res.*, *116*, D07203, doi:10.1029/2010JD014800.

Lau, K.-M., M.-K. Kim, and K. M. Kim (2006a), Aerosol induced anomalies in the Asian summer monsoon: The role of the Tibetan Plateau, *Clim. Dyn.*, *26*(7-8), 855–864, doi:10.1007/s00382-006-0114-z.

Lau, K.-M., M. -K. Kim, and K.-M. Kim (2006b), Asian summer monsoon anomalies induced by aerosol direct forcing: The role of the Tibetan Plateau, *Clim. Dyn.*, *26*(7-8), 855–864, doi:10.1007/s00382-006-10114-z.

Lau, K.-M., et al. (2008), The Joint Aerosol-Monsoon Experiment: A new challenge in monsoon climate research, *Bull. Am. Meteorol. Soc.*, *89*, 369–383, doi:10.1175/BAMS-89-3-369.

Lau, K. M., K. M. Kim, Y. C. Sud, and G. K. Walker (2009a), A GCM study of the response of the atmospheric water cycle of West Africa and the Atlantic to Saharan dust radiative forcing, *Ann. Geophys.*, *27*, 4023–4037, doi:10.5194/Angeo-27-4023-2009.

Lau, K.-M., K.-M. Kim, C. Hsu, and B. Holben (2009b), Possible influences of air pollution, dust and sandstorms on the Indian monsoon, *WMO Bull.*, *58*(1), 22–30.

Lau, W., and K. Kim (2010), Fingerprinting the impacts of aerosols on long-term trends of the Indian summer monsoon regional rainfall, *Geophys. Res. Lett.*, *37*, L16705, doi:10.1029/2010GL043255.

Lau, W. K., and D. E. Waliser (2012), *Intraseasonal Variability in the Atmosphere-Ocean Climate System*, pp. 3183–3193, Springer, Berlin.

Lau, W. K. M. (2014), Desert dust and monsoon rainfall, *Nat. Geosci.*, doi:10.1038/ngeo2115.

Lau, W. K. M., and K. M. Kim (2014), Impacts of aerosols on the Asian Monsoon—An interim assessment, in *Climate Variability and Change*, edited by C. P. Chang and J. M. Wallace, World Scientific Publication Company.

Lebsock, M. D., G. L. Stephens, and C. Kummerow (2008), Multisensor satellite observations of aerosol effects on warm clouds, *J. Geophys. Res.*, *113*, D15205, doi:10.1029/2008JD009876.

L'Ecuyer, T. S., W. Berg, J. Haynes, M. Lebsock, and T. Takemura (2009), Global observations of aerosol impacts on precipitation occurrence in warm maritime clouds, *J. Geophys. Res.*, *114*, D09211, doi:10.1029/2008JD011273.

Le Page, Y., J. M. C. Pereira, R. Trigo, C. da Camara, D. Oom, and B. Mota (2008), Global fire activity patterns (1996–2006) and climatic influence: An analysis using the World Fire Atlas, *Atmos. Chem. Phys.*, *8*, 1911–1924, doi:10.5194/acp-8-1911-2008.

Lee, A. K. Y., P. Herckes, W. R. Leaitch, A. M. Macdonald, and J. P. D. Abbatt (2011), Aqueous OH oxidation of ambient organic aerosol and cloud water organics: Formation of highly oxidized products, *Geophys. Res. Lett.*, *38*, L11805, doi:10.1029/2011GL047439.

Lee, A. K. Y., K. L. Hayden, P. Herckes, W. R. Leaitch, J. Liggio, A. M. Macdonald, and J. P. D. Abbatt (2012), Characterization of aerosol and cloud water at a mountain site during WACS 2010: Secondary organic aerosol formation through oxidative cloud processing, *Atmos. Chem. Phys.*, *12*, 7103–7116, doi:10.5194/acp-12-7103-2012.

Lee, Y. N., and S. E. Schwartz (1983), Kinetics of oxidation of aqueous sulfur (IV) by nitrogen dioxide, in *Precipitation Scavenging, Dry Deposition and Resuspension*, vol. 1, edited by H. R. Pruppacher, R. G. Semonin, and W. G. N. Slinn, Elsevier, New York.

Lensky, I. M., and D. Rosenfeld (2006), The time-space exchangeability of satellite retrieved relations between cloud top temperature and particle effective radius, *Atmos. Chem. Phys.*, 6, 2887–2894.

Lerach, D. G., B. J. Gaudet, and W. R. Cotton (2008), Idealized simulations of aerosol influences on tornadogenesis, *Geophys. Res. Lett.*, 35, L23806, doi:10.1029/2008GL035617.

Levelt, P. F., and R. Noordhoek (2002), OMI Algorithm Theoretical Basis Document Volume I: OMI Instrument, Level 0-1b Processor, Calibration & Operations, *Tech. Rep. ATBD-OMI-01*, Version 1.1, August 2002. [Available at http://www.knmi.nl/omi/documents/data/OMI_ATBD_Volume_1_V1d1.pdf.]

Levin, E. J. T., A. J. Prenni, M. D. Petters, S. M. Kreidenweis, R. C. Sullivan, S. A. Atwood, J. Ortega, P. J. DeMott, and J. N. Smith (2012), An annual cycle of size-resolved aerosol hygroscopicity at a forested site in Colorado, *J. Geophys. Res.*, 117, D06201, doi:10.1029/2011JD016854.

Levy, R. C., L. A. Remer, R. G. Kleidman, S. Mattoo, C. Ichoku, R. A. Kahn, and T. F. Eck (2010), Global evaluation of the Collection 5 MODIS dark-target aerosol products over land, *Atmos. Chem. Phys.*, 10, 10,399–10,420, doi:10.5194/acp-10-10399-2010.

Liepert, B. G., J. Feichter, U. Lohmann, and E. Roeckner (2004), Can aerosols spin down the water cycle in a warmer and moister world?, *Geophys. Res. Lett.*, 31, L06207, doi:10.1029/2003GL019060.

Lin, B., and W. B. Rossow (1996), Seasonal variation of liquid and ice water path in nonprecipitating clouds over oceans, *J. Clim.*, 9, 2890–2902.

Liu, H., D. J. Jacob, I. Bey, and R. M. Yantosca (2001), Constraints from ^{210}Pb and ^{7}Be on wet deposition and transport in a global three-dimensional chemical tracer model driven by assimilated meteorological fields, *J. Geophys. Res.*, 106, 12,109–12,128, doi:10.1029/2000JD900839.

Liu, J., and Z. Li (2014), Estimation of cloud condensation nuclei concentration from aerosol optical quantities: Influential factors and uncertainties, *Atmos. Chem. Phys.*, 14(1), 471–483.

Liu, Y., J. Sun, and B. Yang (2009), The effects of black carbon and sulfate aerosols in China regions on East Asian monsoon, *Tellus*, 61B, 642–656, doi:10.1111/j.1600-0889.2009.00427.x.

Loeb, N. G., and G. L. Schuster (2008), An observational study of the relationship between cloud, aerosol and meteorology in broken low-level cloud conditions, *J. Geophys. Res.*, 113, D14214, doi:10.1029/2007JD009763.

Loeb, N. G., B. A. Wielicki, D. R. Doelling, G. L. Smith, D. F. Keyes, S. Kato, N. Manalo-Smith, and T. Wong (2009), Toward optimal closure of the Earth's top-of-atmosphere radiation budget, *J. Clim.*, 22, 748–766.

Logan, J. A., I. Megretskaia, R. Nassar, L. T. Murray, L. Zhang, K. W. Bowman, H. M. Worden, and M. Luo (2008), Effects of the 2006 El Niño on tropospheric composition as revealed by data from the Tropospheric Emission Spectrometer (TES), *Geophys. Res. Lett.*, 35, L03816, doi:10.1029/2007GL031698.

Lohmann, U., J. Quaas, S. Kinne, and J. Feichter (2007), Different approaches for constraining global climate models of the anthropogenic indirect aerosol effect, *Bull. Am. Meteorol. Soc.*, 88, 243–249.

Lyapustin, A., Y. Wang, I. Laszlo, R. Kahn, S. Korkin, L. Remer, R. Levy, and J. S. Reid (2011), Multiangle implementation of atmospheric correction (MAIAC): 2. Aerosol algorithm, *J. Geophys. Res.*, 116, D03211, doi:10.1029/2010JD014986.

Mahmood, R., and S. Li (2012), Delay in the onset of South Asia summer monsoon induced by local black carbon in an AGCM, *Theor. Appl. Climatol.*, 111(3-4), 529–536, doi:10.1007/s00704-012-0681-3.

Manoj, M. G., P. C. S. Devara, P. D. Safai, and B. N. Goswami (2010), Absorbing aerosols facilitate transition of Indian monsoon breaks to active spells, *Clim. Dyn.*, 37, 2181–2198, doi:10.1007/s00382-010-097-3.

Marshak, A., G. Wen, J. A. Coakley Jr., L. A. Remer, N. G. Loeb, and R. F. Cahalan (2008), A simple model for the cloud adjacency effect and the apparent bluing of aerosols near clouds, *J. Geophys. Res.*, 113, D14S17, doi:10.1029/2007JD009196.

Martin, L. R. (1984), Kinetic studies of sulfite oxidation in aqueous solution, in *SO₂, NO, and NO₂ Oxidation Mechanisms: Atmospheric Considerations*, edited by J. G. Calvert, pp. 63–100, Butterworth, Stoneham, Mass.

Martins, J. V., A. Marshak, L. A. Remer, D. Rosenfeld, Y. J. Kaufman, R. Fernandez-Borda, I. Koren, A. L. Correia, V. Zubko, and P. Artaxo (2011), Remote sensing the vertical profile of cloud droplet effective radius, thermodynamic phase, and temperature, *Atmos. Chem. Phys.*, 11, 9485–9501, doi:10.5194/acp-11-9485-2011.

Martonchik, J. V., R. A. Kahn, and D. J. Diner (2009), Retrieval of aerosol properties over land using MISR observations, in *Satellite Aerosol Remote Sensing Over Land*, edited by A. A. Kokhanovsky and G. de Leeuw, pp. 267–293, Springer, Berlin.

McComiskey, A., and G. Feingold (2012), The scale problem in quantifying aerosol indirect effects, *Atmos. Chem. Phys.*, 12, 1031–1049, doi:10.5194/acp-12-1031-2012.

Meehl, G. A., J. M. Arblaster, and W. D. Collins (2008), Effects of black carbon aerosols on the Indian monsoon, *J. Clim.*, 21, 2869–2882, doi:10.1175/2007JCLI1777.1.

Mehta, V. M., and T. Delworth (1995), Decadal variability of the tropical Atlantic Ocean surface temperature in shipboard measurements and in a Global Ocean-Atmosphere model, *J. Clim.*, 8, 172–190, doi:10.1175/1520-0442(1995)008<0172:DVOTTA>2.0.CO;2.

Meyer, K., S. Platnick, L. Oreopoulos, and D. Lee (2013), Estimating the direct radiative forcing of absorbing aerosols overlying marine boundary layer clouds in the southeast Atlantic using MODIS and CALIOP, *J. Geophys. Res. Atmos.*, 118, 4801–4815, doi:10.1002/jgrd.50449.

Mishchenko, M. I., I. V. Geogdzhayev, B. Cairns, W. B. Rossow, and A. A. Lacis (1999), Aerosol retrievals over the ocean by use of channels 1 and 2 AVHRR data: Sensitivity analysis and preliminary results, *Appl Opt*, 38, 7325–7341.

Mishchenko, M. I., B. Cairns, G. Kopp, C. F. Schueller, B. A. Fafaul, J. E. Hansen, R. J. Hooker, T. Itchkawich, H. B. Maring, and L. D. Travis (2007), Accurate monitoring of terrestrial aerosols and total solar irradiance, *Bull. Am. Meteorol. Soc.*, 88, 677–691.

Mitchell, R. M., S. K. Campbell, and Y. Qin (2010), Recent increase in aerosol loading over the Australian arid zone, *Atmos. Chem. Phys.*, 10, 1689–1699, doi:10.5194/acp-10-1689-2010.

Morcrette, J.-J., et al. (2009), Aerosol analysis and forecast in the European Centre for Medium-Range Weather Forecasts Integrated Forecast System: Forward modelling, *J. Geophys. Res.*, 114, D06206, doi:10.1029/2008JD011235.

Moroney, C., R. Davies, and J.-P. Muller (2002), MISR stereoscopic image matchers: Techniques and results, *IEEE Trans. Geosci. Remt. Sens.*, 40, 1547–1559.

Morrison, A. E., S. T. Siems, and M. J. Manton (2011), A three-year climatology of cloud-top phase over the Southern Ocean and North Pacific, *J. Clim.*, 24, 2405–2418, doi:10.1175/2010JCLI3842.1.

Morrison, H. (2012), On the robustness of aerosol effects on an idealized supercell storm simulated with a cloud system-resolving model, *Atmos. Chem. Phys.*, 12, 7689–7705, doi:10.5194/acp-12-7689-2012.

Morrison, H., and W. Grabowski (2013), Response of tropical deep convection to localized heating perturbations: Implications for aerosol-induced convective invigoration, *J. Atmos. Sci.*, 70(11), 3533–3555, doi:10.1175/JAS-D-13-027.1.

Morrison, H., G. de Boer, G. Feingold, J. Harrington, M. D. Shupe, and K. Sulia (2012), Resilience of persistent Arctic mixed-phase clouds, *Nat. Geosci.*, 5, 11–17, doi:10.1038/ngeo1332.

Muller, J.-P., A. Mandanayake, C. Moroney, R. Davies, D. J. Diner, and S. Paradise (2002), Operational retrieval of cloud-top heights using MISR data, *IEEE Trans. Geosci. Remt. Sens.*, 40, 1532–1546.

Myhre, G., F. Stordal, M. Johnsrud, Y. J. Kaufman, D. Rosenfeld, T. Storelvmo, J. E. Kristjansson, T. K. Berntsen, A. Myhre, and I. S. A. Isaksen (2007), Aerosol-cloud interaction inferred from MODIS satellite data and global aerosol models, *Atmos. Chem. Phys.*, *7*, 3081–3101.

Nakajima, T., and A. Higurashi (1998), A use of two channel radiances for an aerosol characterization from space, *Geophys. Res. Lett.*, *25*(20), doi:10.1029/98GL02151.

Nakajima, T., and M. Schulz (2009), What do we know about large-scale changes of aerosols, clouds, and the radiation budget?, in *Clouds and the Perturbed Climate System, Ernst Strüngmann Forum*, edited by J. Heintzenberg and R. J. Charlson, MIT Press, Cambridge.

Nakajima, T., A. Higurashi, K. Kawamoto, and J. E. Penner (2001), A possible correlation between satellite-derived cloud and aerosol microphysical parameters, *Geophys. Res. Lett.*, *28*, 1171–1174, doi:10.1029/2000GL012186.

Nelson, D. L., M. J. Garay, R. A. Kahn, and B. A. Dunst (2013), Stereoscopic height and wind retrievals for aerosol plumes with the MISR INteractive eXplorer (MINX), *Remote Sens.*, *5*, 4593–4628, doi:10.3390/RS5094593.

Nielsen, J. K., M. Foster, and A. Heidinger (2011), Tropical stratospheric cloud climatology from the PATMOS-x dataset: An assessment of convective contributions to stratospheric water, *Geophys. Res. Lett.*, *38*, L18801, doi:10.1029/2011GL049429.

Nigam, S., and M. Bollasina (2010), "Elevated heat pump" hypothesis for the aerosol monsoon hydroclimate link: "Grounded" in observations?, *J. Geophys. Res.*, *115*, D16201, doi:10.1029/2009JD013800.

Niu, F., and Z. Li (2012), Systematic variations of cloud top temperature and precipitation rate with aerosols over the global tropics, *Atmos. Chem. Phys.*, *12*, 8491–8498, doi:10.5194/acp-12-8491-2012.

Norris, J. R., and M. Wild (2007), Trends in aerosol radiative effects over Europe inferred from observed cloud cover, solar dimming, and solar brightening, *J. Geophys. Res.*, *112*, D08214, doi:10.1029/2006JD007794.

North, P. R. J. (2002), Estimation of aerosol opacity and land surface bidirectional reflectance from ATSR-2 dual-angle imagery: Operational method and validation, *J. Geophys. Res.*, *107*, doi:10.1029/2000JD000207.

Omar, A., et al. (2009), The CALIPSO automated aerosol classification and lidar ratio selection algorithm, *J. Atmos. Oceanic Tech.*, *26*, 1994–2014.

Panicker, A. S., G. Pandithurai, and S. Dipu (2010), Aerosol indirect effect during successive contrasting monsoon seasons over Indian subcontinent using MODIS data, *Atmos. Environ.*, *44*, 1937–1943.

Penkett, S. A., B. M. R. Jones, K. A. Brice, and A. E. J. Eggleton (1979), The importance of atmospheric ozone and hydrogen peroxide in oxidizing sulfur dioxide in cloud and rainwater, *Atmos. Environ.*, *13*, 123–137.

Penning de Vries, M. J. M., and T. Wagner (2011), Modelled and measured effects of clouds on UV Aerosol Indices on a local, regional, and global scale, *Atmos. Chem. Phys.*, *11*, 12,715–12,735, doi:10.5194/acp-11-12715-2011.

Penning de Vries, M. J. M., S. Beirle, and T. Wagner (2009), UV Aerosol Indices from SCIAMACHY: Introducing the SCattering Index (SCI), *Atmos. Chem. Phys.*, *9*, 9555–9567, doi:10.5194/acp-9-9555-2009.

Peters, K., J. Quaas, and H. Graßl (2011), A search for large-scale effects of ship emissions on clouds and radiation in satellite data, *J. Geophys. Res.*, *116*, D24205, doi:10.1029/2011JD016531.

Petters, M. D., and S. M. Kreidenweis (2007), A single parameter representation of hygroscopic growth and CNN activity, *Atmos. Chem. Phys.*, *7*, 1961–1971.

Pinsky, M., and A. P. Khain (2002), Effects of in-cloud nucleation and turbulence on droplet spectrum formation in cumulus clouds, *Q. J. R. Meteor. Soc.*, *128*, 501–533.

Pinsky, M., A. Khain, I. Mazin, and A. Korolev (2012), Analytical estimation of droplet concentration at cloud base, *J. Geophys. Res.*, *117*, D18211, doi:10.1029/2012JD017753.

Prabha, T. V., A. Khain, R. S. Maheshkumar, G. Pandithurai, J. R. Kulkarni, M. Konwar, and B. N. Goswami (2011), Microphysics of premonsoon and monsoon clouds as seen from in situ measurements during the Cloud Aerosol Interaction and Precipitation Enhancement Experiment (CAIPEEX), *J. Atmos. Sci.*, *68*, 1882–1901, doi:10.1175/2011JAS3707.1.

Prospero, J. M., and P. J. Lamb (2003), African droughts and dust transport to the Caribbean: Climate change implications, *Science*, *302*, 1024–1027, doi:10.1126/science.1089915.

Pruppacher, H. R., and J. D. Klett (1997), *Microphysics and Clouds*, 2nd ed., Springer, Dordrecht, Netherlands.

Qian, Y., D. Gong, J. Fan, L. R. Leung, R. Bennartz, D. Chen, and W. Wang (2009), Heavy pollution suppresses light rain in China: Observations and modeling, *J. Geophys. Res.*, *114*, D00K02, doi:10.1029/2008JD011575.

Quaas, J. (2012), Evaluating the "critical relative humidity" as a measure of subgrid-scale variability of humidity in general circulation model cloud cover parameterizations using satellite data, *J. Geophys. Res.*, *117*, D09208, doi:10.1029/2012JD017495.

Quaas, J., O. Boucher, and U. Lohmann (2006), Constraining the total aerosol indirect effect in the LMDZ and ECHAM4 GCMs using MODIS satellite data, *Atmos. Chem. Phys.*, *6*, 947–955.

Quaas, J., O. Boucher, A. Jones, G. P. Weedon, J. Kieser, and H. Joos (2009), Exploiting the weekly cycle as observed over Europe to analyse aerosol indirect effects in two climate models, *Atmos. Chem. Phys.*, *9*, 8493–8501, doi:10.5194/acp-9-8493-2009.

Radke, L. F., and P. V. Hobbs (1991), Humidity and particle fields around some small cumulus clouds, *J. Atmos. Sci.*, *48*, 1190–1193.

Ramanathan, V., and G. Carmichael (2008), Global and regional climate changes due to black carbon, *Nat. Geosci.*, *1*, 221–227, doi:10.1038/ngeo156.

Ramanathan, V., P. J. Crutzen, J. T. Kiehl, and D. Rosenfeld (2001), Aerosols, climate and the hydrological cycle, *Science*, *294*, 2119–2124.

Ramanathan, V., V. C. Chung, D. Kim, T. Bettge, L. Buja, J. T. Kiehl, W. M. Washington, Q. Fu, D. R. Sikka, and M. Wild (2005), Atmospheric brown clouds: Impacts on south Asian climate and hydrological cycle, *Proc. Natl. Acad. Sci. U.S.A.*, *102*(15), 5326–5333.

Randles, C. A., and V. Ramaswamy (2008), Absorbing aerosols over Asia: A GFDL general circulation model sensitivity study of model response to aerosol optical depth and aerosol absorption, *J. Geophys. Res.*, *113*, D21203, doi:10.1029/2008JD010140.

Rangno, A. L., and P. V. Hobbs (2005), Microstructures and precipitation development in cumulus and small cumulonimbus clouds over the warm pool of the tropical Pacific Ocean, *Q. J. R. Meteorol. Soc.*, *131*, 639–673, doi:10.1256/qj.04.13.

Reale, O., K. M. Lau, A. da Silva, and T. Matsui (2014), Impact of assimilated and interactive aerosol on tropical cyclogenesis, *Geophys. Res. Lett.*, *41*, 3282–3288, doi:10.1002/2014GL059918.

Redemann, J., Q. Zhang, P. B. Russell, J. M. Livingston, and L. A. Remer (2009), Case studies of aerosol remote sensing in the vicinity of clouds, *J. Geophys. Res.*, *114*, D06209, doi:10.1029/2008JD010774.

Remer, L. A., et al. (2005), The MODIS aerosol algorithm, products, and validation, *J. Atmos. Sci.*, *62*, 947–973.

Rennó, N. O., et al. (2013), CHASER: An innovative satellite mission concept to measure the effects of aerosols on clouds and climate, *Bull. Am. Meteorol. Soc.*, *94*, 685–694.

Reutter, P., H. Su, J. Trentmann, M. Simmel, D. Rose, S. S. Gunthe, H. Wernli, M. O. Andreae, and U. Pöschl (2009), Aerosol- and updraft-limited regimes of cloud droplet formation: Influence of particle number, size and hygroscopicity on the activation of cloud condensation nuclei (CCN), *Atmos. Chem. Phys.*, *9*, 7067–7080, doi:10.5194/acp-9-7067-2009.

Rosenfeld, D., and T. L. Bell (2011), Why do tornados and hailstorms rest on weekends?, *J. Geophys. Res.*, *116*, D20211, doi:10.1029/2011JD016214.

Rosenfeld, D., and G. Gutman (1994), Retrieving microphysical properties near the tops of potential rain clouds by multispectral analysis of AVHRR data, *Atmos. Res.*, *34*(1–4), 259–283, doi:10.1016/0169-8095(94)90096-5.

Rosenfeld, D., and I. M. Lensky (1998), Satellite-based insights into precipitation formation processes in continental and maritime convective clouds, *Bull. Am. Meteorol. Soc.*, *79*, 2457–2476.

Rosenfeld, D., and C. W. Ulbrich (2003), Cloud microphysical properties, processes, and rainfall estimation opportunities, in *Radar and Atmospheric Science: A Collection of Essays in Honor of David Atlas*, Meteorological Monographs 52, edited by R. M. Wakimoto and R. Srivastava, chap. 10, pp. 237–258, AMS, Boston, Mass.

Rosenfeld, D., and W. L. Woodley (2000), Deep convective clouds with sustained supercooled liquid water down to −37.5°C, *Nature*, *405*, 440–442.

Rosenfeld, D., and W. L. Woodley (2003), Closing the 50-year circle: From cloud seeding to space and back to climate change through precipitation physics, in *Cloud Systems, Hurricanes, and the Tropical Rainfall Measuring Mission (TRMM)*, *Meteorological Monographs* 51, edited by W.-K. Tao and R. Adler, chap. 6, pp. 59–80, AMS.

Rosenfeld, D., R. Lahav, A. P. Khain, and M. Pinsky (2002), The role of sea-spray in cleansing air pollution over ocean via cloud processes, *Science*, *297*, 1667–1670.

Rosenfeld, D., X. Yu, and J. Dai (2005), Satellite retrieved microstructure of AgI seeding tracks in supercooled layer clouds, *J. Appl. Meteorol.*, *44*, 760–767.

Rosenfeld, D., Y. Kaufman, and I. Koren (2006a), Switching cloud cover and dynamical regimes from open to closed Benard cells in response to aerosols suppressing precipitation, *Atmos. Chem. Phys.*, *6*, 2503–2511.

Rosenfeld, D., W. L. Woodley, T. W. Krauss, and V. Makitov (2006b), The structure of severe convective storms in Mendoza, Argentina, *J. Appl. Meteorol.*, *45*, 1261–1281.

Rosenfeld, D., A. Khain, B. Lynn, and W. L. Woodley (2007), Simulation of hurricane response to suppression of warm rain by sub-micron aerosols, *Atmos. Chem. Phys.*, *7*, 3411–3424.

Rosenfeld, D., U. Lohmann, G. B. Raga, C. D. O'Dowd, M. Kulmala, S. Fuzzi, A. Reissell, and M. O. Andreae (2008a), Flood or drought: How do aerosols affect precipitation?, *Science*, *321*, 1309–1313.

Rosenfeld, D., W. L. Woodley, A. Lerner, G. Kelman, and D. T. Lindsey (2008b), Satellite detection of severe convective storms by their retrieved vertical profiles of cloud particle effective radius and thermodynamic phase, *J. Geophys. Res.*, *113*, D04208, doi:10.1029/2007JD008600.

Rosenfeld, D., W. L. Woodley, A. Lerner, G. Kelman, and D. T. Lindsey (2008c), Satellite detection of severe convective storms by their retrieved vertical profiles of cloud particle effective radius and thermodynamic phase, *J. Geophys. Res.*, *113*, D04208, doi:10.1029/2007JD008600.

Rosenfeld, D., X. Yu, G. Liu, X. Xu, Y. Zhu, Z. Yue, J. Dai, Z. Dong, Y. Dong, and Y. Peng (2011), Glaciation temperatures of convective clouds ingesting desert dust, air pollution and smoke from forest fires, *Geophys. Res. Lett.*, *38*, L21804, doi:10.1029/2011GL049423.

Rosenfeld, D., H. Wang, and P. J. Rasch (2012a), The roles of cloud drop effective radius and LWP in determining rain properties in marine stratocumulus, *Geophys. Res. Lett.*, *39*, L13801, doi:10.1029/2012GL052028.

Rosenfeld, D., W. L. Woodley, A. Khain, W. R. Cotton, G. Carrió, I. Ginis, and J. H. Golden (2012b), Aerosol effects on microstructure and intensity of tropical cyclones, *Bull. Am. Meteorol. Soc.*, *93*, 987–1001.

Rosenfeld, D., E. Williams, M. O. Andreae, E. Freud, U. Pöschl, and N. O. Rennó (2012c), The scientific basis for a satellite mission to retrieve CCN concentrations and their impacts on convective clouds, *Atmos. Meas. Tech.*, *5*, 2039–2055.

Rosenfeld, D., R. Wood, L. Donner, and S. Sherwood (2013), Aerosol cloud-mediated radiative forcing: Highly uncertain and opposite effects from shallow and deep clouds, in *Climate Science for Serving Society: Research, Modelling and Prediction Priorities*, edited by G. R. Asrar and J. W. Hurrell, Springer, New York.

Rosenfeld, D., B. Fischman, Y. Zheng, T. Goren, and D. Giguzin (2014), Combined satellite and radar retrievals of drop concentration and CCN at convective cloud base, *Geophys. Res. Lett.*, *41*, 3259–3265, doi:10.1002/2014GL059453.

Rotstayn, L. D., and U. Lohmann (2002), Tropical rainfall trends and the indirect aerosol effect, *J. Clim.*, *15*, 2103–2116, doi:10.1175/1520-0442(2002)015<2103:TRTATI>2.0.CO;2.

Rotstayn, L. D., et al. (2007), Have Australian rainfall and cloudiness increased due to the remote effects of Asian anthropogenic aerosols?, *J. Geophys. Res.*, *112*, D09202, doi:10.1029/2006JD007712.

Ruckstuhl, C., et al. (2008), Aerosol and cloud effects on solar brightening and the recent rapid warming, *Geophys. Res. Lett.*, *35*, L12708, doi:10.1029/2008GL034228.

Russell, P. B., et al. (2002), Comparison of aerosol single scattering albedos derived by diverse techniques in two North Atlantic experiments, *J. Atmos. Sci.*, *59*, 609–619.

Satheesh, S. K., O. Torres, L. A. Remer, S. S. Babu, V. Vinoj, T. F. Eck, R. G. Kleidman, and B. N. Holben (2009), Improved assessment of aerosol absorption using OMI-MODIS joint retrieval, *J. Geophys. Res.*, *114*, D05209, doi:10.1029/2008JD011024.

Schwarz, J. P., J. R. Spackman, R. S. Gao, L. A. Watts, P. Stier, M. Schulz, S. M. Davis, S. C. Wofsy, and D. W. Fahey (2010), Global-scale black carbon profiles observed in the remote atmosphere and compared to models, *Geophys. Res. Lett.*, *37*, L18812, doi:10.1029/2010GL044372.

Schwartz, S. E., C. M. Harshvardhan, and C. M. Benkovitz (2002), Influence of anthropogenic aerosol on cloud optical depth and albedo shown by satellite measurements and chemical transport modelling, *Proc. Natl. Acad. Sci. U.S.A.*, *99*, 1784–1789, doi:10.1073/pnas.261712099.

Seinfeld, J. H., and S. N. Pandis (1998), *Atmospheric Chemistry and Physics*, 1326 pp., John Wiley, New York.

Seiz, G., and R. Davies (2006), Reconstruction of cloud geometry from multi-view satellite images, *Remt. Sens. Environ.*, *100*, 143–149.

Sekiguchi, M., T. Nakajima K. Suzuki, K. Kawamoto, A. Higurashi, D. Rosenfeld, I. Sano, and S. Mukai (2003), A study of the direct and indirect effects of aerosols using global satellite datasets of aerosol and cloud parameters, *J. Geophys. Res.*, *108*(D22), 4699, doi:10.1029/2002JD003359.

Sherwood, S. C. (2002a), Aerosols and ice particle size in tropical cumulonimbus, *J. Clim.*, *15*, 1051–1063.

Sherwood, S. C. (2002b), A microphysical connection among biomass burning, cumulus clouds, and stratospheric moisture, *Science*, *295*, 1272–1275.

Shinozuka, Y., et al. (2009), Aerosol optical properties relevant to regional remote sensing of CCN activity and links to their organic mass fraction: Airborne observations over Central Mexico and the US West Coast during MILAGRO/INTEX-B, *Atmos. Chem. Phys.*, *9*, 6727–6742.

Small, J. D., P. Y. Chuang, G. Feingold, and H. Jiang (2009), Can aerosol decrease cloud lifetime?, *Geophys. Res. Lett.*, *36*, L16806, doi:10.1029/2009GL038888.

Small, J. D., J. H. Jiang, H. Su, and C. Zhai (2011), Relationship between aerosol and cloud fraction over Australia, *Geophys. Res. Lett.*, *38*, L23802, doi:10.1029/2011GL049404.

Snook, N., and M. Xue (2008), Effects of microphysical drop size distribution on tornadogenesis in supercell thunderstorms, *Geophys. Res. Lett.*, *35*, L24803, doi:10.1029/2008GL035866.

Sorooshian, A., G. Feingold, M. D. Lebsock, H. Jiang, and G. L. Stephens (2010), Deconstructing the precipitation susceptibility construct: Improving methodology for aerosol-cloud precipitation studies, *J. Geophys. Res.*, *115*, D17201, doi:10.1029/2009JD013426.

Stevens, B., and G. Feingold (2009), Untangling aerosol effects on clouds and precipitation in a buffered system, *Nature*, *461*, 607–613, doi:10.1038/nature08281.

Stevens, B., G. Vali, K. Comstock, M. C. van Zanten, P. H. Austin, C. S. Bretherton, and D. H. Lenschow (2005), Pockets of open cells (POCs) and drizzle in marine tratocumulus, *Bull. Am. Meteorol. Soc.*, *86*, 51–57.

Stiller, G. P., et al. (2012), Validation of MIPAS IMK/IAA temperature, water vapor, and ozone profiles with MOHAVE-2009 campaign measurements, *Atmos. Meas. Tech.*, *5*, 289–320, doi:10.5194/amt-5-289-2012.

Su, H., D. Rose, Y. F. Cheng, S. S. Gunthe, A. Massling, M. Stock, A. Wiedensohler, M. O. Andreae, and U. Pöschl (2010), Hygroscopicity distribution concept for measurement data analysis and modeling of aerosol particle mixing state with regard to hygroscopic growth and CCN activation, *Atmos. Chem. Phys.*, *10*, 7489–7503, doi:10.5194/acp-10-7489-2010.

Sundström, A., et al. (2013), Estimating the concentration of nucleation mode aerosol particles over South Africa using satellite remote sensing measurements, in *AIP Conference Proceedings*, vol. 1527, pp. 503–506, AIP Publishing, Melville, New York, doi:10.1063/1.4803315.

Suzuki, K., T. Y. Nakajima, and G. L. Stephens (2010), Particle growth and drop collection efficiency of warm clouds as inferred from joint CloudSat and MODIS observations, *J. Atmos. Sci.*, *67*, 3019–3032, doi:10.1175/2010JAS3463.1.

Suzuki, K., G. L. Stephens, S. C. van den Heever, and T. Y. Nakajima (2011), Diagnosis of the warm rain process in cloud-resolvinig models using joint CloudSat and MODIS observations, *J. Atmos. Sci.*, *68*, 2655–2670, doi:10.1175/JAS-D-10-05026.1.

Swietlicki, E., et al. (2008), Hygroscopic properties of submicrometer atmospheric aerosol particles measured with H-TDMA instruments in various environments—A review, *Tellus*, *60B*, 432–469.

Tackett, J. L., and L. Di Girolamo (2009), Enhanced aerosol backscatter adjacent to tropical trade wind clouds revealed by satellite-based lidar, *Geophys. Res. Lett.*, *36*, L14804, doi:10.1029/2009GL039264.

Tao, W.-K., J.-P. Chen, Z. Li, C. Wang, and C. Zhang (2012), Impact of aerosols on convective clouds and precipitation, *Rev. Geophys.*, *50*, RG2001, doi:10.1029/2011RG000369.

Textor, C., et al. (2006), Analysis and quantification of the diversities of aerosol life cycles within AeroCom, *Atmos. Chem. Phys.*, *6*, 1777–1813.

Tian, B., D. E. Waliser, R. A. Kahn, Q. Li, Y. L. Yung, I. Tyranowski, I. V. Geogdzhayev, M. I. Mishchenko, O. Torres, and A. Smirnov (2008), Does the Madden-Julian Oscillation influence aerosol variability?, *J. Geophys. Res.*, *113*, D12215, doi:10.1029/2007JD009372.

Tian, B., D. E. Waliser, R. A. Kahn, and S. Wong (2011), Modulation of Atlantic aerosols by the Madden-Julian Oscillation, *J. Geophys. Res.*, *116*, D15108, doi:10.1029/2010JD015201.

Torres, O. H. J., and P. K. Bhartia (2012), Retrieval of aerosol optical depth above clouds from OMI observations: Sensitivity analysis and case studies, *J. Atmos. Sci.*, *69*, 1037–1053.

Torres, O., P. K. Bhartia, J. R. Herman, A. Sinyuk, P. Ginoux, and B. Holben (2002), A long-term record of aerosol optical depth from TOMS observations and comparison to AERONET measurements, *J. Atmos. Sci.*, *59*, 398–413.

Torres, O., C. Ahn, and Z. Chen (2013), Improvements to the OMI near UV aerosol algorithm using A-train CALIOP and AIRS observations, *Atmos. Meas. Tech. Discuss.*, *6*, 5621–5652, doi:10.5194/amtd-6-5621-2013.

Tosca, M. G., J. T. Randerson, C. S. Zender, M. G. Flanner, and P. J. Rasch (2010), Do biomass burning aerosols intensify drought in equatorial Asia during El Niño?, *Atmos. Chem. Phys.*, *10*, 3515–3528.

Trenberth, K. E., J. T. Fasullo, and J. Kiehl (2009), Earth's global energy budget, *Bull. Am. Meteorol. Soc.*, *90*(2), 311–323.

Tripathi, S. N., A. Pattnaik, and S. Dey (2007), Aerosol indirect effect over Indo-Gangetic plain, *Atmos. Environ.*, *41*, 7037–7047.

Twomey, S. (1977), The influence of pollution on the short wave albedo of clouds, *J. Atmos. Sci.*, *34*, 1149–1152.

van den Heever, S. C., G. L. Stephens, and N. B. Wood (2011), Aerosol indirect effects on tropical convection characteristics under conditions of radiative-convective equilibrium, *J. Atmos. Sci.*, *68*, 699–718.

van der Werf, G. R., et al. (2008), Climate regulation of fire emissions and deforestation in Equatorial Asia, *Proc. Natl. Acad. Sci. U.S.A.*, *105*, 20,350–20,355, doi:10.1073/pnas.0803375105.

Várnai, T., and A. Marshak (2009), MODIS observations of enhanced clear sky reflectance near clouds, *Geophys. Res. Lett.*, *36*, L06807, doi:10.1029/2008GL037089.

Várnai, T., A. Marshak, and W. Yang (2012), Multi-satellite aerosol observations in the vicinity of clouds, *Atmos. Chem. Phys. Discuss.*, *12*, 32,039–32,061, doi:10.5194/acpd-12-32039-2012.

Veefkind, J. P., G. de Leeuw, and P. A. Durkee (1998), Retrieval of aerosol optical depth over land using two-angle view satellite radiometry during TARFOX, *Geophys. Res. Lett.*, *25*(16), 3135–3138, doi:10.1029/98GL02264.

Veefkind, J. P., K. F. Boersma, J. Wang, T. P. Kurosu, N. Krotkov, K. Chance, and P. F. Levelt (2011), Global satellite analysis of the relation between aerosols and short-lived trace gases, *Atmos. Chem. Phys.*, *11*, 1255–1267.

Veselovskii, I., A. Kolgotin, V. Griaznov, D. Müller, K. Franke, and D. Whiteman (2004), Inversion of multiwavelength Raman lidar data for retrieval of bimodal aerosol size distribution, *Appl. Opt.*, *43*, 1180–1195.

Vinoj, V., P. J. Rasch, H. Wang, J. H. Yoon, P. L. Ma, K. Landu, and B. Singh (2014), Short-term modulation of Indian summer monsoon rainfall by West Asian dust, *Nat. Geosci.*, *7*, 308–313, doi:10.1038/ngeo2107.

Wagner, T., M. Penning de Vries, S. Beirle, and J. Zörner (2013), Investigation of trace gas to aerosol relationships over biomass burning areas using daily satellite observations, ESA Living Planet Symposium, Edinburgh, 09–13 Sept.

Wang, C., D. Kim, A. M. L. Ekman, M. C. Barth, and P. J. Rasch (2009), Impact of anthropogenic aerosols on Indian summer monsoon, *Geophys. Res. Lett.*, *36*, L21704, doi:10.1029/2009GL040114.

Wang, H., and G. Feingold (2009a), Modeling mesoscale cellular structures and drizzle in marine stratocumulus, Part I: Impact of drizzle on the formation and evolution of open cells, *J. Atmos. Sci.*, *66*, 3237–3256, doi:10.1175/2009JAS3022.1.

Wang, H., and G. Feingold (2009b), Modeling open cellular structures and drizzle in marine stratocumulus. Part II: The microphysics and dynamics of the boundary region between open and closed cells, *J. Atmos. Sci.*, *66*, 3257–3275, doi:10.1175/2009JAS3120.1.

Wang, P. K., S.-H. Su, Z. Charvát, J. Štástka, and H.-M. Lin (2011), Cross tropopause transport of water by mid-latitude deep convective storms: A review, *Terr. Atmos. Ocean Sci.*, *22*(5), 447–462.

Wang, Q., D. J. Jacob, J. R. Spackman, A. E. Perring, J. P. Schwarz, N. Moteki, E. A. Marais, C. Ge, J. Wang, and S. R. H. Barrett (2014a), Global budget and radiative forcing of black carbon aerosol: Constraints from pole-to-pole (HIPPO) observations across the Pacific, *J. Geophys. Res. Atmos.*, *119*, 195–206, doi:10.1002/2013JD020824.

Wang, Y., and L. Zhou (2005), Observed trends in extreme precipitation events in China during 1961–2001 and the associated change in large-scale circulation, *Geophy. Res. Lett.*, *32*, L09707, doi:10.1029/2005GL022574.

Wang, Y., M. Wang, R. Zhang, S. J. Ghan, Y. Lin, J. Hu, B. Pan, M. Levy, J. Jiang, and M. J. Molina (2014b), Assessing the effects of anthropogenic aerosols on Pacific storm track using a multi-scale global climate model, *Proc. Natl. Acad. Sci. U.S.A.*, *111*(19), 6894–6899.

Wang, Y., R. Zhang, and R. Saravanan (2014c), Asian pollution climatically modulates mid-latitude cyclones following hierarchical modelling and observational analysis, *Nature. Comm.*, *5*, 3098.

Wang, Y., K.-H. Lee, Y. Lin, M. Levy, and R. Zhang (2014d), Distinct effects of anthropogenic aerosols on tropical cyclones, *Nature. Clim. Change*, *4*, 368–373.

Waquet, F., J. Riedi, L. C. Labonnote, P. Goloub, B. Cairns, J.-L. Deuzé, and D. Tanré (2009), Aerosol remote sensing over clouds using the A-train observations, *J. Atmos. Sci.*, *66*, 2468–2480, doi:10.1175/2009JAS3026.1.

Waquet, F., et al. (2013), Retrieval of aerosol microphysical and optical properties above liquid clouds from POLDER/PARASOL polarization measurements, *Atmos. Meas. Tech.*, *6*, 991–1016, doi:10.5194/amt-6-991-2013.

Waquet, F., F. Peers, P. Goloub, F. Ducos, F. Thieuleux, Y. Derimian, J. Riedi, M. Chami, and D. Tanré (2014), Retrieval of the Eyjafjallajökull volcanic aerosol optical and microphysical properties from POLDER/PARASOL measurements, *Atmos. Chem. Phys.*, *14*, 1755–1768, doi:10.5194/acp-14-1755-2014.

Werner, F., F. Ditas, H. Siebert, M. Simmel, B. Wehner, P. Pilewskie, T. Schmeissner, R. A. Shaw, and M. Wendisch (2013), Twomey effect observed from collocated microphysical and remote sensing measurements over shallow cumulus, *J. Geophys. Res. Atmos.*, *119*, 1534–1545, doi:10.1002/2013JD020131.

Wheeler, M. C., and H. H. Hendon (2004), An all-season real-time multivariate MJO index: Development of an index for monitoring and prediction, *Mon. Weather Rev.*, *132*, 1917–1932, doi:10.1175/1520-0493(2004)132<1917:AARMMI>2.0.CO;2.

Wiedensohler, A., et al. (2012), Mobility particle size spectrometers: Harmonization of technical standards and data structure to facilitate high quality long-term observations of atmospheric particle number size distributions, *Atmos. Meas. Tech.*, *5*, 657–685, doi:10.5194/amt-5-657-2012.

Wilcox, E. M. (2012), Direct and semi-direct radiative forcing of smoke aerosols over clouds, *Atmos. Chem. Phys.*, *12*, 139–149, doi:10.5194/acp-12-139-2012.

Wilcox, E. M., Harshvardhan, and S. Platnick (2009), Estimate of the impact of absorbing aerosol over cloud on the MODIS retrievals of cloud optical thickness and effective radius using two independent retrievals of liquid water path, *J. Geophys. Res.*, *114*, D05210, doi:10.1029/2008JD010589.

Wild, M. (2005), Solar radiation budgets in atmospheric model intercomparisons from a surface perspective, *Geophys. Res. Lett.*, *32*, L07704, doi:10.1029/2005GL022421.

Wild, M. (2012), Enlightening global dimming and brightening, *Bull. Am. Meteorol. Soc.*, *93*, 27–37.

Wild, M., and B. Liepert (2010), The Earth radiation balance as driver of the global hydrological cycle, *Environm. Res. Lett.*, *5*, 025203, doi:10.1088/1748-9326/5/2/025203.

Wild, M., B. Trüssel, A. Ohmura, C. N. Long, G. König-Langlo, E. G. Dutton, and A. Tsvetkov (2009), Global dimming and brightening: An update beyond 2000, *J. Geophys. Res.*, *114*, D00D13, doi:10.1029/2008JD011382.

Wild, M., D. Folini, C. Schär, N. Loeb, E. G. Dutton, and G. König-Langlo (2013), The global energy balance from a surface perspective, *Clim. Dyn.*, *40*, 3107–3134, doi:10.1007/s00382-012-1569-8.

Williams, E., and S. Stanfill (2002), The physical origin of the land-ocean contrast in lightning activity, *Applied Physics*, *3*, 1277–1292.

Williams, E., et al. (2002), Contrasting convective regimes over the Amazon: Implications for cloud electrification, *J. Geophys. Res.*, *107*(D20), 8082, doi:10.1029/2001JD000380.

Wind, G., A. M. da Silva, P. M. Norris, and S. Platnick (2013), Multi-sensor cloud retrieval simulator and remote sensing from model parameters— Part 1: Synthetic sensor radiance formulation, *Geosci. Model Dev.*, *6*, 2049–2062, doi:10.5194/gmd-6-2049-2013.

Winker, D. M., M. A. Vaughan, A. H. Omar, Y. Hu, K. A. Powell, Z. Liu, W. H. Hunt, and S. A. Young (2009), Overview of the CALIPSO mission and CALIOP data processing algorithms, *J. Atmos. Oceanic Tech.*, *26*, 2310–2323.

Winker, D. M., et al (2010), The CALIPSO mission: A global 3D view of aerosols and clouds, *Bull. Am. Meteorol. Soc.*, *91*, 1211–1229, doi:10.1175/2010BAMS3009.1.

Winker, D. M., J. L. Tackett, B. J. Getzewich, Z. Liu, M. A. Vaughan, and R. R. Rogers (2012), The global 3-D distribution of tropospheric aerosols as characterized by CALIOP, *Atmos. Chem. Phys. Discuss.*, *12*, 24,847–24,893, doi:10.5194/acpd-12-24847-2012.

Yanai, M., C. Li, and Z. Song (1992), Seasonal heating of the Tibetan Plateau and its effects on the evolution of the Asian summer monsoon, *J. Meteor. Soc. Jpn.*, *70*(1B), 319–351.

Yu, F., X. Ma, and G. Luo (2013), Anthropogenic contribution to cloud condensation nuclei and the first aerosol indirect climate effect, *Environ. Res. Lett.*, *8*, 024029, doi:10.1088/1748-9326/8/2/024029.

Yuan, T., J. V. Martins, Z. Li, and L. A. Remer (2010), Estimating glaciation temperature of deep convective clouds with remote sensing data, *Geophys. Res. Lett.*, *37*, L08808, doi:10.1029/2010GL042753.

Yuan, T., L. A. Remer, and H. Yu (2011a), Microphysical, macrophysical and radiative signatures of volcanic aerosols in trade wind cumulus observed by the A-Train, *Atmos. Chem. Phys.*, *11*, 7119–7132.

Yuan, T., L. A. Remer, K. E. Pickering, and H. Yu (2011b), Observational evidence of aerosol enhancement of lightning activity and convective invigoration, *Geophys. Res. Lett.*, *38*, L04701, doi:10.1029/2010GL046052.

Zhang, H., G. M. McFarquhar, S. M. Saleeby, and W. R. Cotton (2007), Impacts of Saharan dust as CCN on the evolution of an idealized tropical cyclone, *Geophys. Res. Lett.*, *34*, L14812, doi:10.1029/2007GL029876.

Zhang, H., G. M. McFarquhar, W. R. Cotton, and Y. Deng (2009a), Direct and indirect impacts of Saharan dust acting as cloud condensation nuclei on tropical cyclone eyewall development, *Geophys. Res. Lett.*, *36*, L06802, doi:10.1029/2009GL037276.

Zhang, H., Z. L. Wang, P. W. Guo, and Z. Z. Wang (2009b), A modeling study of the effects of direct radiative forcing due to carbonaceous aerosols on the climate in East Asia, *Adv. Atmos. Sci.*, *16*(1), 57–66, doi:10.1007/s00376-009-0057-5.

Zhang, H., A. Lyapustin, Y. Wang, S. Kondragunta, I. Laszlo, P. Ciren, and R. M. Hoff (2011), A multi-angle aerosol optical depth retrieval algorithm for geostationary satellite data over the United States, *Atmos. Chem. Phys.*, *11*, 11,977–11,991, doi:10.5194/acp-11-11977-2011.

Zhang, J., J. S. Reid, and B. N. Holben (2005), An analysis of potential cloud artifacts in MODIS over ocean aerosol optical thickness product, *Geophys. Res. Lett.*, *32*, L15803, doi:10.1029/2005GL023254.

Zhang, J., J. S. Reid, D. Westphal, N. Baker, and E. Hyer (2008), A system for operational aerosol optical depth data assimilation over global oceans, *J. Geophys. Res.*, *113*, D10208, doi:10.1029/2007JD009065.

Zhang, L., D. J. Jacob, X. Liu, J. A. Logan, K. Chance, A. Eldering, and B. R. Bojkov (2010), Intercomparison methods for satellite measurements of atmospheric composition: Application to tropospheric ozone from TES and OMI, *Atmos. Chem. Phys.*, *10*, 4725–4739, doi:10.5194/acp-10-4725-2010.

Zhu, Y., D. Rosenfeld, X. Yu, G. Liu, J. Dai, and X. Xu (2014), Satellite retrieval of convective cloud base temperature based on the NPP/VIIRS Imager, *Geophys. Res. Lett.*, *41*, 1308–1313, doi:10.1002/2013GL058970.

Zieger, P., et al. (2011), Comparison of ambient aerosol extinction coefficients obtained from in situ, MAX-DOAS and LIDAR measurements at Cabauw, *Atmos. Chem. Phys.*, *11*, 2603–2624, doi:10.5194/acp-11-2603-2011.

Ziemke, J. R., and S. Chandra (2003), La Niña and El Niño-induced variabilities of ozone in the tropical lower atmosphere during 1970–2001, *Geophys. Res. Lett.*, *30*(3), 1142, doi:10.1029/2002GL016387.

Zipser, E. J. (1994), Deep cumulonimbus cloud systems in the tropics with and without lightning, *Mon. Weather Rev.*, *122*, 1837–1851.